Experimental Investigation of Moving Surfaces for Boundary Layer and Circulation Control of Airfoils and Wings

Robert Vets

A dissertation
submitted in partial fulfillment of the
requirements for the degree of

Doctor of Philosophy

University of Washington

2015

Reading Committee:

Robert Breidenthal, Chair

Mitsuro Kurosaka

Antonino Ferrante

Program Authorized to Offer Degree:
Aeronautics and Astronautics

University of Washington

Abstract

Experimental Investigation of
Moving Surfaces for Boundary Layer and
Circulation Control of Airfoils and Wings

Robert Vets

Chair of the Supervisory Committee:
Professor Robert Breidenthal
Department of Aeronautics and Astronautics

An experimental study was conducted to assess the application of a moving surface to affect boundary layers and circulation around airfoils for the purpose of altering and enhancing aerodynamic performance of finite wings at moderate Reynolds numbers. The moving surface was established by a wide, lightweight, nylon belt that enveloped a wing's symmetric airfoil profile articulated via a friction drive cylinder such that the direction of the upper surface was in the direction of the free stream. A water tunnel visualization study accompanied wind tunnel testing at the University of Washington, Kirsten Wind Tunnel of finite wings. The defining non-dimensional parameter for the system is the ratio of the surface velocity to the free stream velocity, u_s/U_o. Results show a general increase in lift with increasing u_s/U_o. The endurance parameter, $C_L^{3/2}/C_D$ served as an additional metric for the system's performance. Examining the results of the endurance parameter shows general increase in endurance and lift with the moving surface activated. Peak performance in terms of increased endurance along with increased lift occurs at or slightly above $u_s/U_o = 1$. Water tunnel visualization showed a marked difference in the downwash for velocity ratios greater than 1, supporting the measured data. Reynolds numbers for this investigation were 1.9×10^5 and 4.3×10^5, relevant to the class of fixed wing, Tier-1, Unmanned Aerial Vehicles (UAV).

TABLE OF CONTENTS

LIST OF FIGURES

LIST OF TABLES

GLOSSARY

b: Wing span

c: Wing chord length

c_D: Section Coefiicient of Drag

c_L: Section Coefiicient of Lift

c_L: Section Coefiicient of Lift

psf: Pounds per Square Foot

r: Radial Distance

rpm: Revolutions per MInute

u: x-axis velocity component

u_b: Surface Speed, Belts

u_c: Surface Speed, Cylinder

u_r: Radial Velocity Component

u_s: Surface Speed, General

u_θ: Azimuthal Velocity Component

v: y-axis velocity component

w: z-axis velocity component

A: Amp

AC: Alternating Current

AR: Aspect Ratio

BEC: Battery Elimination Circuit

C_D: Coefiicient of Drag

C_F: Coefiicient of Skin Friction

C_L: Coefiicient of Lift

CFD: Computational Fluid Dynamics

D: Drag Force

DC: Direct Current

ESC: Electronic Speed Control

FAA: Federal Aviation Administration

HLFC: Hybrid Laminar Flow Control

HZ: Hertz, cycles per second

ISR: Intelligence, Surveillance, and Reconnaissance

LFC: Laminar Flow Control

L: Lift Force

L/D: Lift to Drag Ratio

MSL: Mean Sea Level

NLF: Natural Laminar Flow

P_R: Power Required

P: Pressure

PID: Proportional Integral Differential

PPM: Pulse Postion Modulation

Re: Reynolds Number

S: Wing Planform Area

T: Thrust

T_R: Thrust Required

U: Velocity

U_O: Free Stream Velocity

UAS: Unmanned Aerial System

UAV: Unmanned Aerial Vehicle

UWAL: University of Washington Aeronautical Laboratory

V: Volt

V_∞: Free Stream Velocity

W: Weight

α: Angle of Attack

Γ: Total Circulation

μ: Dynamic Viscosity

ρ : Air Density

ACKNOWLEDGMENTS

I'd like to thank Professor Bob Breidenthal for his support, friendship, and encouragement, especially in the final push get this done. My gratitude is also expressed to the professors who have provided their time to participate on the committees and in the exams: Professor Kurosaka, Professor Ferrante, Professor Kutz, and Professor Narang, who was kind enough to join the advisory committee late. I have to express special appreciation to Wanda Frederick for her help with my consistent late registration, navigating the administrative landscape, and general friendship. Thanks also to Professor Bruckner for the opportunity to teach AA-302 and to Paolo Feraboli and his students Federico and Francesco in the Lamborghini Lab; the chicken gun demonstration was the certainly best thing I've witnessed at UW.

Finally, I would like to acknowledge the young men who started Vires Aeronautics. Their eagerness and drive provided the support necessary to complete this journey. I am grateful to Harshil Goel, Zack Hargraves, Jordan Green, and all those who invested in their enthusiasm. I wish them all the best in their endeavors.

DEDICATION

to Jessica

We can take down that Post-It now.

Chapter 1
INTRODUCTION

1.1 Preliminary Comments

The results of an experimental study to investigate the performance of finite wings that incorporate a moving-surface boundary layer control system comprised of a rotating belt that encompasses the airfoil profile across much of the span are presented. Moving surfaces are conceptually, perhaps, the simplest method for boundary layer control, in that the moving surfaces can directly reduce or eliminate the velocity gradient across a viscous boundary layer between the no-slip condition at the surface and the free stream. [54]

Although conceptually simple, accommodating a moving surface over anything but the simplest of geometries is a notable engineering design task. Implementations of moving surface systems, as a result, have been primarily based upon rotating cylinders with limited cases of simple belt configurations, with constant geometry orthogonal to the moving surface's velocity vector. The use of moving surfaces on airfoils and wings has been examined, intermittently, since the dawn of powered flight. Although these systems have been the subject of numerous serious investigations, many concepts appear to have been developed largely at the hands of industrialists or entrepreneurs working from popularized understanding of mechanics, primarily based upon the vague technical nature of the Magnus Effect. This may also result from the paradoxical nature of the science of aerodynamics, making the field a challenge. [12] Conventional academic study of aerodynamics necessarily includes discussion and consideration of rotating cylinders; as such it is conceptually straightforward for their use to have been a persistent line of inquiry in the production of lift and the manipulation of boundary layers.

For this study, wind tunnel testing was performed on wings of three differing aspect

ratios (AR) and two trailing edge configurations. Tests were conducted with and without the moving surfaces. The airfoil for this study was a symmetric NACA 0015 with a nominal design chord length of 30.48 cm (12-inches). Individual belts covered 27.3 cm (10.75-inches) of the wing's span, with multiple belts used on each wing when tested. Wind tunnel experiments were performed at a Reynolds numbers of 1.9×10^5 and 4.3×10^5, well below the transition Reynolds number. [53] Water tunnel visualization studies were conducted to provide insight into the evolution of the flow at differing belt speeds: the surface speed of the belt relative to the free stream, u_s/U_o, serving as the non-dimensional parameter characterizing the overall system.

The primary focus of the study was the relationship between the additional circulation created by the belt system, or the impact on boundary layers, on increasing overall lift capability, aerodynamic efficiency, and endurance capability. The endurance parameter, $C_L^{3/2}/C_D$, has been used with respect to flow control system design and experiments for wings and airfoils and serves as an insightful metric for the system under consideration. [19]

1.2 Scope

Aerodynamic testing at the scale presented here, and at the resulting Reynolds numbers, is typical in the technical literature and the history of the development of aerodynamic systems. Concepts are first proven at small scales, manageable with limited resources and facilities, before growing into more comprehensive and expensive studies required for implementation and validation for full-scale systems. The definition of a full-scale system has traditionally meant manned aircraft, however, with the Global War on Terror and U.S. Military campaigns in Iraq and Afghanistan, UAVs[1] are becoming an increasingly important and notable part of the integrated airspace. [5, 36]

The U.S. Army classifies systems based upon the military echelon that they support, for

[1]The term used in the industry and military is actually UAS, unmanned aerial systems, of which the air vehicle, the UAV, is only a component. The system typically includes ground station and mission support equipment, such as cameras or designators.

example brigade, battalion, or division;[2] the larger the echelon, the larger the platform. [17] In terms of military systems, public attention through media reports focus on the larger systems such as the Northup Grumman Global Hawk RQ-4 and General Atomics MQ-1 Predator or MQ-9 Reaper systems. Given the geo-political nature of the missions these systems support, it is not surprising that they receive considerable media coverage, however less than 500 systems of MQ-1 and MQ-9 combined have been produced and less than 50 of the larger RQ-4's have been produced.[3] Meanwhile, the smaller class of systems, often referred to as Tier-1[4] which includes the Boeing-Insitu ScanEagle and the AeroVironment RQ-20 Puma are becoming integrated into the US Civilian Air Space. Both the Scan Eagle and the Puma received restricted category type certificates by the FAA in 2013 and have been approved for commercial use over land and the arctic. [18] Over 1,000 units each of the Scan Eagle and the Puma have been fielded while over 20,000 of the smaller RQ-11 Ravens have been produced. Industry analysts predict that the market for UAVs will more than triple over the next decade, for a total market of near $100B over the next ten years, with the fastest growth in the civilian sector. [2]

Although the Scan Eagle is a fast flying, swept wing system, the smaller RQ-20 and RQ-11 fly at speeds that are consistent with the scale of experiments performed here and by most early stage research efforts. Table 1.1 provides basic specifications for the RQ-20 and RQ-11 air vehicles. These systems fall under the U.S. Army's brigade echelon system classification providing tactical Intelligence, Surveillance, and Reconnaissance (ISR) to ground forces. The systems are essentially *hardened* radio controlled (RC) aircraft with tactical grade imaging systems and capable autopilots. The systems are typically launched by hand where a running soldier launches the air-vehicle by throwing it, a potentially vulnerable maneuver in hostile

[2]The classification of UAS varies with little uniformity, largely it is left to the report in which the systems are discussed to classify them although clear distinctions do exist based upon logistical considerations and size.

[3]As of 2014

[4]Designation by Tier is not regulated by any U.S. Government agency or department, leaving some ambiguity as to what classifies as a Tier-1 system, at present.

Specifications	
RQ-20A Puma AE	
Wing Span:	9.2 ft (2.8 m)
Length:	4.7 ft
Weight:	13 lbs
Speed:	20 - 40 kts (10.3 - 20.6 m/s)
Range:	$10 - 20$ km
Endurance:	60 -120 minutes
Max. Altitude:	10,500 ft MSL
RQ-11B Raven	
Wing Span:	4.5 ft (1.37 m)
Length:	3 ft
Weight:	4.7 lbs
Speed:	17 - 44 kts (8.7 - 22.6 m/s)
Range:	$5 - 10$ km
Endurance:	60 - 90 minutes
Max. Altitude:	10,000 ft MSL

Table 1.1: RQ-20 and RQ-11 UAV Specifications. From AeroVironment.

environments. Recovery is generally achieved by the autopilot vectoring the air-vehicle to a homing waypoint and executing a preprogrammed *deep-stall* maneuver; essentially crashing to the ground.

The aerodynamic characteristics of finite wings with a moving surface boundary layer control discussed in this dissertation are directly applicable to Puma-scale UAVs.

Chapter 2

BACKGROUND

Circulation theory of lift and boundary layer theory, it can be argued, provided the necessary concepts for the theoretical framework that fostered the development of heavier than air flight. Circulation, in this context within a 2-dimensional flow field, is the integral of a closed path within a vector field, specifically a closed path that envelops a body moving through the vector velocity field. The boundary layer is the thin region near an immersed body where viscous forces are appreciable compared to the inertial forces of the flow, and for which a complete analytical theory has been developed for laminar flow. The addition of a moving surface to an airfoil and wing, investigated in this study, affects the total circulation developed by that wing, increasing lift in general while altering the development of the boundary layer that affects the development of drag through viscous friction of the air and by displacement of the flow about the wing. Further, the boundary layer plays an important role in flow separation and stalling.

2.1 Classical Aerodynamics

Prandtl presented the concept of the boundary layer to the Third International Mathematics Congress, in Heidelberg, in 1904; the paper was published a year later. That a thin layer existed near a wetted surface, a wall along which a flow has been established such as a flat plate or an airplane wing, where the forces of viscosity are significant, appears to have been largely understood before 1904. Prandtl's theory reduced the formidable Navier-Stokes equations into readily integrable equations by assuming that the pressure gradient normal to the wall is negligibly small and that the variation of velocity along the wall, within the layer, is much smaller than the variation normal to the wall; the first analytical solutions

to these equations were provided by Blasius in 1908. Prandtl's original paper was lightly received but the solution of the momentum integral equation by von Karman in 1921 paved the way for applying boundary layer theory across a broad range of engineering applications. In 1951, Schlichting published, what has become the graduate-student standard tome, *Boundary Layer Theory*, a comprehensive textbook on this important aspect of fluid mechanics. Often missed but important, Prandtl's original boundary layer paper included a demonstration of preventing flow separation by removing the boundary layer by suction: the first demonstration of boundary layer control. [62]

Concepts for boundary layer control are generally classified by method; either moving the solid wall reducing the velocity gradient, accelerating or energizing the boundary layer by injecting mass and momentum into it, suction to draw fluid from the boundary layer, preventing transition from laminar to turbulent by providing suitable surface geometry, or thermally by cooling wall. Based upon the development of boundary layer theory, the moving surface is perhaps conceptually the simplest method of boundary layer control. [54]

A technical description of circulation generally starts with a recounting of Magnus who, in 1852, sought to examine the flight for projectiles. He conducted a famous experiment on the lateral deflection of a rotating cylinder in a cross flow. Although he did not measure the magnitude of the induced force, he demonstrated what has become known as the Magnus Effect. These effects had been well known in gunnery and observations had been recorded with regard to the flight of tennis balls with back spin at least as far back as 1671. None-theless, the Magnus Effect has inspired numerous inventive, if not particularly scientific, devices. The most famous are probably the 1924 Flettner rotor ships, the Buckau and Barbara. With large rotating cylinders replacing sails, one ship successfully crossed the Atlantic. It was reported that driving the rotors consumed less power than equivalent screw propulsion. Several aircraft designs, notably the Ames rotor plane[1] in the same period, attempted to

[1]Butler Ames was a U.S. Congressman and not Joseph Ames the physicist for whom the NASA Ames Research Center is named.

replace wings with rotors as well. [59, 61].

Rayleigh in 1877 presented the first mathematical model for the potential flow about a rotating cylinder, a cylinder with circulation. [52] His efforts are said to have stalled, however, as he was unable to describe the manner in which friction between the fluid and the rotating cylinder produced circulation. Scores of investigations on rotating cylinders have been conducted and continue to the current day with over 100 papers published in the last decade alone.

Lanchester, in 1894, was the first to make the connection between the concepts of circulation and lift, although his ideas were not widely accepted in Cambridge at the time and were not published until 1907. Kutta, independently, made the connection between circulation and lift in Munich in 1902. The quantitative expression for the relationship between circulation and lift would be developed, again independently, by Joukowski in Moscow in 1906 resulting in the Kutta-Joukowski theorem: $L = \Gamma \rho_\infty V_\infty$. This deceptively simple relation would provide the foundation for thin airfoil theory developed by Munk a decade later that lead to rapid growth in the field of inviscid aerodynamics. [7]

2.2 Rotating Cylinders and Moving Surfaces to Enhance Airfoil Lift

It isn't surprising that incorporating rotating cylinders into wings might be a concept of interest. In the mid 1920's, Wolff appears to have been the first to look at the effect of airfoils "fitted with rotatory cylinders" using an airfoil that approximated a Gottingen 386 with a cylinder that truncated a portion of the leading edge, the diameter of the cylinder nearly the maximum thickness of the airfoil. The airfoil had a 185 mm chord and experiments were run at a Reynolds number of 2.2×10^5. With a cylinder surface velocity 3.4 times the free stream of 16.7 m/s, Wolff reported 90% increase in lift for a maximum C_L of 1.22, nearly twice that of the base airfoil, 0.64, with a stated decrease in drag. Wolff also reported that the gap between the cylinder and the airfoil reduced the cylinder's contribution to lift at higher angles of attack. [76–78]

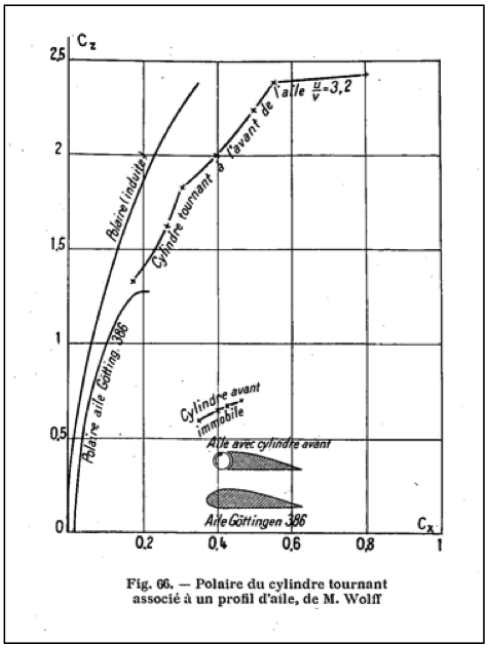

Fig. 66. — Polaire du cylindre tournant associé à un profil d'aile, de M. Wolff

Figure 2.1: Wolff Leading Edge Cylinders, from Favre

Favre, who would later become known for mass averaging techniques in turbulence research, conducted a study on a moving surface boundary layer control system on the upper surface of Joukowski airfoil in his PhD thesis at the University of Paris in 1938. His interest appears to have been to use the moving surface as means to re-attach separated flows, i.e. to recover stalled wings.[2]

Favre briefly describes earlier and contemporary works on moving surface airfoils, including Hubert, who tested a variety of belt configurations in 1925. One had the lower surface moving against the mean flow and along a portion of the leading edge, increased lift by 17%, with drag increased at low angle of attack and decreased at higher angles of attack. Figure 2.2 shows Hubert's results as provided by Favre. Mention is also made of a patented configuration in which the wing was comprised of a series of belts that envelope and

[2]The thesis is written in French without an English translation and without, apparently, an accompanying publication. I have selectively translated parts of the thesis in order to address elements relevant to the effort described herein.

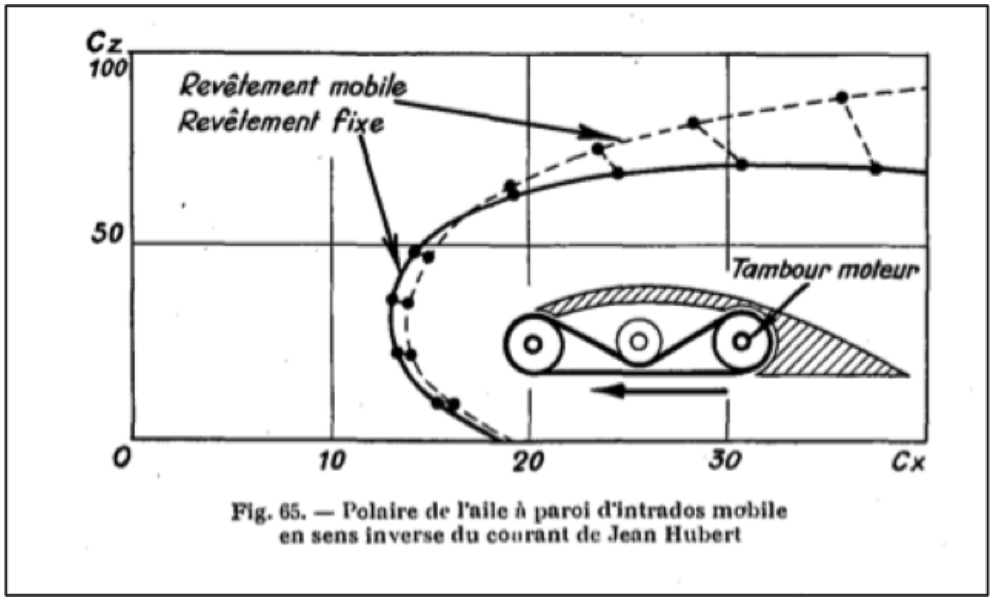

Figure 2.2: Hubert Moving Surface Airfoil, from Favre

establish the airfoil profile. Favre mentions that no results for that system were available. A number of patents were issued in the early 1930's for various wing configurations with moving surfaces, including a single wide belt covering a whole wing, wings having leading edge cylinders similar to those tested by Wolff, wings with the trailing edge replaced with a rotating cylinder, and a wide array of configurations with blowing or suction. In spite of the active entrepreneurial activity at the time, Favre's work appears to stand as the primary scientific investigation and received mention in Schlichting's brief section on moving surface boundary layer control.

Favre used a Joukowski airfoil with the upper surface and leading edge covered in a belt tested in an open return wind tunnel at a Reynolds numbers of 1×10^4 with surface velocity ratios generally below three, see Figure 2.3. Favre tested a number of belt configurations: one wide belt and various combinations of narrow belts covering the same span. His data suggested little or no difference in performance as long as the equivalent span was covered. Favre's results were impressive, demonstrating a peak C_L of 3.5 with stall delayed to 55

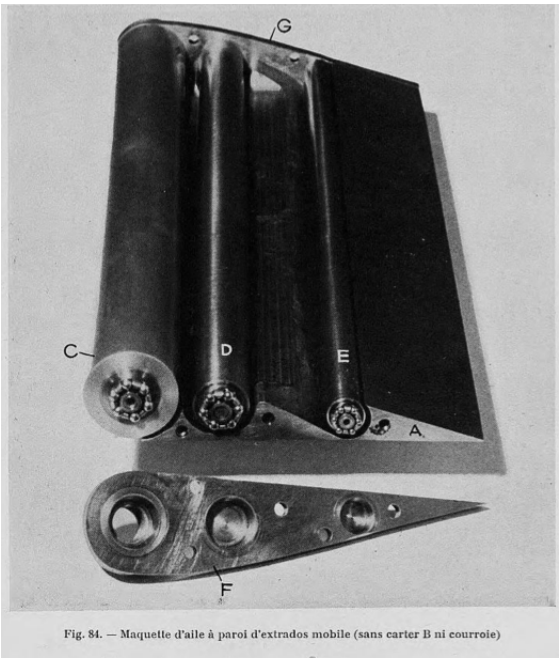

Figure 2.3: Favre's Moving Surface Model, from Favre

degrees, nearly a 300% increase in lift. [21] Figure 2.4 presents the summary of Favre's data.

With the onset of World War II in 1939 and the subsequent change in aerospace research priorities (missiles and jet engines) following the war, there was a lull in moving surface aerodynamics research for nearly 30 years. Alvarez-Calderon and Arnold performed small scale testing in 1961 for a rotating cylinder flap system where the leading edge of the flap was replaced by a rotating cylinder. Their encouraging results, showing an increasing range of angle-of-attack with attached flows, prompted a series of full scale wind tunnel tests at NASA Ames with two and four-propeller aircraft variants leading to eventual flight testing of a North American Rockwell YOV-10A twin-engine aircraft with 12-inch cylinders at the 70% chord flap hinge, Figure 2.5. With an 11,000 pound gross take-off-weight, stabilized approaches were reported at between 28-31 m/s (62-69 mph) corresponded to a lift coefficient of 4.3; the stall speed of the OV-10A is 64 m/s (144 mph). [15]

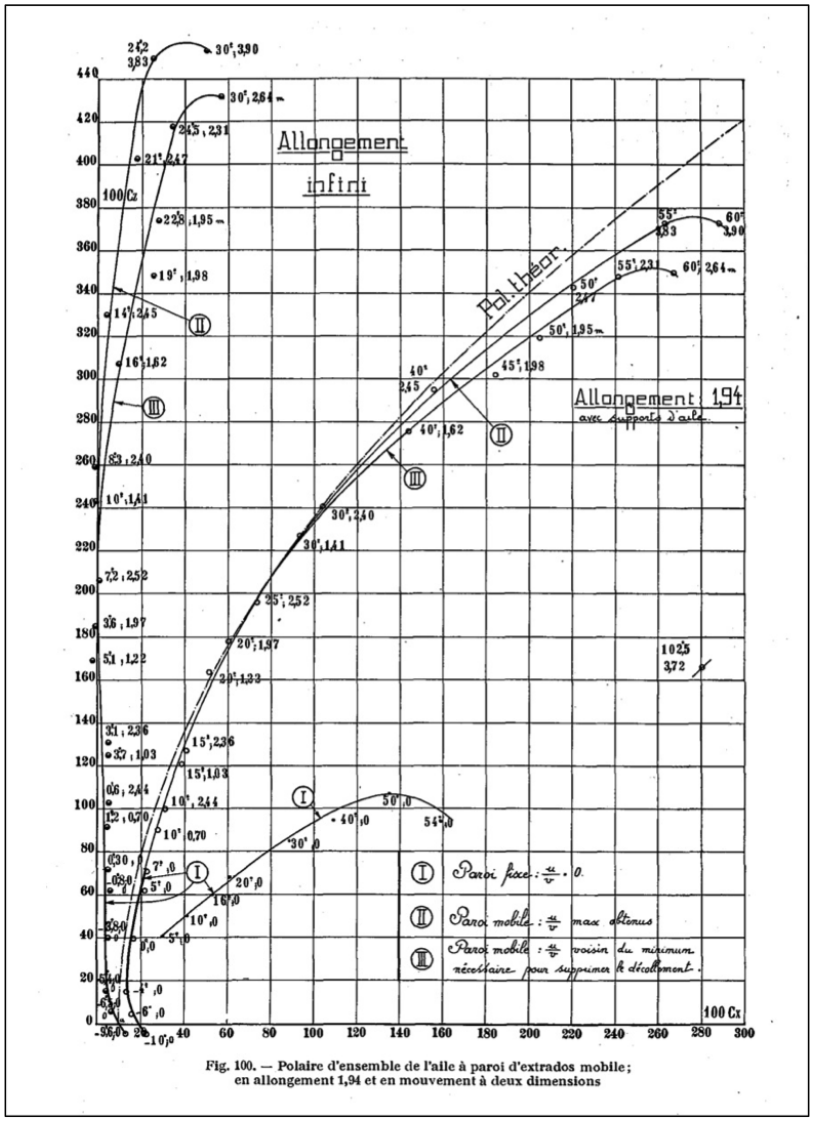

Fig. 100. — Polaire d'ensemble de l'aile à paroi d'extrados mobile; en allongement 1,94 et en mouvement à deux dimensions

Figure 2.4: Favre Moving Surface Data, from Favre

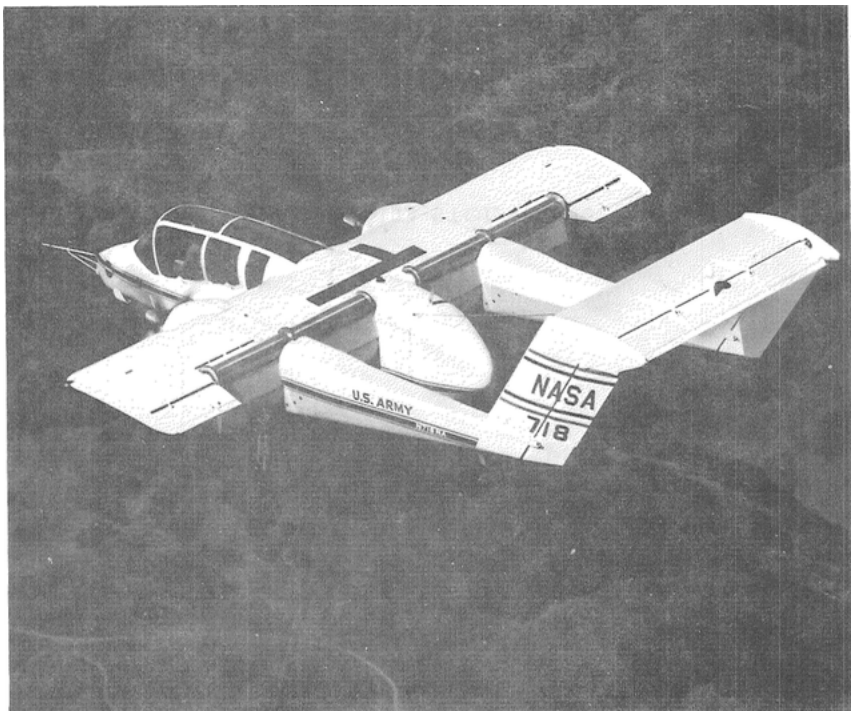

Figure 2.5: North American Rockwell YOV-10A with cylinder flaps

In 1976, Tennet reported using a rotating cylinder at the trailing edge for circulation control of a symmetric airfoil producing a C_L of 1.2 with a velocity ratio of three at a zero angle of attack. [63] In the 1980's, circulation control and circulation control airfoils became terms associated with the use of jets blowing across the upper, aft section of an airfoil just before the trailing edge or flaps, where a circulation airfoil refers to an airfoil with an ellipsoid trailing edge. The Coanda affect is exploited in these studies to preserve attached flow and increase the net airfoil circulation. This remains an active field of study. [48]

Starting in the late 1980's, Modi and his researchers at the University of British Columbia, Vancouver, conducted a nearly two-decade study boundary layer control by use of rotating cylinders to inject momentum into a boundary layer. Their work included airfoil applications, over the road trucks, and stationary bluff bodies representative of civil structures such as tall buildings, bridge towers, and other bodies subject to wind design loads. [44]

Airfoils studies were conducted with a 15% thickness, symmetric, Joukowski airfoil [3] with a range of configurations for the placement of cylinders within the airfoil including the leading edge, the trailing edge, two locations on the upper surface, and combinations of cylinders. Tests were conducted primarily at a Reynolds number of 4.62×10^4, with some at 2.31×10^5. The plain airfoil had a maximum C_L of 0.88. With a leading edge cylinder operating at a velocity ratio of 4, the system produced a C_L of 2.0 without affecting the slope of the lift curve. With the cylinder on the upper side of the leading edge a $C_L = 2.35$ was observed. Combining cylinders at the leading edge and on the forward upper surface a maximum C_L of 2.73 was reached. [39] Mokhtarian would suggest that an optimum location for an upper surface cylinder might exist off the leading edge. [45] Trailing edge cylinders were found to act like flaps shifting the C_L curve to the left and increasing lift at small angles of attack; they noted an increase of C_L from 0.35 to 1.5, or 330%, at 4 degrees angle of attack. Lower drag at higher angles of attack was also noted.

---

[3] They also studied NACA 63-218 airfoils but in his review paper in which he chronicled the work of his research program Modi chose to focus on the Joukowski airfoil on which the most comprehensive set of studies was conducted.

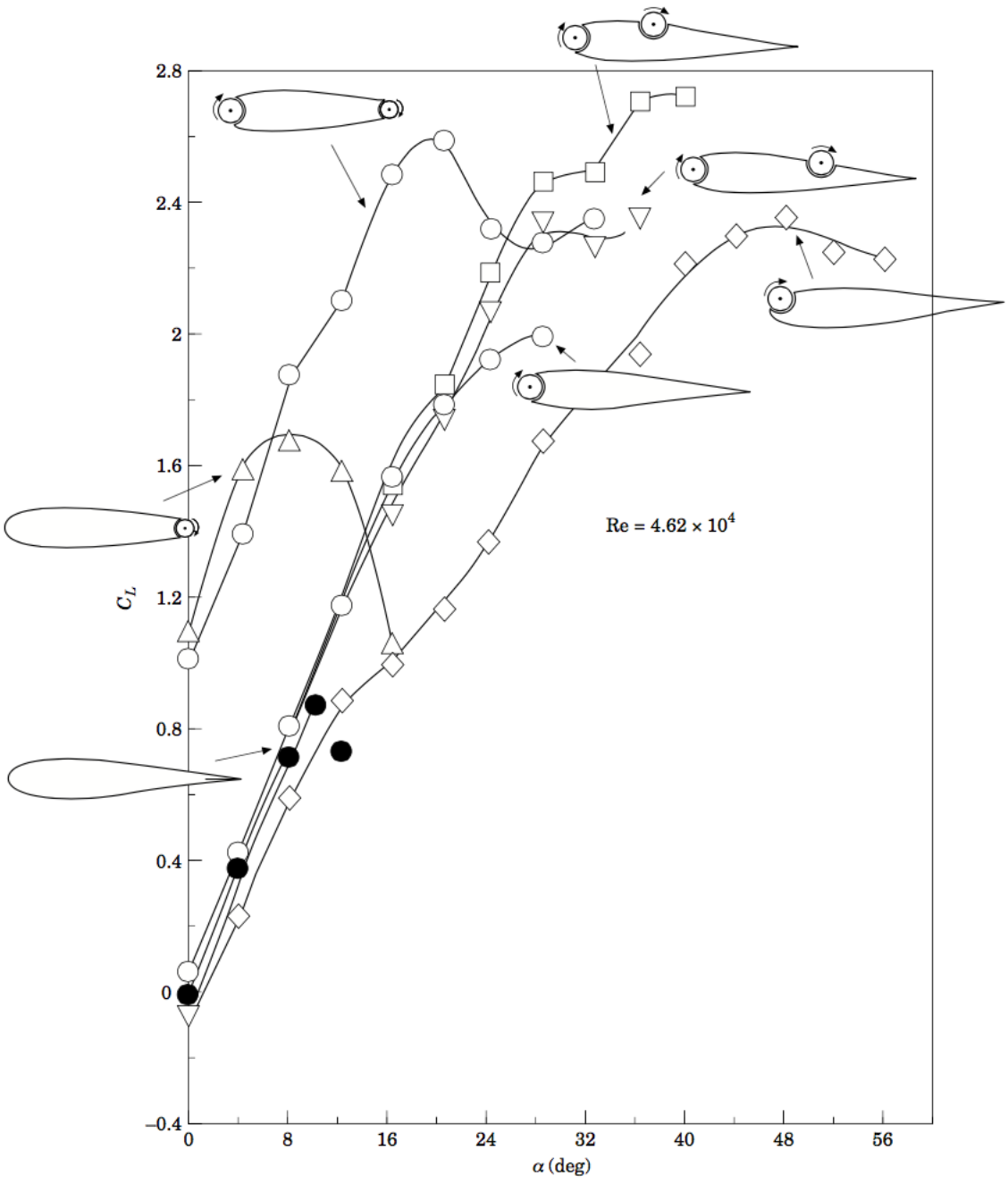

Figure 2.6: Modi et al., Cylinder Data, $u_c/U_o = 4$, from Modi

Leading edge and upper surface cylinders had a diameter that was 10% of the chord and achieved a velocity ratio of four at 8000 rpm. It was noted that although lift performance improved with increasing velocity ratio, the improvements progressively diminished becoming "virtually negligible" at velocity ratios greater than five, $u_c/U_o > 5$. The typical gap between the leading edge cylinder and the airfoil body was 1 mm; increasing it to 5 mm essentially eliminated the effectiveness of the cylinders.

Al-Garni conducted a study on a NACA 0024 airfoil with a 200 mm chord, a 25 mm diameter (12.5% chord) rotating leading edge cylinder, and a 40mm (20% chord) plane flap at a Reynolds number of 6.5×10^4. A maximum cylinder velocity ratio of 4 produced a 92% increase in lift. A modest increase in drag at 10-degrees angle of attack, that increased slightly with increasing cylinder speed was also noted. At higher angles of attack, 20-degrees and above, although lift increased and stall was significantly delayed, notable increase in drag was attributed to the increased adverse pressure differential created by the cylinder at the leading edge. In experiments combining the rotating cylinders with a plain flap the addition of 30 degrees of flaps, increased a total lift 130%. Smoke flow visualization showed the suppression of boundary layer separation as a result of the cylinder rotation. The images show little difference in terms of the locus of the leading edge stagnation point, although sharper velocity gradients near the stagnation point with increasing cylinder speed are evident. [6]

Newer technologies have been investigated for the purposes of boundary layer control on wings. Walker, in 2006, discussed the use of piezo-electric actuated surfaces for subsonic lift enhancement on multi-element airfoils by energizing the boundary layer through vortex amalgamation, a phenomena reported to occur when surface forcing frequencies are sub-harmonics of the vortex passage frequency. At a free-stream velocity of 20 m/s and 15 degrees angle-of-attack, an increase of 10% C_L was reported. [73]

Favier, in 2008, looked at hydrophilic surfaces on a NACA 0012 to induce positive velocity gradients at the wall to delay boundary layer separation. Experiments showed an 8% increase

in lift. His analysis suggested that this corresponds to a slip velocity at the wall of between 10 and 20%.

Vorobeiv, in 2013, looked at using plasma actuators for lift enhancement on NACA 0009 airfoils for UAV applications with mixed results. Although improvements in lift of nearly 40% were observed, there was a large variation in the results with notable negative consequences across the range angles of attack and free stream velocities explored.

For aeronautical applications, preventing the transition to turbulent flow has become known as *natural laminar flow* where surface geometry is defined to provide favorable pressure gradients delaying transition. For wings this has been found to be sweep-limited with poor off-cruise performance. *Laminar Flow Control* has become a term associated with providing suction or blowing over broad extents of aerodynamics surfaces to maintain laminar conditions. *Hybrid Laminar Flow Control* blends these techniques with favorable geometry and limited suction or blowing, for wings primarily in the region of the leading edge. The Boeing 787-9 and 777-X include such techniques on the vertical fins of the empennage. It should be noted that all of these techniques, NLF, LFC, HLFC are often termed Laminar Flow Control and are employed well beyond the transition Reynolds number (approximately 1×10^6) and thus are considered cruise flight technologies. [30, 31]

2.3 Overview

The study presented in this dissertation looks at a moving surface circulation and boundary layer control system in which the entire surface of the airfoil is articulated via a moving belt, more in following with Favre and his contemporaries than the cylinder-based systems of Modi et al.. The airfoil tested was the NACA 0015, with 15% maximum thickness. In addition to investigating the net effect of the moving surface on lift, this study looks at finite wings of differing aspect ratios; 5, 7, and 9. Wind tunnel experiments were conducted to measure aerodynamic forces, while a water tunnel visualization study was performed to gain some insight into the nature of the flow field provided by the moving surface. In addition to

the standard coefficients of lift and drag (C_L and C_D) across a range of angles of attack, the endurance parameter ($C_L^{3/2}/C_D$) is used as a metric to evaluate the efficacy of such a system. Like previous studies, the velocity ratio of the surface velocity to free stream velocity, u_s/U_o, serves as the primary non-dimensional parameter for the system.

Chapter 3
TECHNICAL COMMENTS

The moving surface added to a wing's airfoil section, as instantiated here, can be expected to directly affect the net circulation around the airfoil in a manner similar to that of rotating cylinders to create supplemental lift. At the same time, the moving surface will directly affect the boundary layers that develop over those surfaces. The net effect of these flow field modifications are ultimately recognized by the forces of lift and drag. Conceptually, adjusting the moving surface speed might provide the ability to deterministically control the circulation or boundary layer to use the system to achieve a desired flight characteristic. An example of this might be to increase lift to reduce airspeed on ISR flights or to improve launch and recovery operations of small UAVs.

This chapter briefly summarizes the relevant aspects of the mechanics of flight, circulation, and boundary layers as they relate to the experimental study presented. Comprehensive references are widely available: Anderson, Schlichting, and Thwaites, to name a few.

3.1 Forces of Flight

The mechanics of powered flight are based upon two sets of orthogonal forces: the aerodynamic forces of lift and drag, and their mechanical system counterparts of weight and thrust, Figure 3.1. For level, un-accelerated, flight the lifting force (L) equals the weight (W) while thrust (T) equals drag (D). [1] The relative motion of air over a wing creates dynamic pressure, the aerodynamic quantity q, traditionally expressed in units of pound per square foot.[1]

[1]Owing to the predominance of the use of English units in aerodynamics, especially with q, this dissertation makes uses English units when appropriate based upon sources and context. The design of the tests and the model were primarily done with English units.

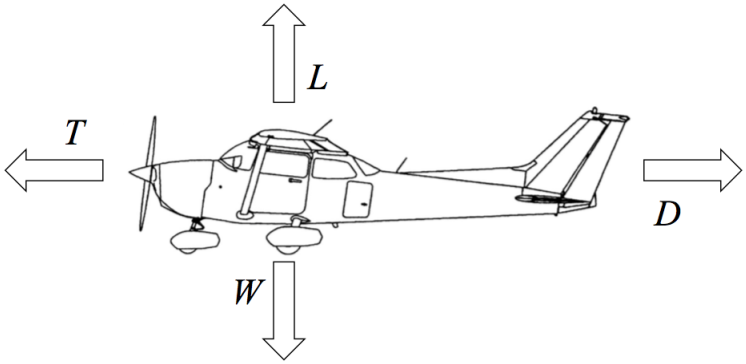

Figure 3.1: Forces of Flight

$$q_\infty = \frac{\rho_\infty V_\infty^2}{2}$$

Non-dimensional coefficients of lift and drag, C_L and C_D, facilitate comparison between experiments, analyses, tests, designs, and systems. The coefficients relate the forces of lift and drag to the dynamic pressure over a reference planform area, S. Section coefficients based upon airfoil chord and unit measure of span are denoted as c_L and c_D.

$$C_L = \frac{L}{q_\infty S}$$

$$C_D = \frac{D}{q_\infty S}$$

The endurance parameter, $C_L^{3/2}/C_D$, relates aerodynamic efficiency, the ratio of Lift to Drag, to power required to maintain constant airspeed.[2] Power required is the product of

[2]The parameter $C_L^{3/2}/C_D$ is a more general than the traditional Breguet's range equation and derivative endurance equation as those are primarily used for analysis at the aircraft level where fuel load is also considered.

thrust required to overcome drag and airspeed:

$$P_R = T_R \, V_\infty$$

For steady flight:

$$\frac{L}{D} = \frac{W}{T} = \frac{C_L}{C_D}$$

$$T_R = \frac{W}{C_L/C_D}$$

Rearranging C_L:

$$V_\infty = \sqrt{\frac{2W}{\rho_\infty \, S \, C_L}}$$

Required power takes the form:

$$P_R = \frac{W}{C_L/C_D} \sqrt{\frac{2W}{\rho_\infty \, S \, C_L}}$$

$$P_R = \sqrt{\frac{2W^2 \, C_D}{\rho_\infty \, S \, C_L^3}}$$

$$P_R \propto \frac{1}{C_L^{3/2}/C_D}$$

Maximum endurance occurs when required power is minimized, i.e. when the term $C_L^{3/2}/C_D$ is maximized for a given configuration. $C_L^{3/2}/C_D$ has started been used a figure of merit, along with the standard aerodynamic coefficients, for evaluating flow control systems.

3.2 Potential Flow

Euler's equations establish the basic model of fluid motion as a set of dependent velocity vector and pressure scalar fields. By relating a reference frame moving with a fluid element

to a spatially fixed frame, the equations of motion for incompressible, perfect (inviscid) fluids are:

$$\frac{\partial u}{\partial t} + u\frac{\partial u}{\partial x} + v\frac{\partial u}{\partial y} + w\frac{\partial u}{\partial z} = -\frac{1}{\rho}\frac{\partial P}{\partial x}$$

$$\frac{\partial v}{\partial t} + u\frac{\partial v}{\partial x} + v\frac{\partial v}{\partial y} + w\frac{\partial v}{\partial z} = -\frac{1}{\rho}\frac{\partial P}{\partial y}$$

$$\frac{\partial w}{\partial t} + u\frac{\partial w}{\partial x} + v\frac{\partial w}{\partial y} + w\frac{\partial w}{\partial z} = -\frac{1}{\rho}\frac{\partial P}{\partial z}$$

A line through the fluid that is everywhere tangent to the velocity vector is a streamline; integrating Euler's equation along that streamline, yields the Bernoulli equation (eq. 3.1) relating pressure and velocity. The Bernoulli equation is widely used as the basis for all introductory discussions of aerodynamics, even though it is frequently inappropriately applied.

$$\frac{1}{2}V^2 + \frac{P}{\rho} + g\,z = constant \tag{3.1}$$

Assuming that a perfect fluid is irrotational permits the use of potential functions[3] to establish set of linear differential equations relating velocity potential functions to stream functions, where constant stream functions are streamlines. The linear functions allow complex flow fields to be developed by superimposing simpler flows (uniform flow, source, sink, doublet, and vortex) in a careful manner. Potential flow need only maintain continuity by satisfying Laplace's equation, $\nabla^2\psi = 0$. Since by definition flow does not cross streamlines, they can effectively represent solid surfaces. Bernoulli's equation facilitates the evaluation of local pressure on these *surfaces*. Sophisticated methods of analysis and design for aircraft aerodynamics based upon potential flow are still widely employed today. [28]

[3] A concept adopted from electrodynamics.

Consider potential flow around a cylinder in a uniform cross flow, created by combining a source-sink doublet and uniform flow. The addition of a vortex, at the center of the cylinder, sets the cylinder rotating. The vortex strength, Γ, is defined in terms of the circulation of its streamlines.

$$\Gamma = \oint V \cdot ds$$

The flow field about a rotating cylinder in polar coordinates is given by:

$$u_r = V_\infty (1 - \frac{a^2}{r^2}) \cos\theta$$

$$u_\theta = -V_\infty (1 + \frac{a^2}{r^2}) \sin\theta - \frac{\Gamma}{2\pi\, r}$$

With increasing circulation, the streamlines about a rotating cylinder change change shape with the with two stagnation points coalescing on one side of the cylinder, the non-symmetric flow producing a net force in the opposite direction, as shown in Figure 3.2 from Kuethe and Chow. Prandtl directly related the surface of a rotating cylinder to the induced velocity in potential flow. He conjectured that the maximum circulation the cylinder could generate was when the stagnation streamlines converged (case c in the figure). This corresponds to maximum $C_{L_{max}}$ of 4π. [50] For a considerable time, maximum values of C_L for rotating cylinders were not observed to be nearly that high, although careful analysis suggested much higher values are possible. [24] Takomaru & Dimotakis, in 1993, reported C_L values over 15 for rotating cylinders at Reynolds number of 3.8×10^3 with high rotation rates $u_c/U_o = 10$.

Classic aerodynamics uses complex analysis to conformally map an airfoil profile into a rotating cylinder in potential flow. [65] The pressure distribution on the surface of the cylinder is determined and mapped back to the airfoil geometry, from which the aerodynamic forces can be calculated. Since the vortex strength determines the location of the stagnation points and consequently the pressure distribution, establishing the value is paramount to the method. The *Kutta condition*, establishes the airfoil's trailing edge as the terminus of

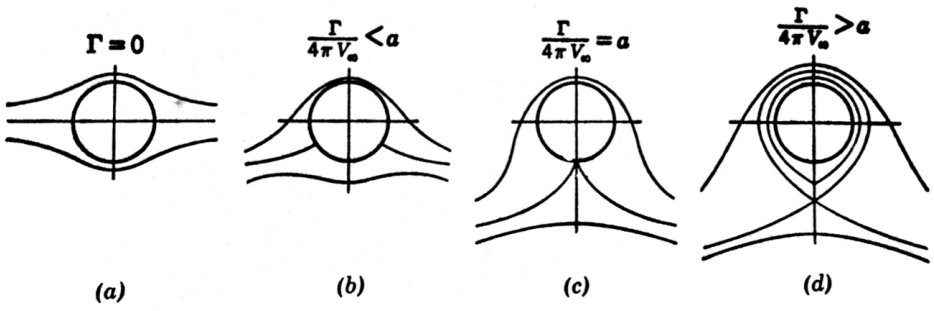

Figure 3.2: Potential flow about a cylinder in cross flow, from Kuethe

the downstream stagnation streamline, establishing the value of Γ. In potential flow, lift is created by the pressure distribution that results from circulation induced by the vortex. If $\Gamma = 0$, then the stagnation stream lines would appear as shown in Figure 3.3a. The Kutta condition properly anchors the trailing edge stagnation point, as shown. In the case where a moving surface can be viewed as superimposing additional circulation, it would be expected that the stagnation points would follow the trend observed for rotating cylinders, converging on the lower surface and eventually separating from the surface.

3.3 Boundary Layers

Prandtl recognized that to a high level of approximation, that the pressure gradient normal to the plane, across which a flow transverses, is negligibly small while, additionally, the variation of velocity along the plane, within the layer, is much smaller than that normal to the plane. With these approximations, the Boundary Layer equation for uniform flow over a flat plate becomes:

$$u\frac{\partial u}{\partial x} + v\frac{\partial u}{\partial y} = -\frac{1}{\rho}\frac{dP}{dx} + \nu\frac{\partial^2 u}{\partial x^2} \tag{3.2}$$

The no-slip approximation provides $u = 0$ at $y = 0$ and beyond the edge of the boundary layer, the velocity reaches the freestream $u = U_o$ at $y \Rightarrow \infty$. The exact solutions of Blasius produce a parabolic velocity profile for laminar flow. In the simplest construct, that of a

flat plate with no pressure gradient, a surface moving in the direction of the free stream will reduce the size of the boundary layer by reducing the velocity gradient, ultimately eliminating it at $u_s/U_o = 1$. At higher speeds, an advancing boundary layer could be defined driven by a sharp positive velocity gradient that would diffuse, or inject, momentum into the free stream. In the case of the airfoil, where the velocity distribution on the surface varies along the chord, it is not possible to maintain a consistent relative local velocity to match the boundary layer. For the NACA 0015, the maximum section thickness is at the 30% chord location, beyond which the pressure gradient becomes increasingly adverse. The adverse pressure gradient can lead to separation and stall where the moving upper surface will delay or prevent separation and stall as demonstrated by Favre. The surface advancing ahead of the flow will create a viscous region transferring momentum to the free stream, further suppressing separation against the adverse pressure gradient. This is observed with rotating cylinders and upper surfaces, and in general terms contributes to the net circulation of the overall flow. [61]

Where the moving surface moves against the free stream a more precarious situation arises. The motion of the wall increases the relative velocity of the flow, increasing the velocity gradient and enhancing the development of the boundary layer. Further, skin-friction is proportional to the velocity gradient at the surface. For a laminar boundary layer, on a flat plate with no pressure gradient, the skin-friction drag coefficient $C_{Df} = \frac{1.328}{\sqrt{Re_c}}$ based upon the length, c, of the plate while for turbulent boundary layers $C_{Df} = \frac{0.074}{Re_c^{0.2}}$. [22] In the range of Reynolds numbers from 2×10^5 and 6×10^5 both turbulent and laminar boundary layers are possible. [54]

The most simplistic model of the moving surface employed in this investigation is that of a flat plate with surfaces set in motion such that the upper surface moves at the speed and direction of the free stream, eliminating the boundary layer and all skin friction, while the lower surface moves against the free stream at the free stream velocity doubling the relative velocity, effectively doubling the Reynolds number. In the laminar case doubling the Reynolds number reduces the friction coefficient by 30% and for the turbulent case by

13%. Overly simplistic, and certainly not correct, a net decrease in skin friction is implied as possible. If doubling of the Reynolds number also causes a transition from a laminar to turbulent boundary layer a notable skin friction increase would be recognized: 90% at a Reynolds number of 2×10^5 and 130% for 4×10^5. Still, the contribution to drag by skin friction are relatively small; for the case discussed here, 0.0029 to 0.0015 for the laminar cases, and 0.0064 to 0.0048 for the turbulent.[4]

3.4 Streamlines

In potential flow for a rotating cylinder, increasing circulation leads to the convergence of the stagnation streamlines as shown in Figure 3.2c. With increases in circulation, the streamlines separate from the surface, Figure 3.2d. For an airfoil section at a small angle-of-attack, conformally mapped to a cylinder in a cross flow, without circulation, the stagnation streamlines appear similar to those shown in Figure 3.3a. The downstream stagnation streamline terminates on the upper section of the wing and the forward stagnation streamline on the underside. The Kutta condition defines the trailing edge of the airfoil as the stagnation streamline's terminus which fixes the value of circulation and establishes the overall streamline patterns, Figure 3.3b.

Moving surfaces, as applied here, are intended to increase total circulation of the airfoil. Considering the moving surface airfoil in potential flow, without circulation, the stagnation streamlines would terminate at similar locations on the upper and lower surfaces as a nominal airfoil. Arbitrary increases in circulation produce analogous effects as that for a cylinder, the convergence of the stagnation streamlines on the underside of the airfoil, eventually meeting at a single point. Similar to the case of the streamlines on a cylinder, with further increases in circulation the airfoil stagnation points would eventually separate from the surface as shown in Figure 3.4. Potential flow without an equivalent Kutta condition.

With the trailing edge replaced by a curved rotating surface, a partial cylinder, the de-

[4]Values cited are for 2×10^5 and 8×10^5, the later values corresponding to doubling the velocity for the 4×10^5 condition.

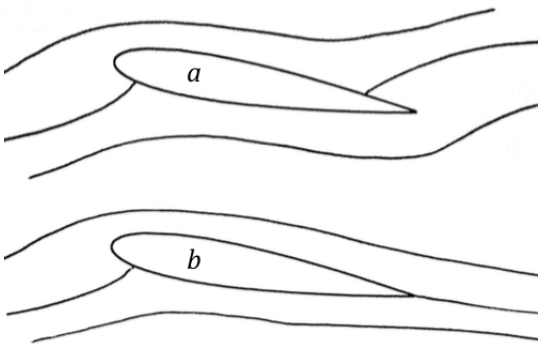

Figure 3.3: Airfoil Streamlines. ***a***: Potential flow without circulation, $\Gamma = 0$. ***b***: With Kutta condition and circulation, $\Gamma > 0$.

terministic location for the Kutta condition is lost. The sharp trailing provided a convenient anchoring point for the stagnation streamline with airflow from the upper and lower surfaces merging at the point. For real airfoils, it has long been understood, the sharp edge does not exist, due to the physical nature of materials and manufacturing. With the development of boundary layers on the upper and lower surfaces, the edge of the boundary layers, by what ever definition chosen, provide *bounding* streamlines for the flow at the aft section of the airfoil. The stagnation streamline at the trailing edge, where the Kutta condition is applied, is essentially an *apparent* streamline between the bounding streamlines, residing in the thin region of *dead water*.

If the rounded trailing edge can be viewed in isolation from the flow around the airfoil, then at low Reynolds number and without motion of the surface, a stagnation streamline on the aft edge of the cylindrical surface might be expected similar to that for a cylinder in a cross flow. For this to occur, of course, the larger potential flow field would require some amount of circulation; equivalent to that had the Kutta condition been applied. With the moving surface activated, additional circulation is produced within the flow field. Viewed locally, the trailing edge continues to resemble a cylinder, now rotating. The aft stagnation streamline may advance along the underside of the trailing edge, again like a rotating cylinder in a cross

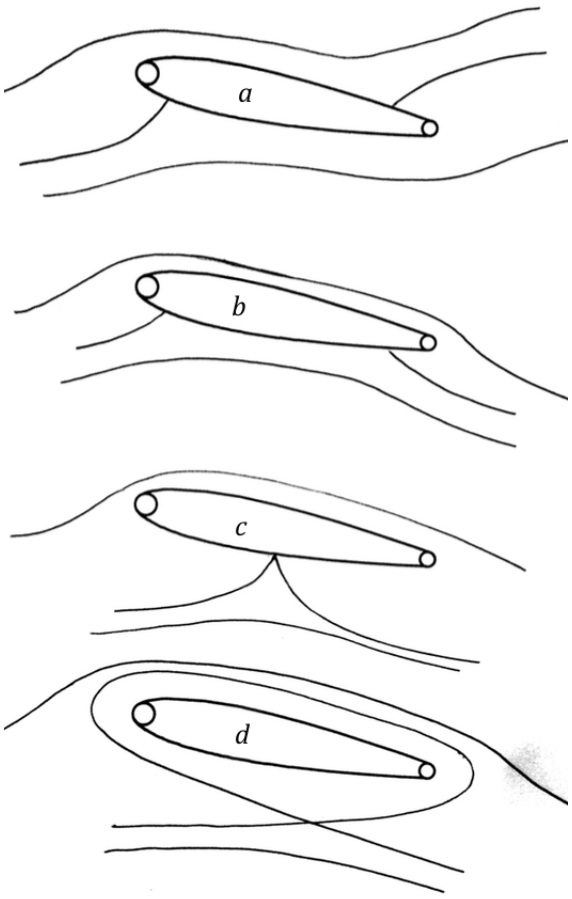

Figure 3.4: Streamlines, Moving Surfaces, Potential flow with increasing circulation, resulting from the action of the moving surface, without a Kutta condition. ***a***: Potential flow without circulation, $\Gamma = 0$. ***b***: With circulation, $\Gamma > 0$. ***c***: $\Gamma >> 0$. ***d***: $\Gamma >>> 0$.

flow. Without an analog to the Kutta condition, as the moving surface speed increased, providing additional circulation, the flow would develop as pure potential flow, again Figure 3.4.

It is possible that an analog to the Kutta condition might exist where the rear stagnation point, or an *apparent* rear stagnation point, may be fixed at a given geometric location. One defining factor may be determined by the upper surface streamlines. The moving surface on the upper side of the airfoil, moving with the free stream, will delay or prevent the development of the boundary layer entirely for velocity ratios of one and above. As the flow is induced to rotate with the trailing edge surface, the streamlines just off the body will follow suit.

Unlike the upper surface, the moving surface on the lower surface enhances the development of the boundary layer. If the outer edge of the lower boundary layer serves as a defining streamline, and the boundary layer were to remain relatively thin, then there would be a point where the momentum of the induced free stream from the rotating surface balances that of the outer edge of the lower surface boundary layer. This would define the locus of the apparent stagnation point. At a unity velocity ratio this balance would likely occur near the tangent point of the cylinder to the airfoil; the point where the circumferential velocity is essentially equal and opposite to the free stream.

At velocity ratios higher than unity, it is difficult to disregard the adverse effect the moving surface has on the pressure side boundary layer. Growing due to the increased velocity gradient, the outer edge of the boundary layer would move farther from the physical surface while the upper surface flow would continue to provide a bounding streamline that closely conformed to the geometric body. The momentum of the convecting lower surface free stream will prevent the advance of the trailing stagnation point forward, as the pure potential flow case might allow. The region about the tangent to the trailing cylinder and the aft airfoil body would provide a potential locus for a bounded stagnation point, an analogy to the Kutta condition.

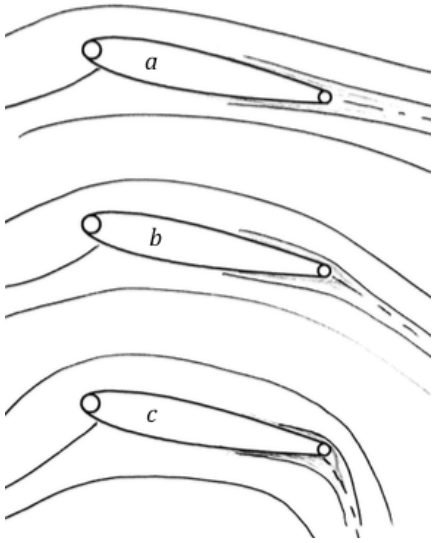

Figure 3.5: Streamline Evolution, Moving Surfaces. With increasing circulation with bounding streamlines and an analog for the Kutta condition.

a: Potential flow without circulation, $\Gamma = 0$. ***b***: With circulation, $\Gamma > 0$; $u_c/U_o < 1$. ***c***: $\Gamma >> 0$; $u_c/U_o \geq 1$.

Chapter 4

EXPERIMENTAL PROGRAM OVERVIEW

4.1 System Description

The effects of a moving surface to influence the boundary layer and net circulation of a wing were examined through wind tunnel testing to measure the aerodynamic forces, with and without the system operating, on finite wings of three different aspect ratios. Water tunnel studies were used to visualize the flow field around the airfoil section. In this investigation, the moving surface consisted of a lightweight nylon fabric belt that enveloped the wing's airfoil cross section, Figure 4.1, along a constant span.

The belt was driven such that it moved in the direction of the free stream on the upper surface, the direction of lift-producing circulation in potential flow, while the underside of the wingś surface moved against the free stream flow. This configuration was chosen for its overall simplicity and novelty of such a system.[1] In terms of a viable implementation for a fielded system, routing the belt through the structure of the wing, as Favre did, introduces numerous complexities to the wing box design and load bearing structure, inevitably resulting in additional weight to that already imposed by the system.

The NACA 0015 symmetric airfoil, with 15% chord maximum thickness and nominal chord length of 30.48 cm (12-inches), was selected for the wing's cross section. Leading and trailing edges were replaced with rotating cylinders, the leading edge cylinder operating as a friction drive *pulley* for the belt powered by a DC electric motor, and the trailing edge cylinder serving as an idling pulley. The NACA 0015 airfoil was well suited to accommodate

[1]The sponsor of the research, Vires Aeronautics, installed and flew a similarly configured system on a Hangar 9 Toledo Special RC airplane, essentially a clip on device installed over the model airplane's existing wings. The observed performance of the non-instrumented flights was part of the motivating factor behind this research effort and some of the design decisions for the test system.

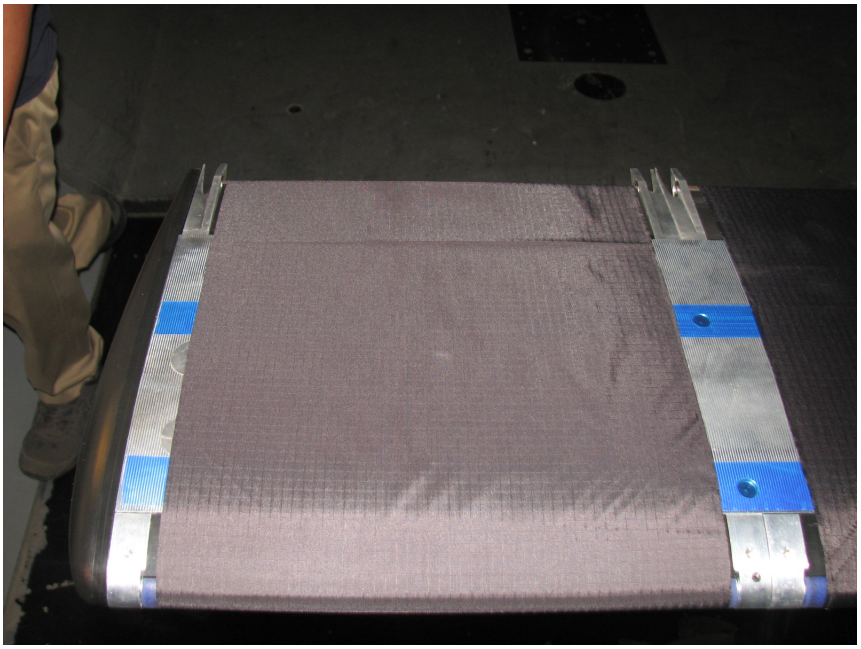

Figure 4.1: Moving Surface Belt

the 19.05 mm (0.75-inch) diameter leading edge cylinder with minimal dimensional deviation to the leading edge radius.

Rotational speeds of the leading edge cylinder were limited to below 15,000 rpm. This speed bound the maximum permissible velocity ratio that could be tested. Although higher speed motors are available and it is possible to add a gearbox, rotating systems above 15,000 or 20,000 rpm require specific details to provide sufficient rigidity and precise balancing of the rotating system, necessitating a notable engineering effort.[2] The preference in this study was to focus on a system configuration that might have been, reasonably, suitable for implementation on an RQ-20 class UAV. Table 4.1 shows the design trade space for the direct drive motor speeds at representative velocity ratios to keep drive motor speeds below 15,000rpm. Two different configurations for the trailing edge were tested in both the water

[2]Earlier studies on cylinders alone were similarly limited to this range. The practical limit of roughly 15,000 rpm for rotating cylinders restricts the otherwise interesting results of the previous cylinder studies with $u_c/U_o > 4$.

Motor Speeds (RPM)			
q		u_c/U_o	
(psf)	0.25	0.5	1.0
1	2,277	4,553	9,106
5	5,082	10,164	*20,328*
10	7,186	14,372	*28,744*
20	10,164	*20,328*	*40,656*

Table 4.1: Motor Speed vs u_c/U_o for 19 mm diameter leading edge shaft.

and wind tunnels. The sharp trailing edge was replaced with one of two diameter idling shafts, or cylinders; one was 6.3 mm (0.25-inch) in diameter and the other 12.6 mm (0.5-inch), see Figure 4.2. The centerline is constant length in all profiles illustrating the amount of chord truncated by the addition of the cylinders.

Water tunnel studies were conducted at far lower free stream velocities; limited to 60 cm/s by the water tunnel and a different drive motor solution was implemented. Higher velocity ratios were achievable in the water tunnel, but testing was limited to a maximum of $u_s/U_o = 2.0$ to correspond to the range of wind tunnel testing conducted.

The speed of the belt, or the tangential surface velocity, is the only relevant physical quantity introduced by the system. The system's performance is characterized by the non-dimensional velocity ratio of the surface speed, u_s, to the free stream velocity, U_o, u_s/U_o. [3] This parameter has been consistently used for rotating cylinders and other moving surface systems.

The velocity ratio was the primary variable of interest in water tunnel, where the Reynolds number varied from roughly 1×10^4 to 4×10^4. Wind tunnel testing was performed with at Reynolds numbers between 1.9×10^5 and 6.1×10^5, with the most relevant testing performed

[3]This could be expressed as u_b/U_o for the belt. u_c/U_o has been used for cylinders in the literature. Here the more general u_s/U_o for surface is typically used.

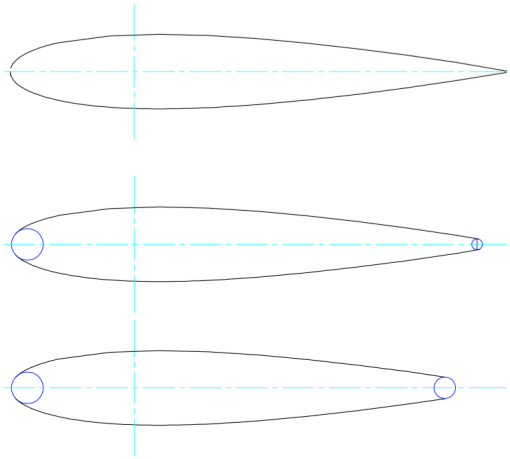

Figure 4.2: Airfoil Profiles, NACA0015. *Top:* Standard airfoil. *Center:* With 6.3 mm diameter trailing edge cylinder and 19.05 mm leading edge cylinder. *Bottom* With 12.6 mm diameter trailing edge cylinder and 19.05 mm leading edge cylinder.

at 4.3×10^5 and below, for both varied velocity ratio and wing configuration. For general reference, at nominal flight speeds, an RQ-20 operates at Reynolds numbers between 3×10^5 and 6×10^5, depending upon the reference chord length and operational altitude relative to mean sea level (MSL). In terms of system design, a 35-knot airspeed corresponds to 18 m/s surface speed for a velocity ratio of 1.0; for the 19.05 mm (0.75-inch) diameter drive cylinder used here that requires a rotational speed of 18,046 rpm.

4.2 General Description

The water tunnel and wind tunnel used a common physical model, the water tunnel employing a single span section of the wind tunnel model. The base wind tunnel model was constructed to the specifications in Table 4.2

The base model consisted of two wings, each of 63.5 cm (25-inches) inches span, with a center body fairing to accommodate the wind tunnel mount. Two sets of wing extensions, each 30.48 cm (12-inches) in span, were developed to provide aspect ratios of seven and nine; the differing wing configurations are referred to as AR-5, AR-7, and AR-9. One of the AR-9

Specifications	
Airfoil:	NACA 0015
Wing Span:	1.52, 2.13, and 2.74 m (5, 7, and 9 ft)
Chord:	30.48 cm (12-inch) nominal
Sweep:	zero
Dihedral:	zero
Taper:	zero

Table 4.2: Test System Specifications

wing extensions was used as the water tunnel model. Each of the 30.48 cm span sections had its own moving surface system, with the root wing having two separate moving belts. Each of the belts was 27.3 cm (10.75-inches) wide, providing 90% span wise surface coverage. Details on the design and fabrication of the wind tunnel model are described below Section 6.2.2.

Chapter 5

WATER TUNNEL EXPERIMENTS

5.1 Objective

Water tunnel studies were used to qualitatively assess the effects of different velocity ratios, u_s/U_o, on the evolution of the flow field in the region about the airfoil. Specific interest was on the down wash as the velocity ratio increased. It was also of interest to consider the behavior of the trailing edge stagnation point, in connection with the Kutta condition, given the sharp trailing edge is replaced by a rotating rounded surface.

Water tunnel experiments were conducted with two model configurations: one had a 6.3 mm (0.25-inch) diameter trailing edge cylinder and the other a 12.7 mm (0.5-inch) diameter trailing edge cylinder. The angle of attack for the visualization studies were 0, +6, +11, for the 6.3 mm diameter trailing edge and 0, +5, +10, +20-degrees for the 12.7 mm diameter trailing edge. The difference between the two sets was the result of indexing the model's test fixture on the water tunnel frame. Sets of digital images were taken for velocity ratios, u_s/U_o, of 0.1, 0.25, 0.5, 0.75, 1.0, 1.25, 1.5, and 2. Movies were also taken as an aid in assessing the images, the movies are not included in this dissertation, however, they were helpful in describing the images presented.

5.2 Experimental Set-Up

5.2.1 Facility

Studies were conducted with the Large Water Tunnel at the University of Washington, Aeronautics and Astronautics department's Fluid Dynamics Laboratory. The Large Water Tunnel has a 3 m (10-foot) long test section with a 0.82 m (3-foot) by 0.82 m (3-foot) cross section. An AC induction motor powers the main pump with a variable-frequency drive

providing variable water speeds in the test sections. The mean flow rate in the test section is a linear function of the drive frequency and corresponds to 1 cps/Hz, with a maximum flow rate of 60 cm/s. For example, a drive frequency of 10 Hz would provide a flow of 10 cm/s and a drive frequency of 2.5 Hz would provide 2.5 cm/s, and so on. A carefully designed converging inlet section, along with a large array of flow straighteners provides a clean flow to the test section. To avoid boundary layer effects from the walls of the test section, experiments were performed with the test model forward in the test section.

A constant displacement, metering pump provided a stream of dye, consisting of food coloring and water, through 20-gauge hypodermic tubing to points in the flow field of interest. The pump controller used a potentiometer to regulate the flow. The potentiometer setting was determined by observing the dye emanating from the end of the hypodermic tubing. Keeping the flow rate as low as possible improved the flow of dye; too high and the small tubing produced relatively high Reynolds number turbulent jets which were to be avoided. Images were captured with a digital camera. After the initial set of testing, a white background was installed in the tank to improve the contrast of the images.

5.2.2 Test Model

A single AR-9 wing extension section from the wind tunnel model was used as the model for all water tunnel studies, see Section 6.2.2. The wing section was suspended by the skin's shear ties under a mounting plate fastened to a four bar linkage that served as the test frame, Figure 5.1. The base leg of the four-bar linkage was clamped to the upper railings of the water tunnel test section to hold the frame in place. The test model mounting plate was machined square and had a compassed miter square attached to it to register the angle of the wing section to the mean flow, specifically the walls of the test section. Articulating the linkage provided the means to alter the angle of attack of the wing relative to the mean flow. The test frame was set manually and secured into position for each configuration.

The leading edge drive cylinder was powered by a belt drive attached to a Pittman GM8212-31, 19.1V, DC gear motor, with a 60.5:1 gear reduction, Figure 5.2. A Sorensen LS

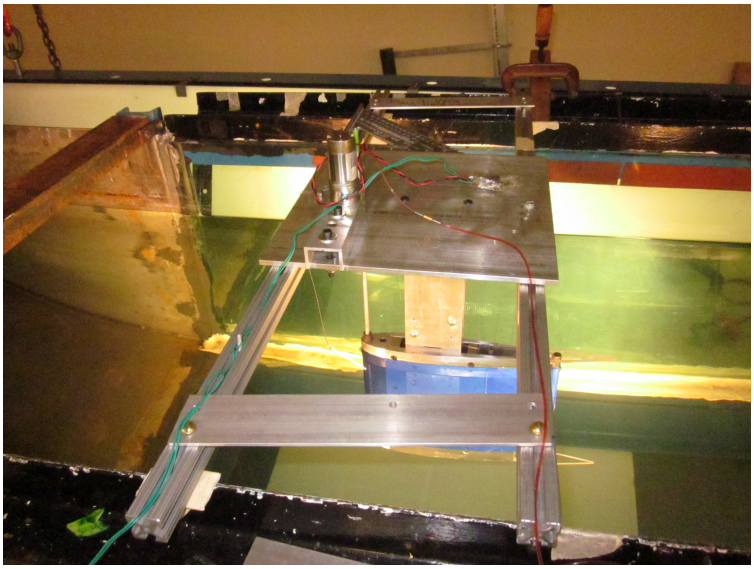

Figure 5.1: Water Tunnel Model Mount

30-3, 30V, 3-amp power supply, used in voltage mode, provided powered to the motor. The surface speed of the belt, u_s, was determined by setting the voltage of the power supply to a fixed value and then making five separate measurements, by stopwatch, of the time required for the belt to complete a single revolution. Timing references were fixed marks on the belt the wing section. For the image studies, drive shaft voltages were limited to maintain the surface velocity at either 1.5 or 5 cm/s, corresponding to values of roughly 4.5 to 5 volts and 10 to 11 volts, and the speed of the water was adjusted for the desired velocity ratio.

The trailing edge sections, aft of the rear spar, were built up structures of water-jet cut acrylic, and were constructed specifically for the water tunnel, Figure 5.3. Given the relatively low speeds, the rear shafts were supported in nylon axle bushings. The structure was designed to snap together but was secondarily bonded with methacrylate.

Belts for the water tunnel were made from 0.65-ounce nylon sailcloth from North Sails, they were 25.4 cm (10-inch) wide and and glued together with the wing section serving as a mandrel. Different belts were required for each trailing edge. The advancing edge of the belt seam, the edge that approached the cylinders, was shaped as a chevron to minimize the

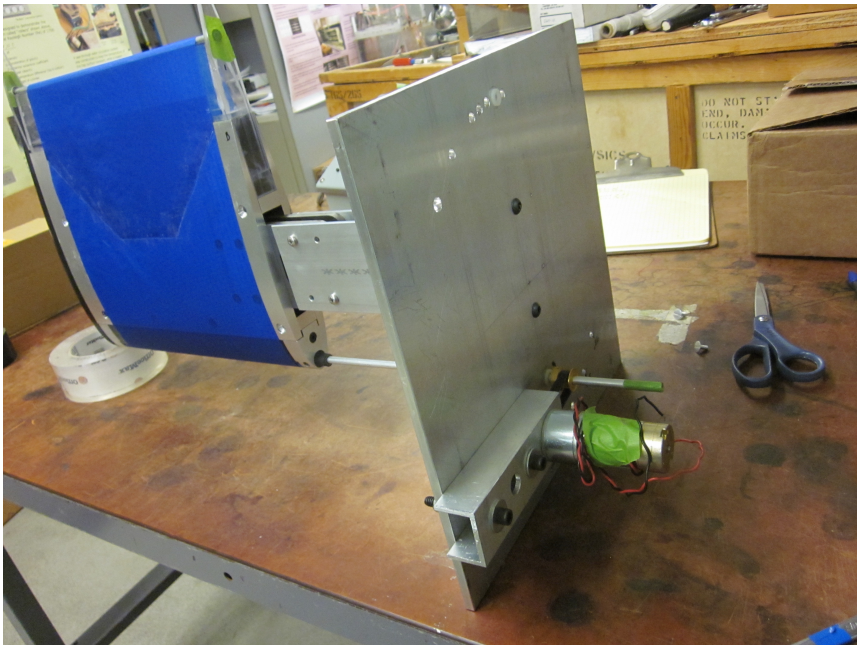

Figure 5.2: Water Tunnel Model

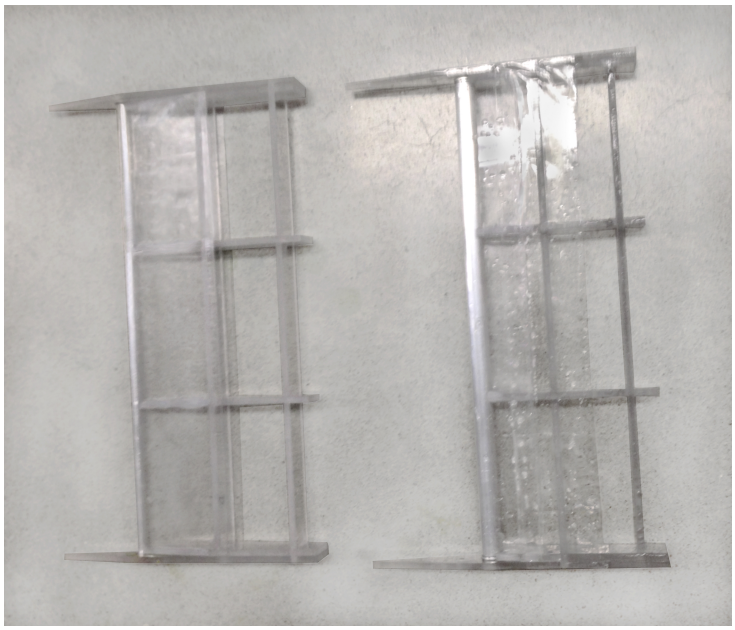

Figure 5.3: Water Tunnel Model Trailing Edge Assemblies

thickness change of the belt due to the seam that traversed the leading and trailing edge cylinders. Flat seams were found to cause a thumping as the belt circumnavigated the wing section and interfered with the smooth operation of the motor.

5.2.3 Test Plan

With the specific model installed in the water tunnel test section, surface speed checks were conducted at the beginning and middle of each day and any time the test model was altered. The different trailing edges affected the voltage required to maintain a specific moving surface velocity. Voltage settings were established to maintain the belt speed at either 1.5 cm/s or 5 cm/s and the speed of the water was set by adjusting the pump motor drive frequency for the desired velocity. The series of velocity ratios were run for a set angle of attack. At the end of the sequence, the angle of attack would be adjusted and the next sequence of would be run. The slowest water speeds were run first, consequently, the velocity ratios started at 2.0 and were reduced from there.

5.3 Results

The water tunnel visualization studies were conducted in two general sets, one for each of the two trailing edge configurations. The flow field changes with increasing velocity ration are generally more pronounced at angles of attack greater than zero.

5.3.1 Configuration 1

Configuration 1 used the 6.3 mm (0.25-inch) trailing edge cylinder. These were the first studies attempted and the contrast of the images was less than ideal. The images are sufficient to resolve changes in the flow field as the velocity ratio is increased, particularly when viewed on a computer screen. All the sets of images presented for Configuration 1 are of the upper side trailing edge. The velocity ratio for all the image sets progresses from velocity ratio $u_s/U_o = 0.1$ to 2.0.

Zero Degrees Angle of Attack

Figure 5.4 shows the set of eight images with the airfoil set at a 0-degrees angle of attack. The dye is injected near the surface at roughly 1/5 chord forward of the trailing edge. At the lower velocity ratios the development of the boundary layer on the upper surface is observable by the spread in the dye, which clearly contracts with increasing surface speed. There is little discernable change to the overall flow pattern as the belt speed increases up to $u_s/U_o = 1.0$. Beyond this point there is an apparent increase in the downwash. At 1.25 this downwash becomes clearly apparent and at $u_s/U_o = 1.5$ and 2.0 increases notably. At $u_s/U_o = 1.25$, there appears to be a clearly defined *apparent stagnation point* at the apex of the trailing edge, the point furthest aft on the model. The characterization of a feature in the flow that can be described as an apparent stagnation point is based upon the presence of dye in close proximity to the surface from which a clear streak is emanating where the flow is apparently behaving independently on either side. Downstream of this point, in the wake, the flow then shows typical wake and shear flow behavior. From this point a shedding vortex street is visible, progressing with moderate but noticeable downwash. At $u_s/U_o = 2.0$, the apparent stagnation point clearly has moved to the underside of the trailing edge cylinder and the downwash is strongly present.

Six Degrees Angle of Attack

Figure 5.5 show more pronounced change in the flow pattern for the sequence at 6 degrees angle of attack. Up to $u_s/U_o = 0.75$ the flow appears largely unchanged. The apparent stagnation point is not nearly as defined in this sequence, however, the flow noticeably changes at $u_s/U_o = 1.0$. At 1.25 and 1.5 the increase in the downwash is evident and by 2.0 the downwash is substantial. For Configuration 1, this set of images shows the most pronounced evolution of trailing edge flow field with increasing relative velocity.

Eleven Degrees Angle of Attack

Figure 5.6 provides a notably different set of images for the 11-degree angle of attack sequence. For $u_s/U_o = 0.5$ and below, the images did not provide clear wake structure, and at 0.25 there was clearly an issue with the dye. At the increased angle of attack, this airfoil would be subject to boundary layer growth and perhaps some separation in the aft section, although the airfoil would not be expected to have fully stalled. It is likely that a poor set-up for the hypodermic needle exacerbated the condition. There is less distinction between the $u_s/U_o = 0.75$ and 1.0 cases in this sequence, however the wake has become more structured than the slower cases. Both of the 0.75 and 1.0 show nicely structured flow with a slight amount of down wash. Progressing to 1.25 and beyond, the amount of downwash increased dramatically over the 6-degree angle of attack case.

5.3.2 Configuration 2

Configuration 2 used the 12.6 mm (0.5-inch) trailing edge cylinder. The contrast in these images was drastically improved by a white polyethylene sheet that was installed on the side and bottom of the water tunnel with revised lighting. Demand for the water tunnel from another research effort prevented redoing Configuration 1 with the improved background.

Two trailing edge image sets were captured for each Configuration 2 sequence, one for each of the upper and lower surfaces. The lower surface images sets provide for additional insight when compared to the upper surface alone as with Configuration 1. An additional set of images were also taken for 20-degrees angle of attack, where the bare airfoil would certainly have been expected to be fully stalled.

Zero Degrees Angle of Attack

Figures 5.7 and 5.8 show the same general evolution of the flow that was observed with Configuration 1, with the 6.3 mm (0.25-inch) trailing edge cylinder. An interesting difference is that the larger diameter cylinder provides broader *dead water*, effectively increasing the

scale of the experiment. The diffusive nature of the evolving boundary layer on the upper surface and unstructured wake at lower velocity ratios is more apparent. Viewed from below, the lowest velocity shows indications of potentially two apparent stagnation points, at the top and the bottom of the cylinder, the *stronger* of the two at the top.

At $u_s/U_o = 0.25$, this dual apparent stagnation condition has clearly collapsed into single point, favoring the stronger point on the upper surface. This upper apparent stagnation is evident from both sets of images, and persists until $u_s/U_o = 0.75$ where the stagnation point has definitively moved to the apex of the trailing edge. The downwash is not strong at 0.75. Although there is clearly shear flow mixing evident below the airfoil, the presence of strong concentrations of dye at the airfoil midplane suggests little bulk downwash. At $u_s/U_o = 1$, this is no longer the case and a definitive downwash induced by the moving belt is now apparent. By 1.5 the apparent stagnation point has moved to the underside of the cylinder along with considerably stronger downwash.

Five Degrees Angle of Attack

Figures 5.9 and 5.10 show the airfoil advanced to 5-degrees angle of attack. At the lowest velocity ratio, the dual apparent stagnation points on the trailing edge appear to have been eliminated. What had been the stronger of the two, the upper apparent stagnation point is now well defined and has a slight bias to the upper surface. For velocity ratios below $u_s/U_o = 0.75$, the flow in the lee of the trailing edge cylinder appears balanced and there is evidence of boundary layer development on the aft section of the airfoil. At $u_s/U_o = 1.0$, the flow has started to change although the clearly altered downwash is most prominent at and above $u_s/U_o = 1.0$. The lower side image, especially $u_s/U_o = 2.0$, shows a dominate apparent stagnation point well along the underside of the airfoil.

Ten Degrees Angle of Attack

Increasing to 10-degrees angle of attack, Figures 5.11 and 5.12 the flow shows essentially the same characteristics as that at 5-degrees angle of attack. The stagnation points are essentially

unchanged, and at $u_s/U_o = 0.75$ the division between the clean flow above the airfoil midline and strongly mixed fluid below is continued. At $u_s/U_o = 0.1$, the underside images might be thought suggest that a stagnation point might lie on the upper surface, but the upper surface images suggest a considerable boundary layer. The apparent stagnation point moves to the underside of the trailing edge cylinder at $u_s/U_o = 1.0$. Above 1.0 the stagnation point again begins to move along the underside of the cylinder along with increasing downwash but not substantially different than for the 5-degree case. Most telling is the underside image at $u_s/U_o = 2.0$, a clear belt of dye a moderate distance away from the airfoil that clearly shows evidence of the induced far field circulation and downwash around the trailing edge of the airfoil. The clean band of fluid also illustrates that the development of the boundary layer is suppressed and flow remains attached to the upper surface.

Twenty Degrees Angle of Attack

At 20-degrees angle of attack, Figures 5.13 and 5.14 the base airfoil is expected to have stalled. The $u_s/U_o = 0.1$ images shows a substantial, fine scale mixing and diffusion of dye at the upper area of the trailing edge cylinder, where the *strong* apparent stagnation points had been observed. This suggests that at these low velocity ratios the airfoils has indeed stalled. Increasing the velocity to $u_s/U_o = 0.25$, the previously observed flow structure begins to re-emerge and the streak of dye on the airfoil's upper surface, evidence of a laminar boundary layer, becomes more pronounced. By $u_s/U_o = 0.5$ the emergence of an apparent stagnation point returns toward the upper side of the rear cylinder. Beyond $u_s/U_o = 1.0$ the stagnation point and overall flow progress similar to lower incidence angle sequences. At $u_s/U_o = 2.0$ the sharp far-field dye streak is again present. Although the angle of the image is different, the general shape is qualitatively the same.

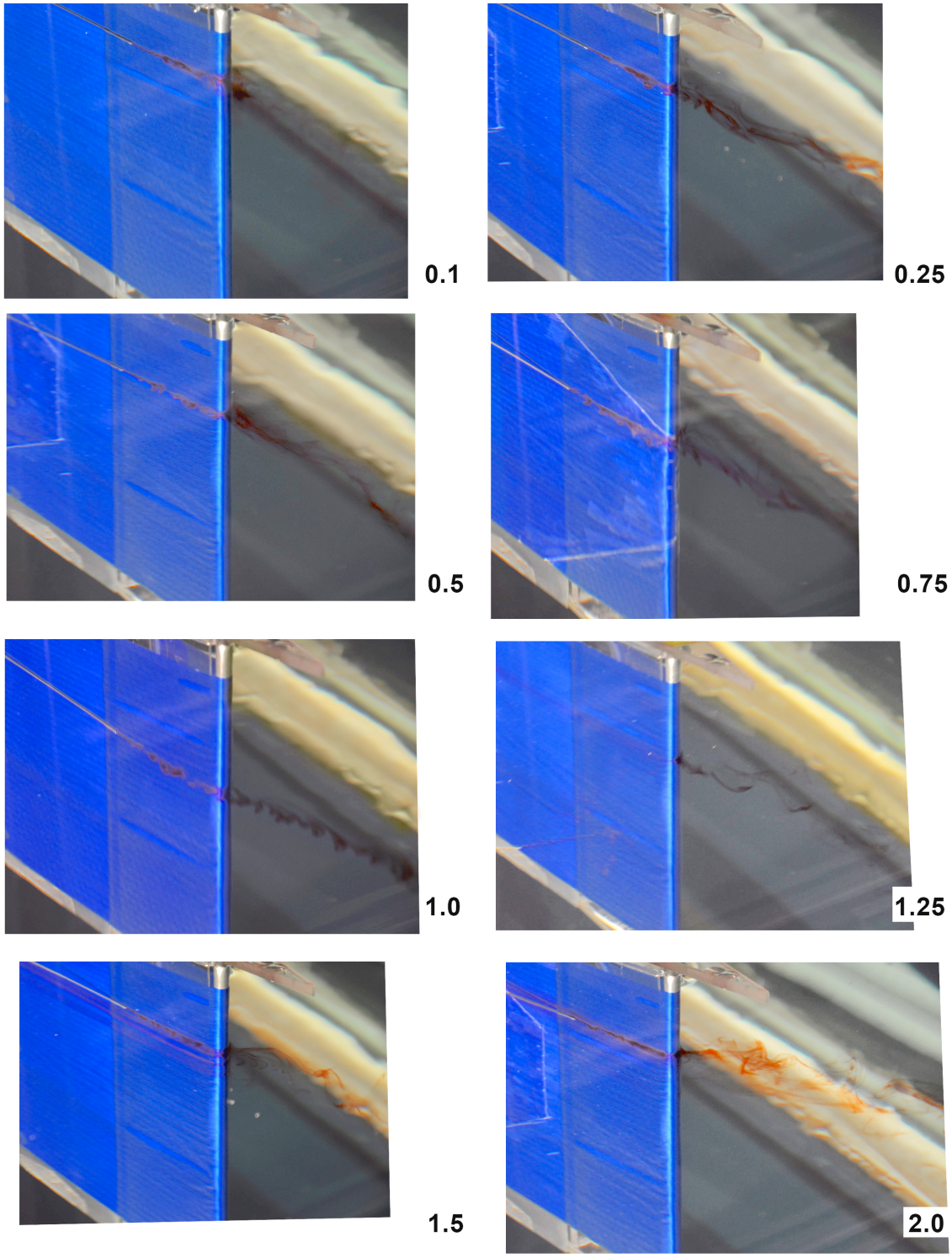

Figure 5.4: Water Tunnel Images. Zero degrees α, Configuration 1

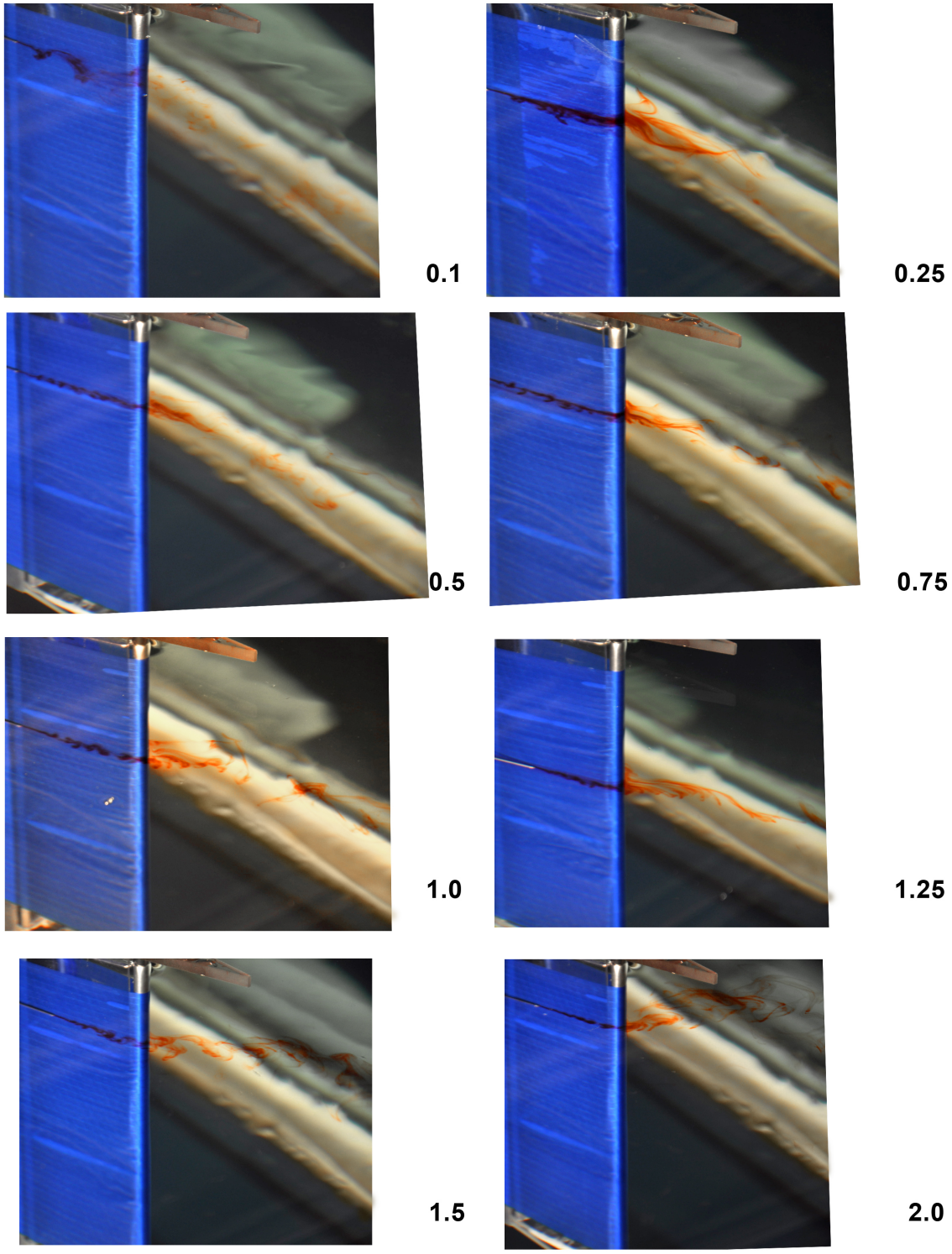

Figure 5.5: Water Tunnel Images. Six degrees α, Configuration 1

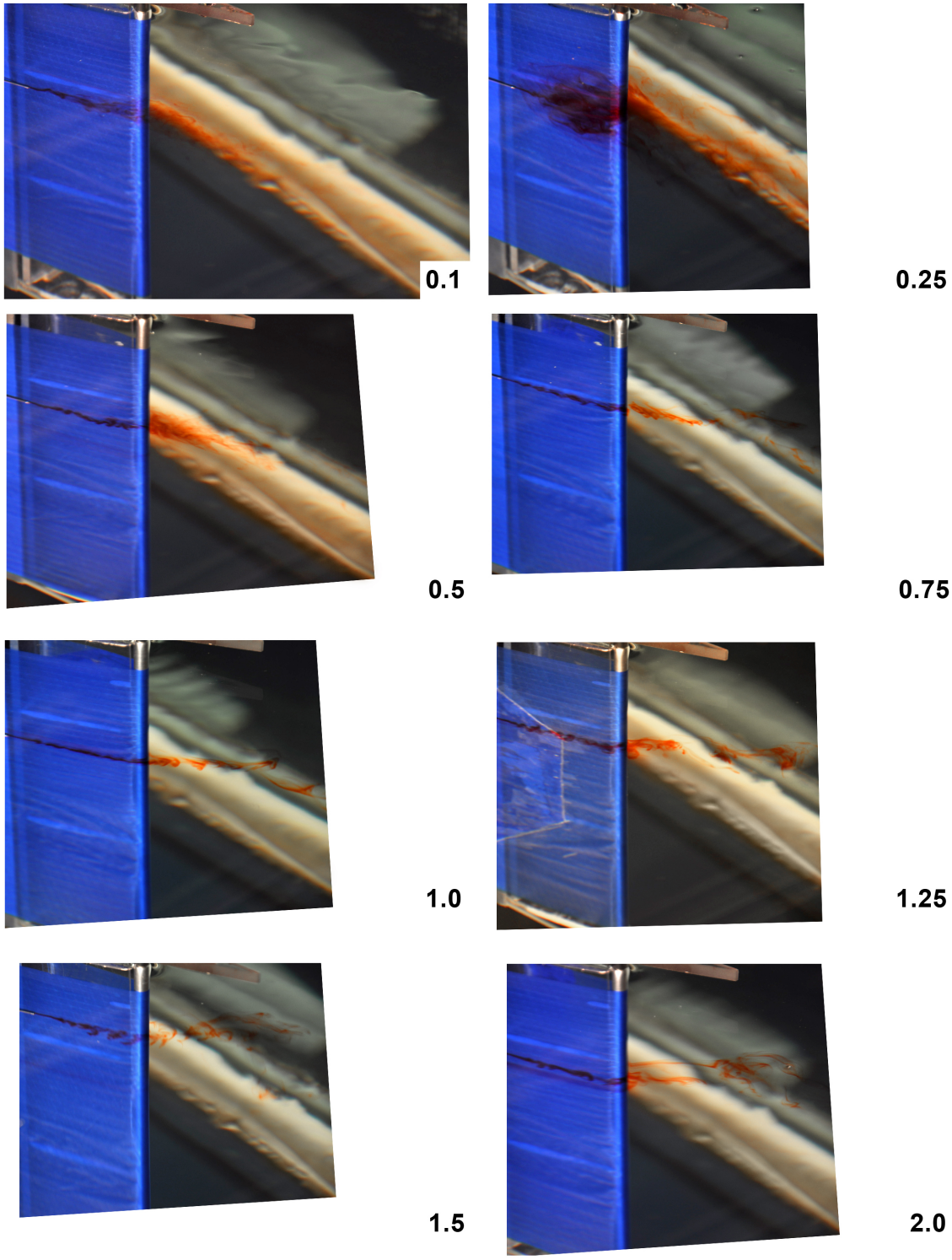

Figure 5.6: Water Tunnel Images. Eleven degrees α, Configuration 1

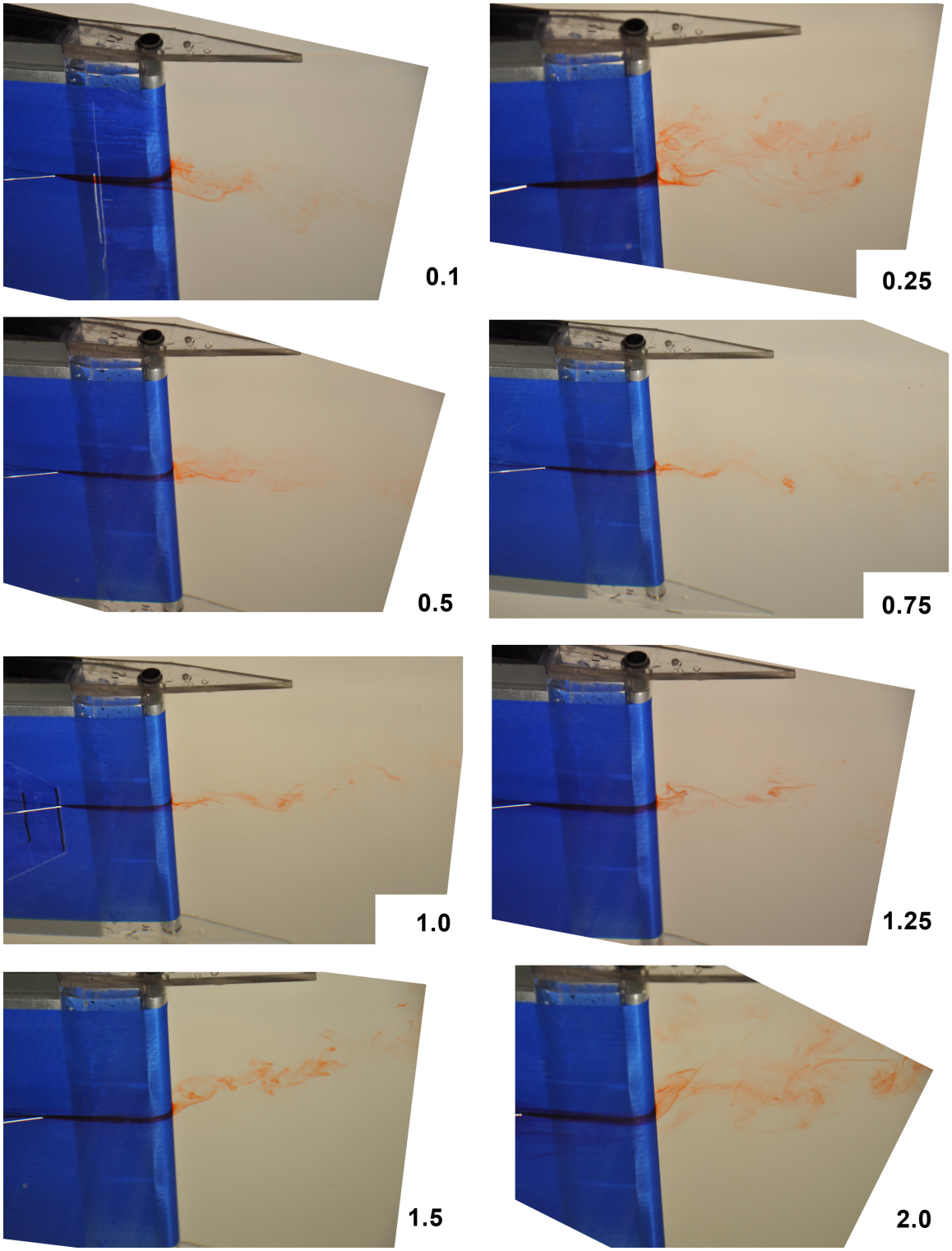

Figure 5.7: Water Tunnel Images. Zero degrees α, Upper, Configuration 2

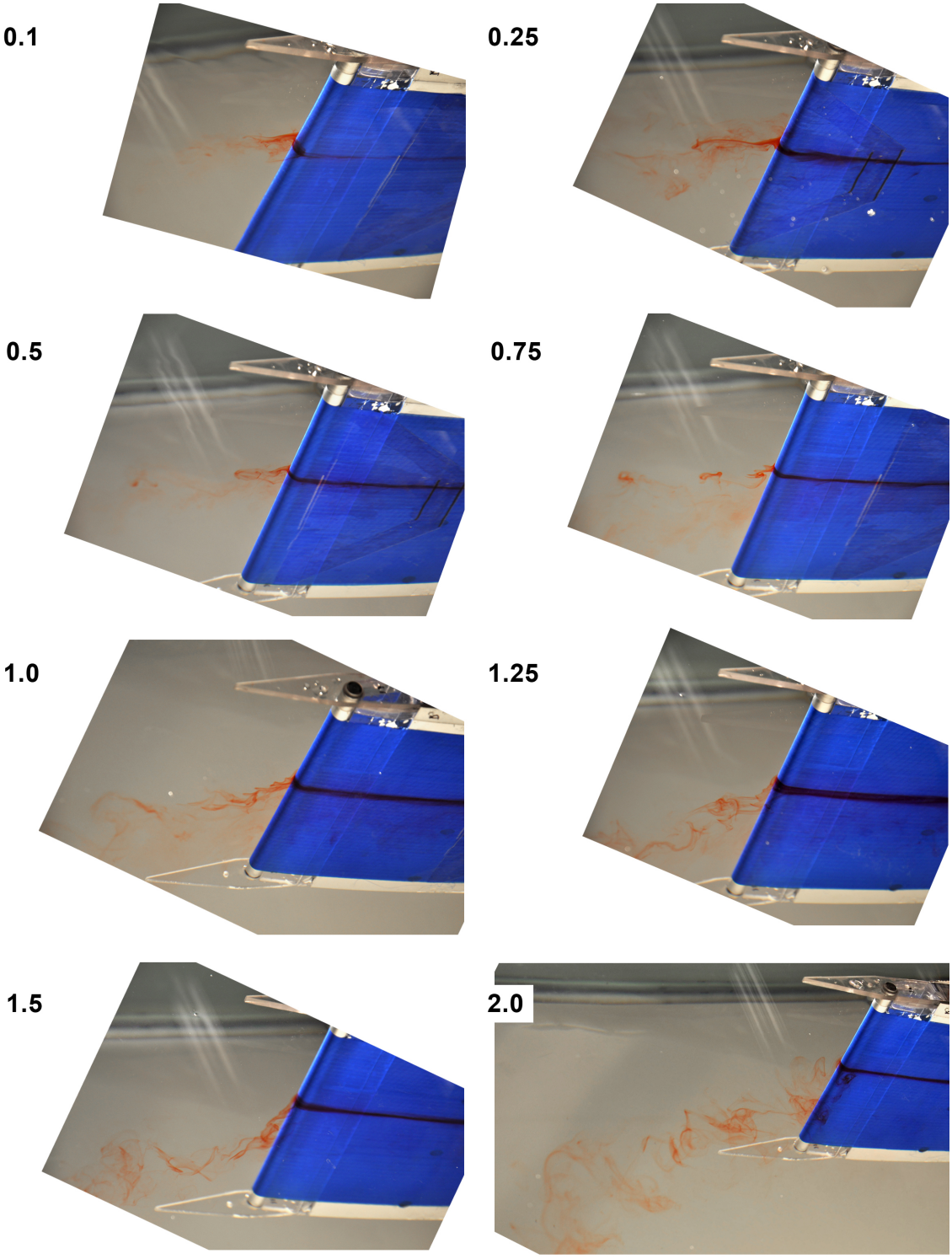

Figure 5.8: Water Tunnel Images. Zero degrees α, Lower, Configuration 2

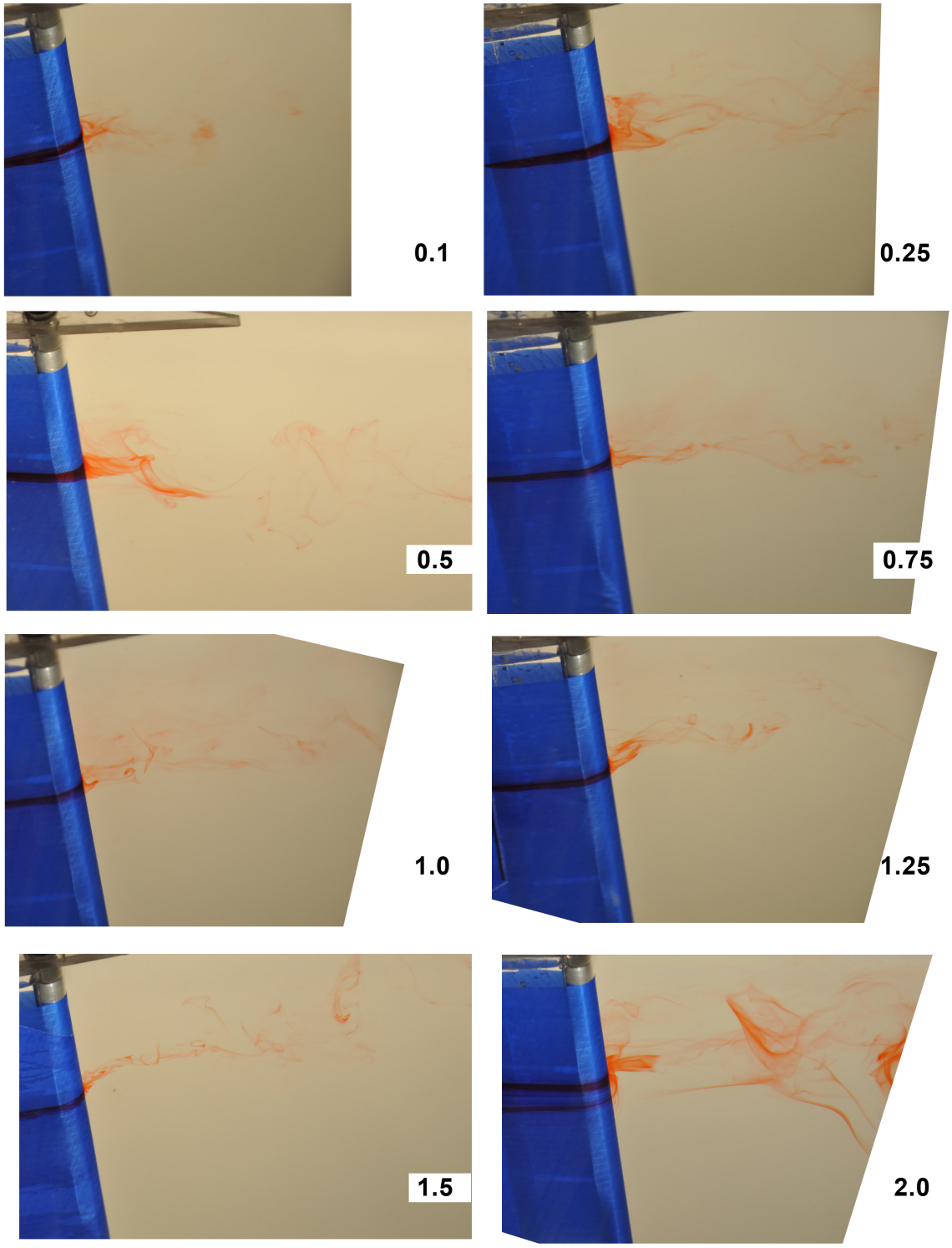

Figure 5.9: Water Tunnel Images. Five degrees α, Upper, Configuration 2

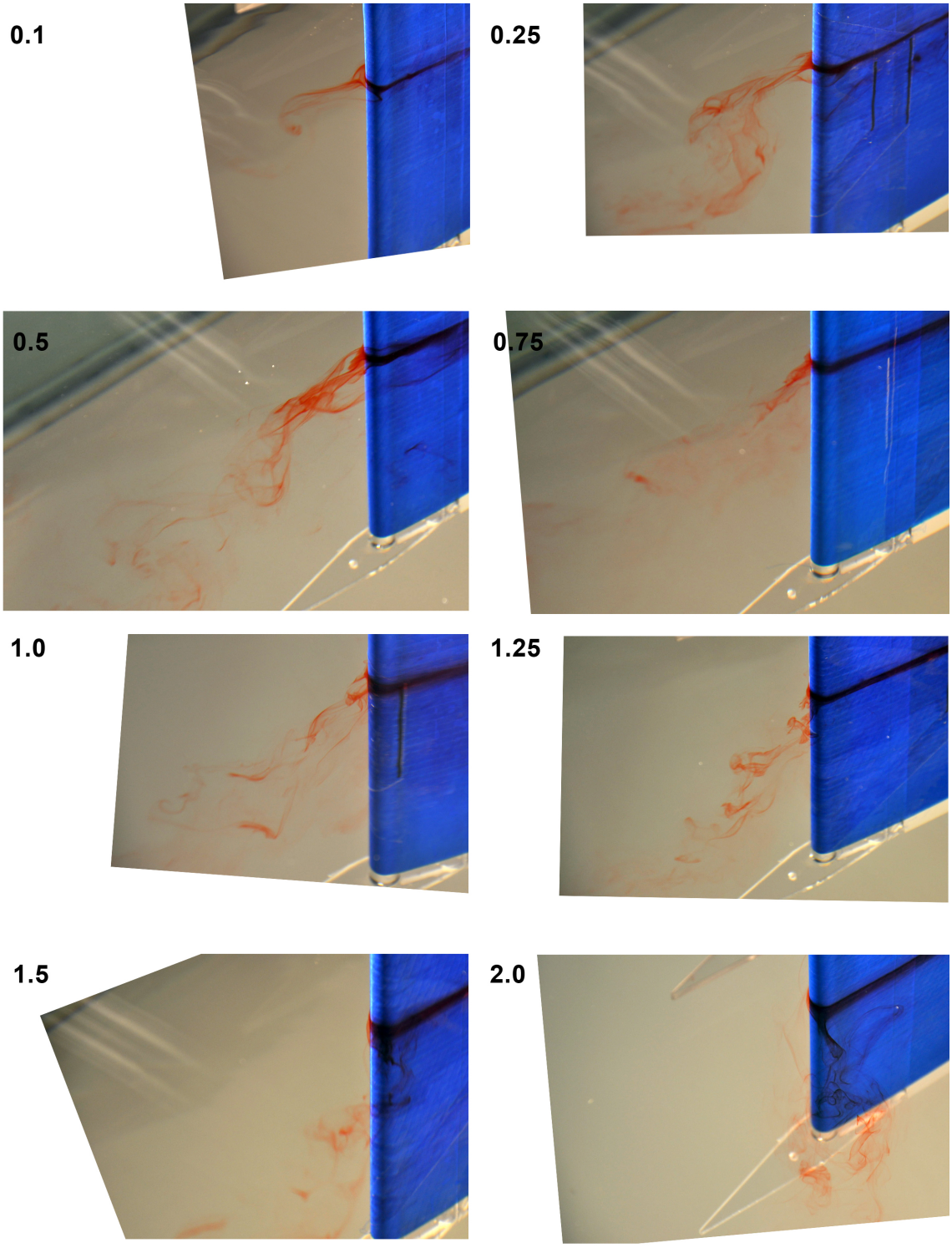

Figure 5.10: Water Tunnel Images. Five degrees α, Lower, Configuration 2

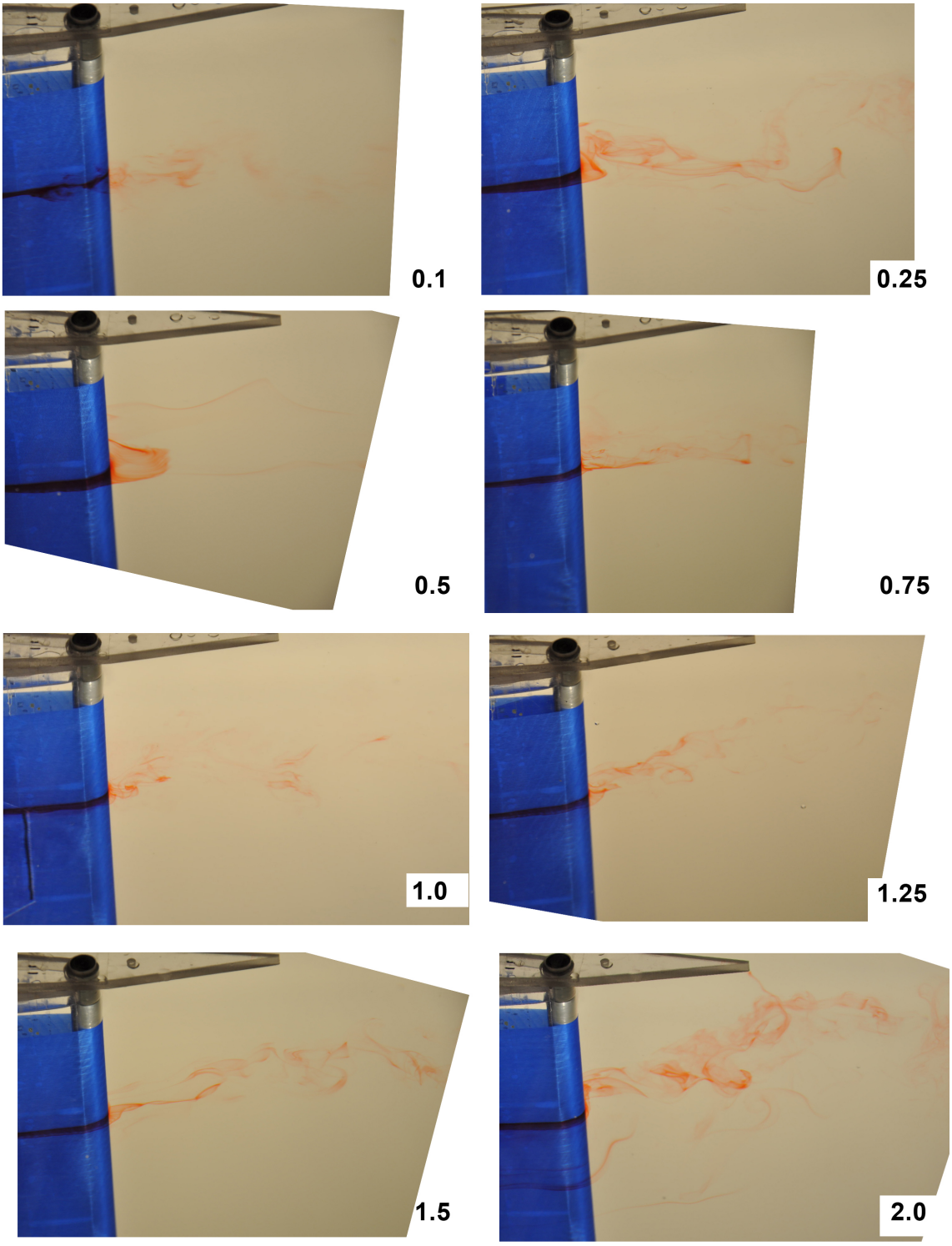

Figure 5.11: Water Tunnel Images. Ten degrees α, Upper, Configuration 2

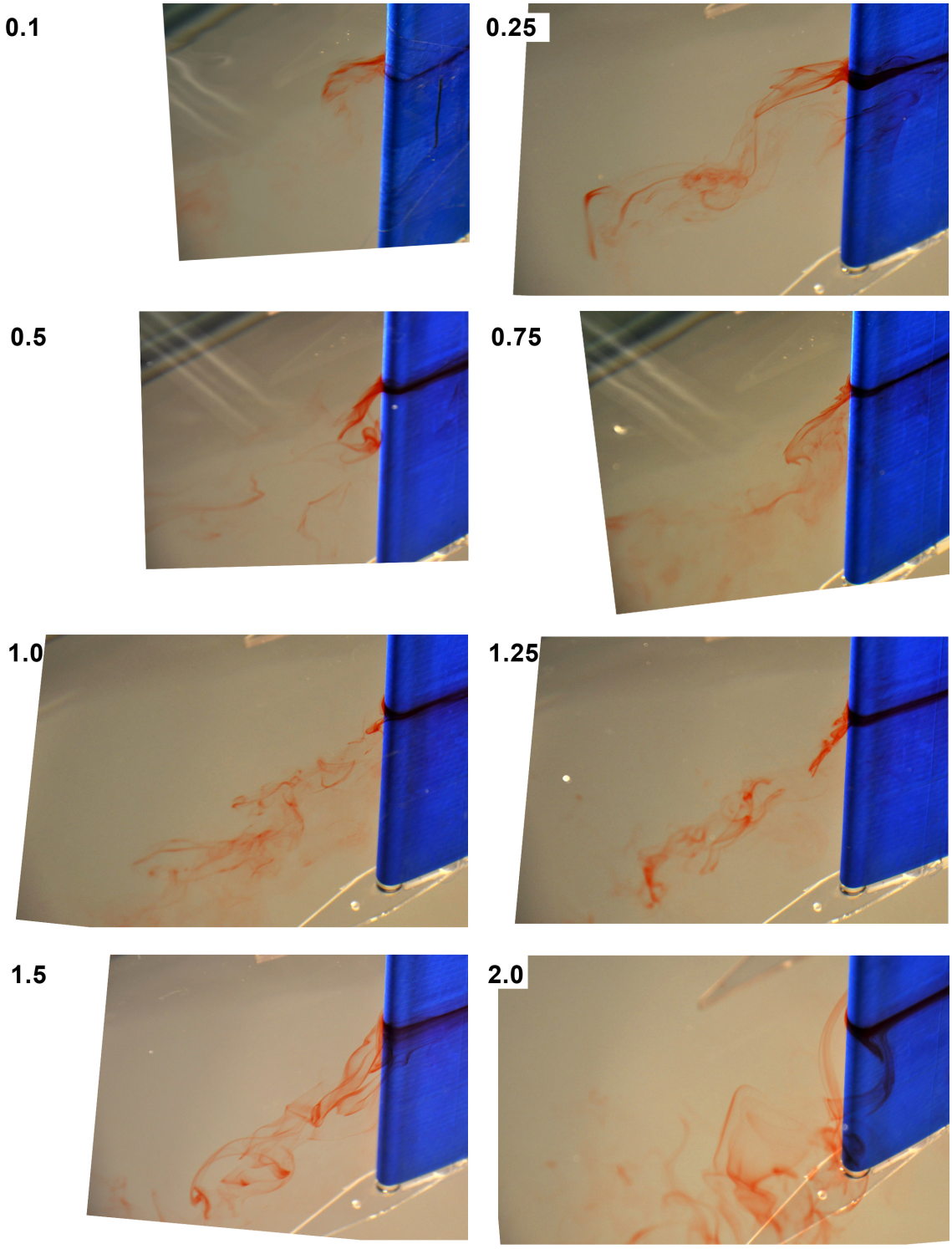

Figure 5.12: Water Tunnel Images. Ten degrees α, Lower, Configuration 2

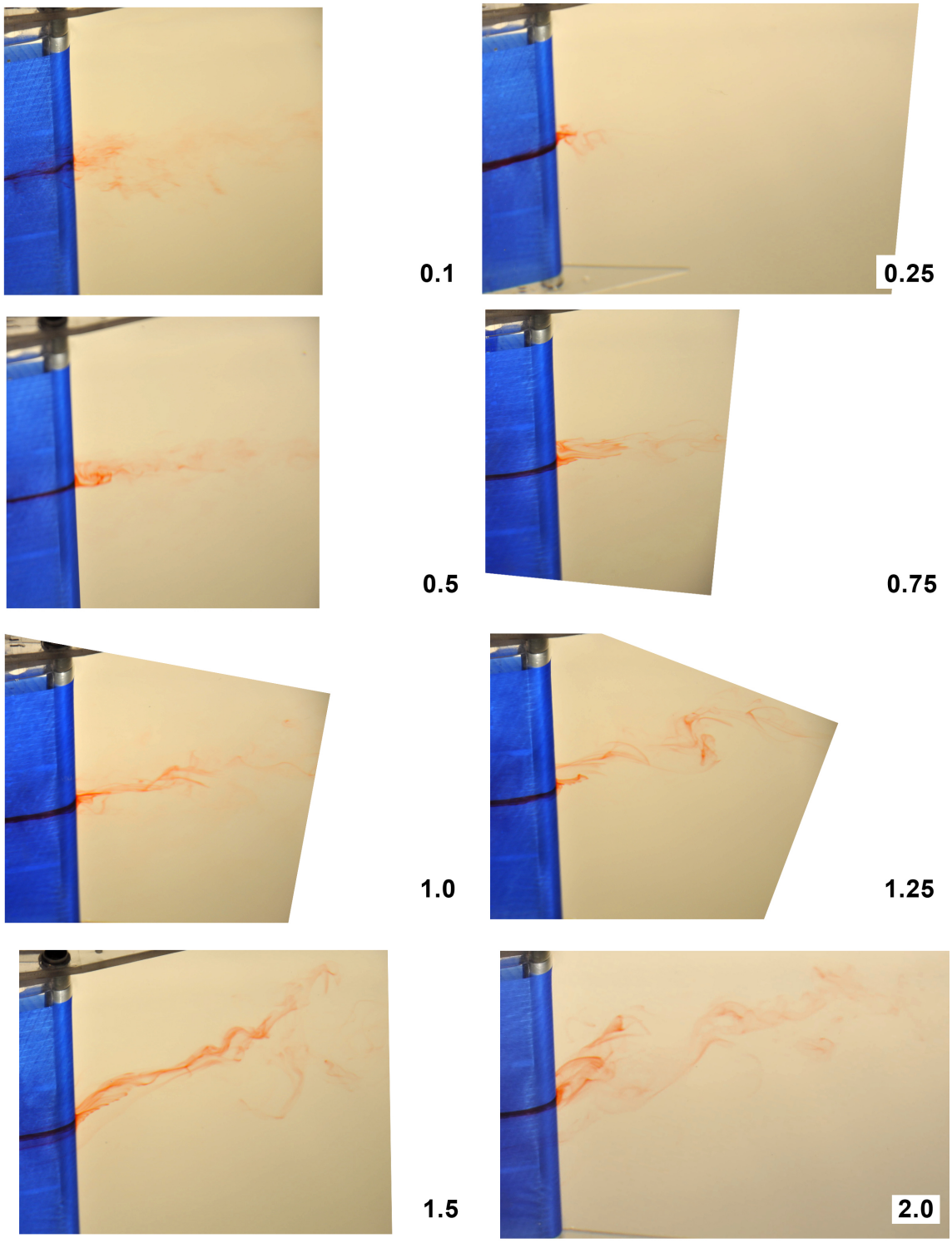

Figure 5.13: Water Tunnel Images. Twenty degrees α, Upper, Configuration 2

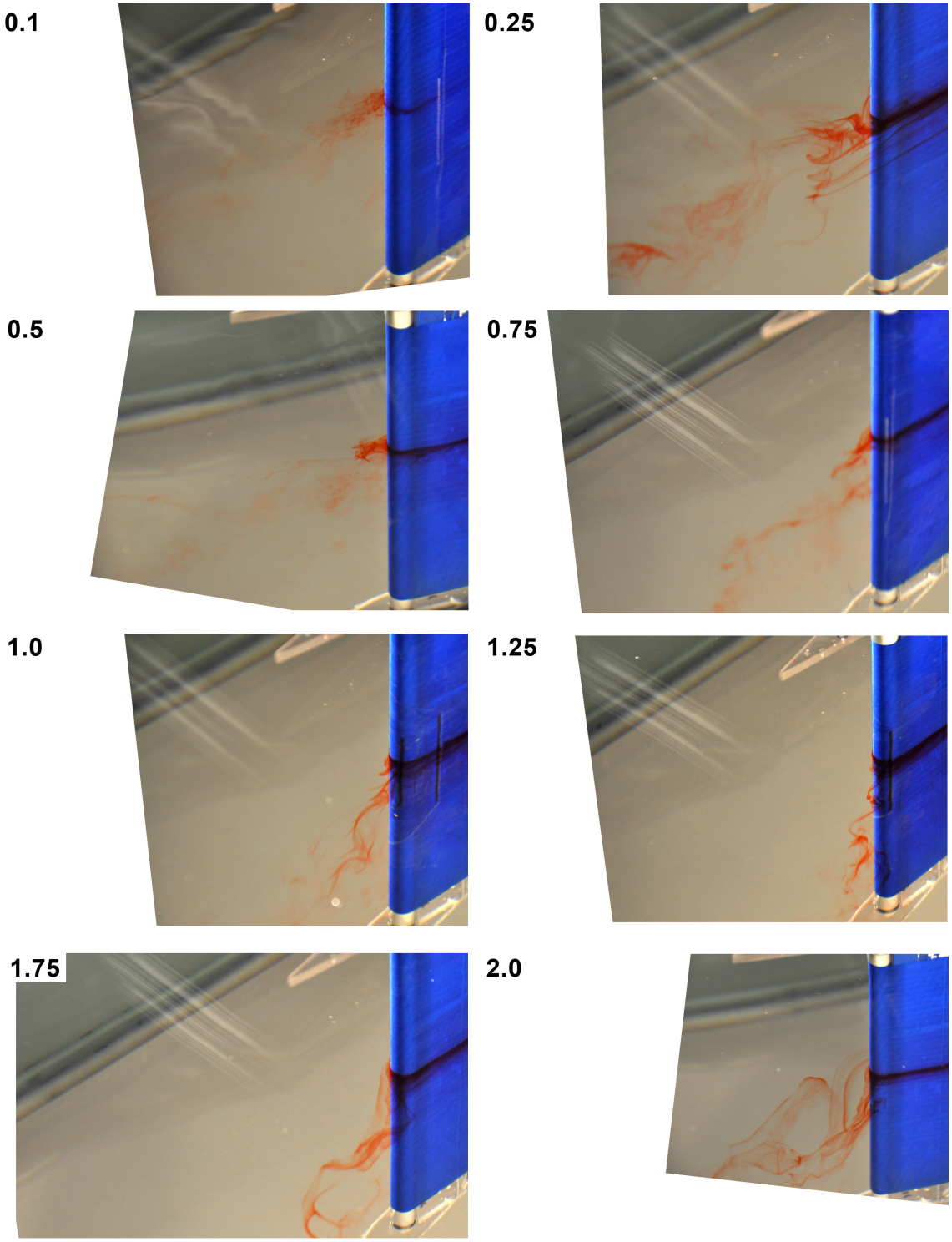

Figure 5.14: Water Tunnel Images. Twenty degrees α, Lower, Configuration 2

Chapter 6
WIND TUNNEL EXPERIMENTS

6.1 Objectives

Wind tunnel testing was conducted to measure the aerodynamic forces on a finite wing with a moving surface system. Tests were mostly performed at a dynamic pressure of $q = 1$ psf, corresponding to a Reynolds number of 1.9×10^5, based upon the nominal airfoil chord of 30.48 cm (12-inches). At that dynamic pressure, a velocity ratio of one required the moving surface to traverse at 8.9 m/s; test were conducted with the moving surface velocity ratio up to $u_s/U_o = 1.5$. Tests were also conducted on the bare wing and with only leading edge cylinders rotating at dynamic pressures up to $q = 20$ psf, corresponding to Reynolds Numbers up to 8.6×10^5.

Baseline tests were conducted with a wing that had aspect ratio of 5. Wings with aspect ratios of 7 and 9 were also tested, the later representative of Tier-1 UAV systems. These configurations will be referred to as AR-5, AR-7, and AR-9 henceforth. Two trailing edge configurations were tested on the AR-5 wing: one with a trailing edge idling cylinder diameter of 6.3 mm (0.25-inch) and one of 12.6 mm (0.5-inch). Although these trailing edge configurations had the same geometry as those tested in the water tunnel, the trailing edges were physically different models. The wind tunnel test matrix is shown in Table 6.1.

6.2 Experimental Set-Up

6.2.1 Facility

Wind tunnel tests were conducted at the University of Washington Aeronautical Laboratory's (UWAL) Kirsten Wind Tunnel. The Kirsten Wind Tunnel is a double-return, closed circuit wind tunnel with a rectangular test section that is eight feet tall, twelve feet wide, and ten

Test Conditions						
q	u_c/U_o					
(psf)	0	0.1	0.25	0.5	1.0	1.5
AR-5, Bare Wing						
1	•					
5	•					
10	•					
20	•					
AR-5, Leading Edge Cylinders						
1			•	•	•	•
5		•	•	•		
10		•	•	•		
AR-5, Moving Surfaces						
1	•	•	•	•	•	•
5	•					
10	•					
20	•					
AR-5, Alternate Trailing Edge						
1	•		•	•		
AR-5, End Plates						
1				•	•	
AR-7						
1	•		•	•		
AR-9, Inner Belts						
1	•		•	•	•	•
5	•	•	•	•		
AR-9, Full Belts						
1	•	•				

Table 6.1: Wind Tunnel Moving Surface Test Matrix

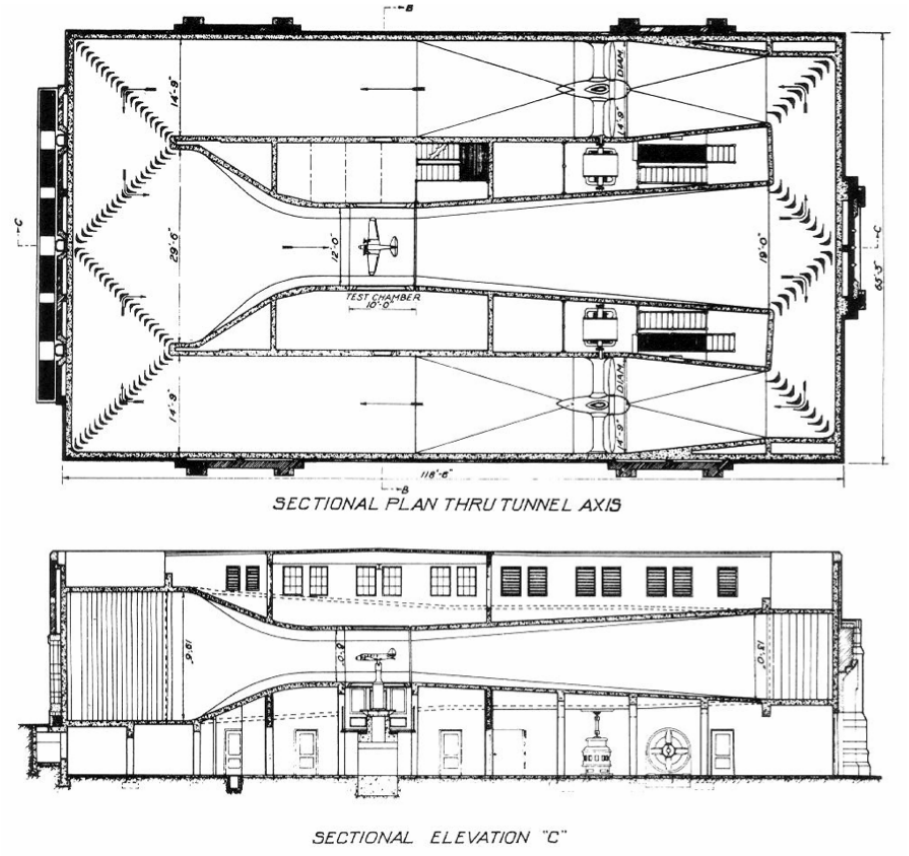

Figure 6.1: UWAL Kirsten Wind Tunnel

feet long with 45 degree, 1.5-foot filleted corners and vented to the atmosphere, Figure 6.1. The wind tunnel's two 14-foot, 9-inch diameter, seven blade, fans are each powered by a 500 hp DC motor, which can produce over 200 mph air speed in the test section. For this study, peak test conditions were 128 mph. [71]

A six component external balance, located beneath the floor of the test section, simultaneously measured force and moment data in three axes. The forces were converted to voltages by electromagnetic potentiometers, which were amplified and converted to digital numbers in engineering units. All signals pass through a 1 Hz low-pass filter before being sent to the data acquisition computer. [71] Aerodynamic force data reduction was performed

using the standard UWAL customer data collection package and software. Classic wall corrections were applied to the data, with deltaw = 0.1115, 0.10843, and 0.11105 assigned by UWAL. Shindo's simplified blockage corrections were also applied based upon the test wing geometry as part of the data reduction performed by UWAL.

6.2.2 Test Model

The wind tunnel base model consisted of a finite wing with a constant chord, zero sweep, aspect ratio of 5, and a NACA 0015 symmetric airfoil. The center body fairing for the wing to wind tunnel mount served also a surrogate for the body of an aircraft.

The wing model was produced as an aluminum skin on spar architecture without ribs. Increasing the aspect ratio of the test model to seven and nine was accommodated by two sets of wing extensions. The wings were connected to a steel wingback that mounted to the Wind Tunnel balance through an articulating trunnion with the angle of attack set by a pitch arm. The model included an integrated moving surface belt system, with 1.9 cm (0.75-inch) diameter drive rollers at the leading edge, driven by brushless electric motors, and idling cylinders at the trailing edge. Each wing had its own moving surface system with independent motors and controls.

The center wing box section was 25.4 cm (10-inches) wide and root wing sections were 63.5 cm (25-inch) in span for the AR-5 configuration. Two sets of outboard wing sections each of 30.48 cm (12-inch) span were constructed to provide the AR-7 and AR-9 configurations. Wings tips were half bodies of revolution of the NACA 0015 airfoil, bolted on to the outer most face of the wing and provided an additional 4.6 cm (1.8-inches) of total span; the additional span of the wingtips was not included in the plan form dimensions.

The leading edge 19.05 mm (0.75-inch) diameter shaft, or cylinder, drove the moving surface aerodynamic belts with torque motors mounted internal to the center body structure. Power and control for the motors was provided by remote service through a 19.05 mm (0.75-inch) access shaft in the wind tunnel mounting strut.

The leading edge cylinders were constructed of 1.59 cm (5/8-inch nominal) diameter 6061

aluminum tubes, 27.4 cm (10.8-inches) long, with a 0.063-inch thick vulcanized silicon rubber coating. The cylinder coating was crowned to aid centering of the belts as they rotated with the outer three inches of the shaft tapered a total of 0.76 mm (0.030-inches); this is typical in conveyor belt systems and belt drive machinery. The remaining 3 cm (1.19-inch) of the 30.48 cm (12-inch) span wing sections accommodated axle bearings and drive couplings. The shaft sizes were held to less than one foot in length to avoid whirling frequencies at the rotational speeds of interest. The leading edge cylinder and axle assemblies were mounted within shaped Delrin blocks that made up the leading edge mounted to the wing's forward spar.

Trailing edge shafts were fabricated from simple aluminum tubing. The chord wise location of the shafts corresponded to the point where the airfoil surface would be tangent to the diameter of the shaft as shown in Figure 4.2. Since the trailing edge shafts were idling shafts, they were neither coated nor tapered. Both leading and trailing edge shafts used high-speed, low-profile, axle bearings.

6.2.3 Structural Design

The wind tunnel model's wing structure was designed and built in traditional wing-box architecture, with forward and aft spars and upper and lower skins making up a torque tube. The spars and skins were machined from 6061-aluminum, Figure 6.2. Steel shear ties between the spar sections transferred bending loads while a second set of steel shear ties transferred torsion through the skins. Unbrako, high-strength fasteners were used for all load-bearing connections. The fastener pitch between the skins and spars varied on the wing extensions, accommodating reduced torque at outward span locations. Based on the results of Favre and Modi, a conservative lift load factor of three was applied to nominal and extrapolated NACA 0015 coefficient of lift data, resulting in two primary structural design load cases for the model with total wing loading of 200 psf; 15-degrees angle of attack at $q = 40$ psf for the AR-7, and 45 degrees angle of attack at $q = 20$ psf for the AR-9. A limit load factor of 1.5 was applied to the maximum loads for design structural integrity purposes.

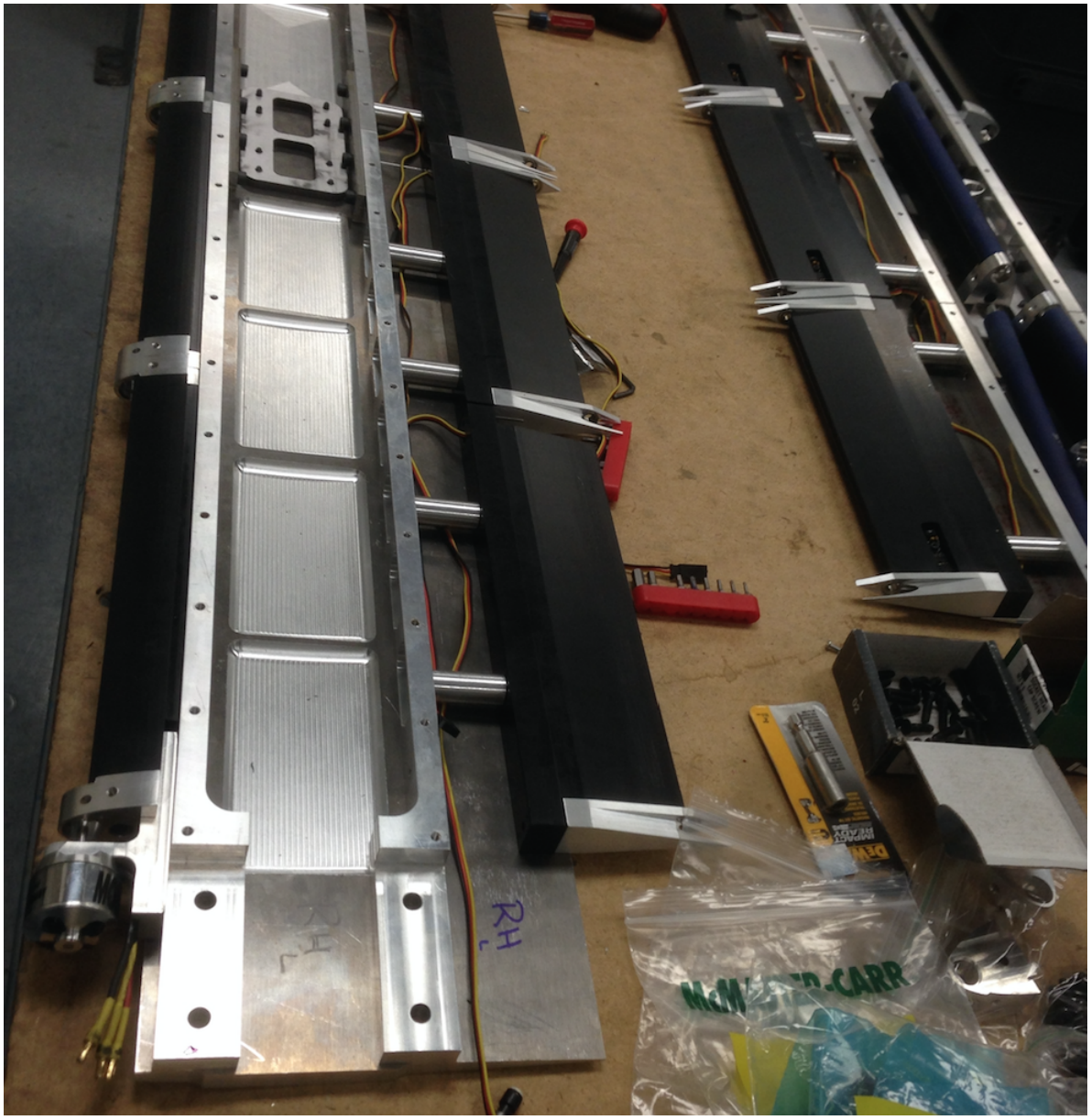

Figure 6.2: Wind Tunnel Model, Structure and Edges

With the center of pressure for symmetric airfoils is at the 1/4 chord location, the wing box was designed to resist aerodynamic induced moments due to the center of pressure, the resultant line of action of aero-forces on the airfoil section, being off-set from the wing box's neutral axis. The effective moment arm was 3.7 cm (1.46-inches) from the center of pressure. At higher angles of attack the center of pressure moves aft, this was disregarded.

6.2.4 Motors, Power, and Control

The moving surface belt drive system was designed and built using commercially available components and was built such that it could have been integrated into a flying system. The only functional difference between the test model and what could be integrated into a similar scale UAV was the electronic and power systems where the control of the belt speed was accomplished through a laptop computer and the batteries were replaced with laboratory power supplies. All of the associated circuitry, power, and controls, for each wing's motor, were set-up on the balance deck below the wind tunnel test section.

The 19 mm (0.75-inch) leading edge cylinders were driven from the wing root via direct drive, attached by vibration isolating couplings, to Grayson Hobby Monster Jet brushless motors rated for 2400 rpm/V. The motors had a maximum efficiency of 80% at 20-45 amps with a peak current capacity of 55 amps for 60 seconds. These motors are generally produced for RC aircraft jet drives and were selected for the their ability to provide adequate torque at 20,000 rpm.

The system batteries were replaced with separate power supplies for each wing system. One was a 20 V, 40 A system and the other 15 V, 60 A system; both systems were operated at a nominal 14.8 volts. The power supplies were connected directly to their motor Electronic Speed Control (ESC) as though they were batteries. Each motor used a Castle Creations Phoenix Edge 200 ESC that supports maximum continuous current up to 200 amps. The auxiliary port on the controllers were programmed to output encoding ticks from the motor providing feedback for Proportional-Integral-Differential (PID) controllers that were hosted on a dedicated Arduino Uno for each motor. The controllers were mounted to an external

heat sink.

Castle Creations Serial Links (CCSL) were configured for pass through mode, enabling both logging and control of each ESC. The i/o protocol used was I2C, the frequency was set at 400 kHz, and the ESC addresses were set at 8 and 71 for the two ESC's. Throttle control for the motors was based upon a 16 bit Pulse Position Modulation (PPM) signal, with 0 corresponding to a 1 ms, 0%, throttle setting and 65,535 to a 2 ms, 100%, throttle setting. These signals were generated by the micro-controllers on the dedicated Arduino Uno for each motor circuit. The result maintained constant motor speed to within +/- 70 counts. ESC data was logged with Castle Link V3.56.17. Unfortunately, there was no system or universal time stamp for the data logs, so care was needed in handling and saving the log files. The serial link was powered through the ESC's Battery Elimination Circuit (BEC).

The motor control and drive system maintained constant motor speed, and therefore leading edge cylinder rotational speed. However, the parameter of interest was primarily the tangential speed of the belt itself. The belt drive was a friction drive system, relying on friction between the belt and the drive cylinder/roller to transmit motion to the belt. Unfortunately, the belt could slip on the drive roller under some test conditions, which was visibly apparent. The speed of the belts were, nominally, monitored by Parallax QTI Line Sensors, #550-27401, infrared sensors embedded into the lower side of the trailing edge. A simple timing circuit was implemented on Arduino Mega 2560 allowing for a total of 8 timing circuits. Encoders were vinyl strips (electrical tape) that were opaque to the infrared sensors and secured under the chevron flap of the belt.

Belts were fabricated for the 6.3 mm (0.25-inch) trailing edge configurations from 1.1-ounce rip-stop nylon fabric. These belts were pre-made and sewn with sealed seams. The inside circumference of the belts was 60.3 cm (23.75-inches). The flat patterns had chevron shaped leading edges to minimize the material cross section of the seams as the belts traversed the shafts; the pointed side was in the direction of the belt travel. Belts for the 12.6 mm (0.5-inch) trailing edge tests were fabricated on site by gluing the belts using the wing as a mandrel, the same method employed for the water tunnel belts. These belts were made

from 0.65 oz. polyester sailcloth, which was lighter but stiffer than the rip-stop nylon. The chevron design was also employed but encoder strips were not. For tests with these belts the belt speed was set or verified by use of a stroboscope.

6.2.5 Trailing Edges

Trailing edge cylinders were mounted in trailing edge body sections that consisted of an aft spar body section secured to the aft spars with a set of standoffs. Free to mechanically float, the body sections were not subject to the twisting or bending of the main wing structure. Axle bearings were housed in floating axle plates with tapered chord extensions sized to provide adequate races for the high-speed bearings. Each of the axle housings had a spring tensioning mechanism to provide minor amounts of tension in the belts via adjustable lead screws that were set independently. Two sets of trailing edge assemblies were constructed, one for each trailing edge cylinder diameter, due to the different chord wise location of the trailing edge cylinder.

The wind tunnel model was mounted to the UWAL Single Strut using the small trunnion with 25.4 mm (1-inch) pins along with the 17.2 pitch arm set at a radius of 12.7 cm (5-inch). To cover the trunnion block and pitch arm mounts, as well as to provide shielding for the motors, a center body was designed that consisted of an NACA 0015 upper surface with the chord extended to 45.72 cm (18-inch) along with a lower surface that maximized to an NACA 0018 for the span of the trunnion ears. Both upper and lower surfaces transitioned to the standard 30.48 cm (12-inch) chord NACA 0015 airfoil section. Wing tips, trailing edge aft bodies, and the model center body were machined from black Delrin; all other components were made from aluminum.

Airspeed Reference Values			
q	Air Speed		Reynolds
(psf)	(mph)	(m/s)	Number
1	20	8.94	1.9×10^5
5	44.7	19.98	4.3×10^5
10	63.2	28.25	6.12×10^5
20	89.5	40.01	8.67×10^5

Table 6.2: Dynamic Pressure, Airspeeds, and Reynolds Number

6.3 Test Summary

6.3.1 Test Plan

Wind Tunnel testing comprised of a series of test sequences, each consisted of a set of test runs for a specific configuration. Within each series, subsequent test runs would alter another parameter, primarily the velocity ratio. For non-moving system tests this it was usually the mean stream velocity. Each test run consisted of a sweep of the wingś angle of attack at a set airspeed. The bulk of the testing was performed with the AR-5 wing fitted with the 6 mm diameter trailing edge cylinder, which served as the general reference for the AR-7 and AR-9 wing configurations. Test sequences were conducted with bare wings with no moving surface, with only the leading edge cylinders rotating, and with the belt based moving surface system. The belt based moving surface system was tested at dynamic pressures of $q = 1$ and $q = 5$ while other testing was conducted up to $q = 20$. Velocity ratios, u_b/U_o, tested were: 0.1, 0.25, 0.5, 1.0, and 1.5. The belt based moving surface system was not able to meet all the speed ratios under all test conditions.

For reference, Table 6.2 the dynamic pressures, with equivalent air speeds, and test Reynolds numbers upon a nominal chord of 30.48 cm (12-inch) and air properties of $1.41 \times 10^{-5}\, m^2/s$ for kinematic viscosity and nominal density of $1.2\, kg/m^3$:

Three standard aerodynamic plots are presented for assessing the effectiveness and characteristics of the moving surface system. The first is the standard coefficient of lift, C_L, versus the angle of attack, alpha. The lift coefficient serves as a direct analog for the total circulation $L = \rho_\infty V_\infty \Gamma$. The second is the ratio of Lift to Drag (L/D) versus the angle of attack, which provides a measure of aerodynamic efficiency and is a useful relationship for airplane performance calculations. [7] The final plot is the endurance parameter $C_L^{3/2}/C_D$ versus the coefficient of lift used to assess endurance and lift.

6.3.2 Test Procedure

Execution of individual test runs was relatively straightforward. Each day's testing sequences and parameters would be established to minimize the amount of time required to reconfigure the test model. Due to the construction and assembly of the wing extensions, it was more efficient to build up and test the AR-9 wing before the AR-7.

Once the test model was in the established configuration, all gaps and seams in the model were sealed with blue Mylar (polyethylene terephthalate) tape. Counter-bores for the heads of the structural fasteners in the wing skins and center body were covered with aluminum dots. For the moving surface tests, the system would be given a checkout to ensure it was operating nominally before the wind tunnel test section was secured and the wind was turned on. Motors were set to predefined speeds and the belt response checked either by encoder or stroboscope, once the system was ready, data collection logging would be initiated. Tuning the tension of the belt to establish proper belt speed was done by carefully adjusting the rear axle mounts. If the tension were too low, the belts would slip and if tension were too high the motors would start to draw excessive amounts of current.

With the model ready, the wind tunnel test section airflow would be established with the test model at a zero degree angle of attack. Once the wind speed reached a stable value, the model would be moved to negative 9 degrees angle of attack and the test run would begin. Force data was collected and the model was transitioned to a new angle of attack. The angle of attack ranged from negative 9 to positive 33 degrees, referred to as an alpha sweep, in

3-degree increments.

Wind tunnel results are discussed beginning with the AR-5 wing based upon the model configurations that include no belts, leading edge cylinders only, belts not actuated, belts actuated, and with the alternate trailing edge. The results of the AR-7 and AR-9 configurations are then discussed. As noted above, the execution of the tests did not proceed in that order. In the discussion, the angle of attack values mentioned are the nominal test values, the exact values as measured by the UWAL position sensors would vary up to 0.5-degrees, although they were typically between 0.18 and 0.34-degrees and consistently above the set value. The data collected and post processed by UWAL is provided in Appendix A for all the test runs discussed in this dissertation and several that were not but might be of interest, for example the center-body alone.

6.4 Additional Notes

A couple of technical concerns arose during test that warrant brief mention.

The intent had been to record power consumption for the motors and the speed of the belts during each of the test runs. During the execution of the tests, these parameters were continually monitored, however the data that was recorded was of poor quality and will not be reviewed.

For power, inappropriately configured speed controller data recording left only data recorded manually available for early test runs. A further complication arose due to the fact that the speed controller did not time stamp the data that it logged. That this was a regret was not immediately apparent. During testing, pre-test system checks resulted in relatively large data logs. With multiple spin-ups of the system the long data records were were difficult to correlate with the test points. Through careful analysis of the available data, the the data in Table 6.3 presents the nominal power consumption for the system, per wing when the belt system was operating properly. This data can only be viewed as general in nature. The range of belt data is for two belts in both the AR-5 and AR-9 inner belt configurations.

Nominal Current Draw in Amps			
u_s/U_o (reference motor speed)			
$0.25(2300rpm)$	$0.5(4500rpm)$	$1.0(9000rpm)$	$1.5(13,600rpm)$
Cylinders			
0.7	1	1.8	2.3
Moving Surface Belts			
5 to 6	7.5 to 9	14 to 20	21 to 27

Table 6.3: Power Consumption in Amps for nominal, reference conditions.

Another concern, which also had a large effect on power consumption, had to do with the performance of the belts. When the belts operated smoothly, as intended, power consumption was relatively modest and fell into the range indicated in the table. When the belts performed poorly, power consumption could become excessive.

One of two failure modes for the belts were observed. The first was a lack of sufficient tension in the belt to maintain the set speed. This could allow the belts to slip and didn't increase power consumption. Motor speed set points were adjusted above the nominal values as needed to keep the belt speeds within about 10% of the desired value. Over tensioning the belts would result in excessive power consumption. A stroboscope was employed as a check on the operation of the belts before each test once the encoder data was deemed unreliable.

The second failure mode was when the belts failed to remain centered, either due to having stretched or having been tensioned in an imbalanced manner. When the belts deviated too far, the free edge could gather at the axles and bind the drive system; massive spikes in current would result, several of these events led to a power supply fault. Further when the belts would deviate in their path the encoder strip embedded in the belt would fail to register with the optical sensor.

All of the operational issues with respect to belt speed and motor power inconsistencies would have been alleviated with a positive drive mechanism were the belt was mechanically

driven by the motor using a system akin to a gear drive and toothed belt. In all 104 test runs were conducted over five days of wind tunnel testing, the results of 48 of those tests are reported on here.

Chapter 7

ASPECT RATIO 5, BARE WING

As a reference, the AR-5 wing planform in a bare configuration was tested fitted with the smaller diameter trailing edge cylinder. Both the leading edge and trailing edge cylinders gaps were sealed with Mylar tape and the moving surface belts were not installed. Figure 7.1 shows the model in the wind tunnel. Angle of attack sweeps were conducted starting with a dynamic pressure of $q = 1$ psf, increasing in subsequent tests to $q = 5$, 10, and finally 20 psf. Peak values for each test run are provided in Table 7. Figure 7 shows the Coefficient of Lift, C_L, versus angle of attack for the set of q tested.

At $q = 1$, the peak C_L of 0.672 occurs at an angle of attack of 12-degrees and by 15-degrees, the wing has stalled. As q increases to 5 psf, the peak C_L increases to 0.734 at 12-degrees angle of attack. A further increase of q to 10 psf shows a similar C_L of 0.745 at 12-degrees angle of attack, but the peak C_L of 0.765 occurs at an angle of attack of 15-degrees. At $q = 20$, the same trend is observed with $C_L = 0.744$ at 12-degrees angle of

AR-5, $u_b/U_\infty = 0$			
q	C_L	$C_L^{3/2}/C_D$	L/D
1	0.672	7.97	10.84
5	0.734	9.94	13.4
10	0.765	10.71	15.31
20	0.831	10.79	14.79

Table 7.1: Aspect Ratio 5, Base Wing

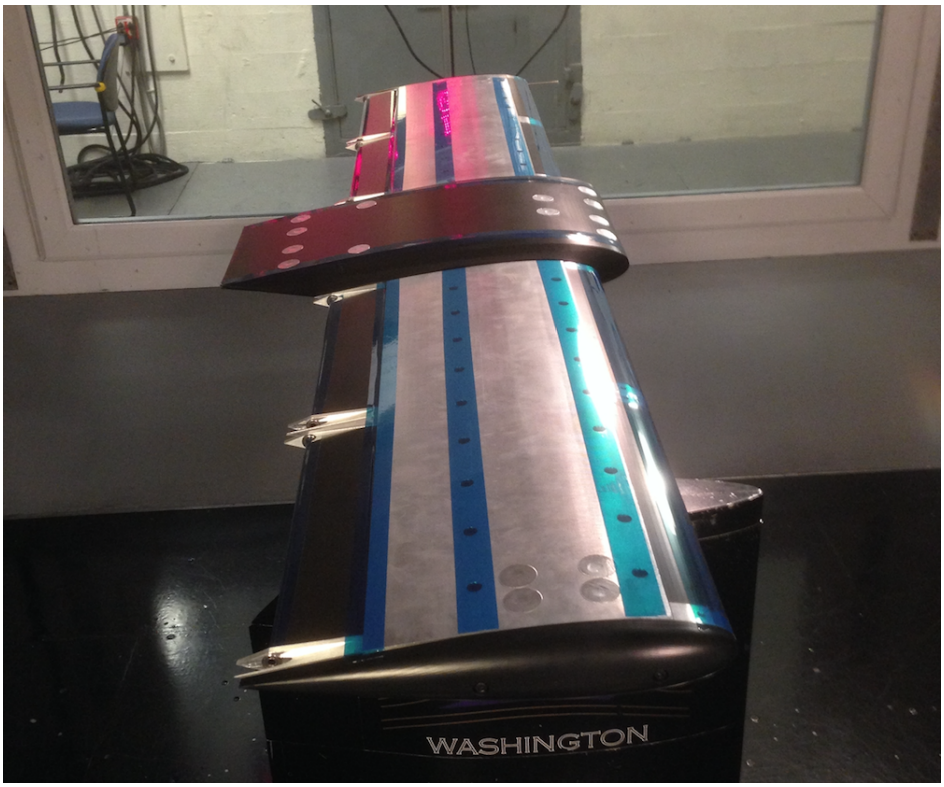

Figure 7.1: AR-5 Wing, Bare

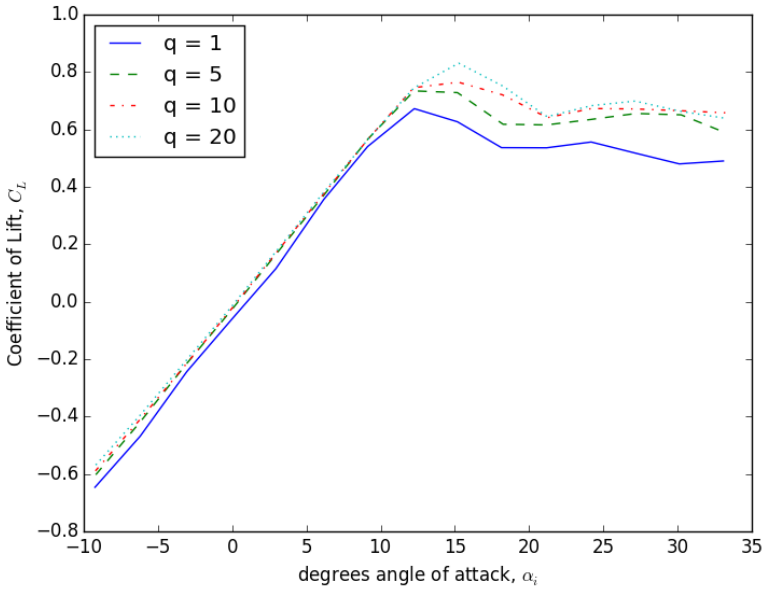

Figure 7.2: Base Wing, Lift Coefficient, Aspect Ratio 5

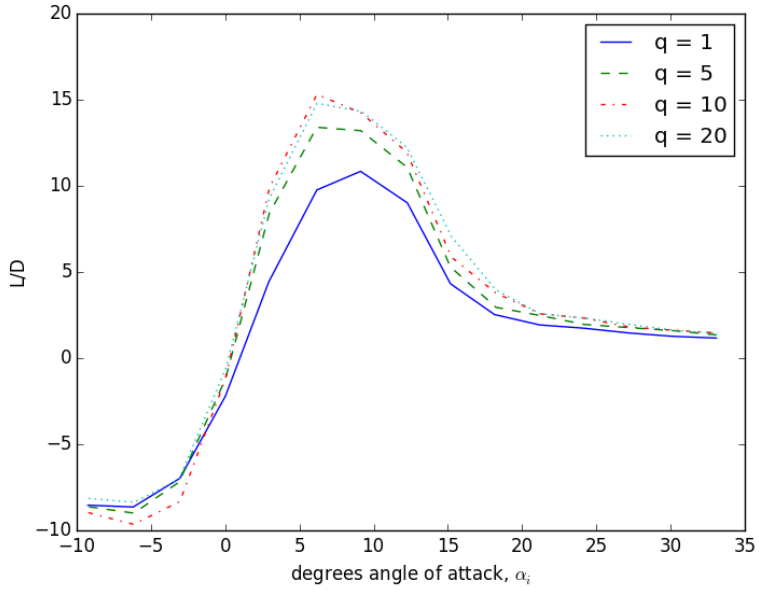

Figure 7.3: Base Wing, L/D, Aspect Ratio 5

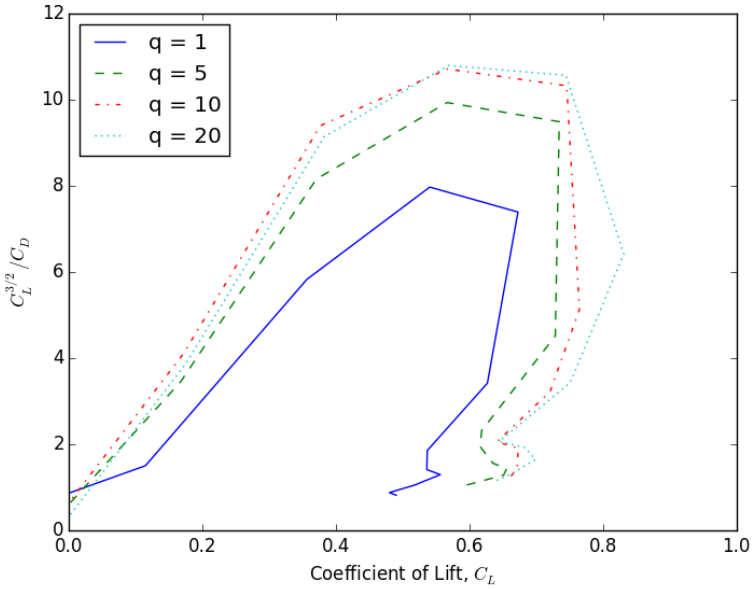

Figure 7.4: Base Wing, Endurance Parameter, Aspect Ratio 5

attack and $C_L = 0.831$ at 15-degrees angle of attack.[1] The slope of the C_L curve, in the linear region, flattens slightly with increasing q. Starting with C_L/degree $\alpha = 0.0658$ at $q = 1$, the lift slope progressively decreases to 0.0642 at $q = 5$, to 0.0635 at $q = 10$, and 0.0626 at $q = 20$. The C_L curve for the $q = 1$ case is offset slightly downward from the other curves, which largely overlay each other in the linear region.

Figure 7 shows the Lift over Drag (L/D) ratio versus the angle of attack for each run, where it can be seen that by an angle of attack of 12-degrees the wing has started to lose aerodynamic efficiency and beyond an angle of attack of 15-degrees has effectively stalled for all cases. The peak L/D for $q = 1$ occurs at an angle of attack of 9-degrees while all other dynamic pressures it occurs at 6-degrees. Peak L/D values increase by 24% between $q = 1$ and $q = 5$, and another 14% at $q = 10$. This trend starts to reverse with a 3% drop at $q = 20$.

[1] At $q = 40$ psf, the peak C_L is 0.819 measured at 15-degrees angle of attack, data is not discussed here, but is provided in Appendix A.

Figure 7 shows the endurance parameter $C_L^{3/2}/C_D$ vs C_L for the base configuration. At the baseline airspeed, $q = 1$, $C_L^{3/2}/C_D = 7.97$ with $C_L = 0.540$ at an angle of attack of 9-degrees. This decreases slightly to 7.39 with a C_L of 0.672 at an angle of attack of 12-degrees. The stalling behavior at 15-degrees angle of attack can also be seen by the sharp decrease in the curve. Increasing q to 5 psf, a dramatic increase of $C_L^{3/2}/C_D$ to 9.94 is observed with C_L= 0.566, again at 9-degrees angle of attack, this decreases to 9.49 with $C_L = 0.734$ at 12-degrees. Increasing the airspeed beyond $q = 10$ psf had only minor effect. The data show similar values of $C_L^{3/2}/C_D$ for both $q = 10$ and $q = 20$, with corresponding C_L values of approximately 0.57 at 9-degrees angle of attack and 0.74 at 12-degrees.

Chapter 8

LEADING EDGE CYLINDERS

A series of tests were conducted with only the leading edge cylinders employed as the moving surface. The trailing edge cylinder was sealed identically in the same manner as the bare airfoil. The leading edge cylinder tests largely replicate the leading edge cylinder experiments of earlier researchers, although most of those tests were focused on section properties not a finite wing. Tests were performed in groups by airspeed with cylinder rotational speed, velocity ratio u_c/U_o, increasing for each test run. Table 6.1 presents the set of tests conducted, data is presented by dynamic pressure. Note that in all cases the $u_c/U_o = 0$ data presented is that of the bare, sealed airfoil presented above.

It is well known that the gap provided to accommodate a leading edge cylinder produces a leakage path that detrimentally affects aerodynamic performance if not sealed. With a primary focus on belts as the moving surface, sealing the cylinder gap was not undertaken. Larger gaps are worse than smaller and the gap by design was small compared to that in the literature at less than 0.75 mm. In the results discussed below, the intent was to compare the leading edge cylinders as they would be used to enhance performance over the base airfoil. In total, the regret for not have executed non-rotating leading edge cylinder tests is minor.

8.1 Leading Edge Cylinders at $q = 1$

Figure 8.2 shows the leading edge cylinder results for $q = 1$, for a Reynolds number of 1.9×10^5, with the cylinder velocity ratio increasing progressively from $u_c/U_o = 0.25$ to 1.5.

For velocity ratio $u_c/U_o = 0.25$, the peak C_L has decreased 10% from the bare wing to 0.604, the peak is still occuring at 12-degrees angle of attack. For $u_c/U_o = 0.5$, the peak C_L recovers to 0.657 with a delayed peak occuring at an angle of attack of 15-degrees along with

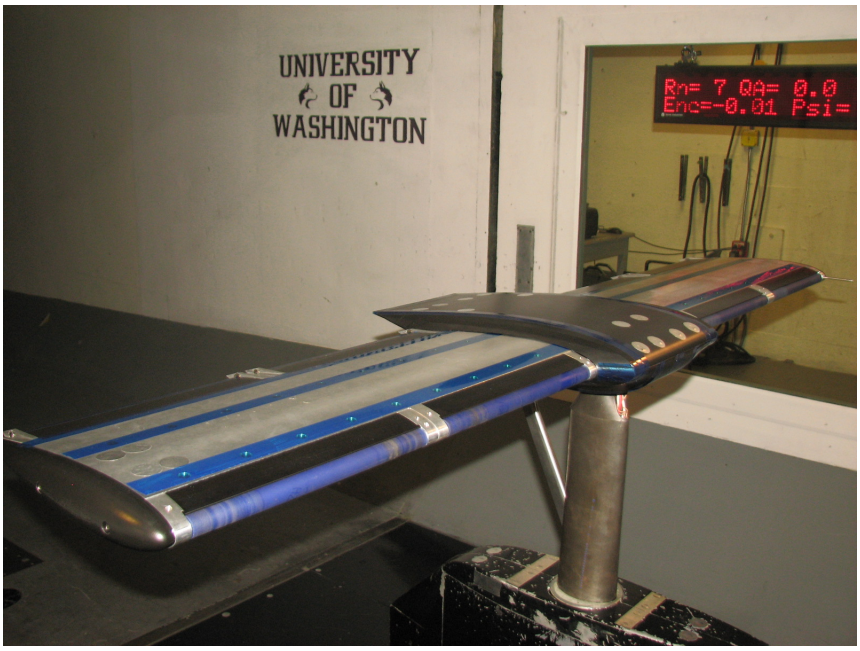

Figure 8.1: AR-5 Wing, Leading Edge Cylinders

Cylinders, AR-5, q=1			
u_c/U_0	C_L	$C_L^{3/2}/C_D$	L/D
0.0	0.672	7.97	10.84
0.25	0.604	6.53	9.07
0.5	0.657	6.92	9.48
1.0	0.827	7.43	10.03
1.5	0.847	7.66	10.34

Table 8.1: Leading Edge Cylinders, $q = 1$

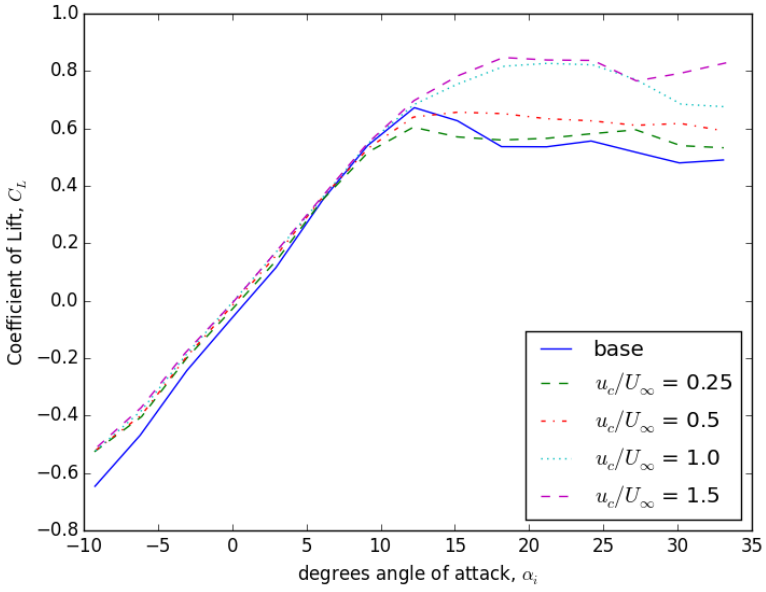

Figure 8.2: Leading Edge Cylinders, Lift Coefficient, $q = 1$

a fairly flat C_L profile between 12 to 21-degrees.

For $u_c/U_o = 1$, the motors operate at roughly 9,000 rpm and develop a peak C_L of 0.827 at 21-degrees angle of attack which maintatins a fairly flat profile between 18 and 24-degrees. For $u_c/U_o = 1.5$, the motor speed increases to 13,600 rpm and the data shows the same briad range of C_L with a peak of 0.847 occurring at an angle of attack = 18-degrees. C_L improvement is observed to only be achieved with $u_c/U_o > 1$.

Lift to Drag data shown in Figure 8.3 suggests that the flat C_L regions observed when u_c/U_o >1 produce shallower stall behavior. The figure also shows that the leading edge cylinder L/D values are bound by the bare airfoil, with peaks remaining at 9-degrees angle of attack. For the best case, $u_c/U_o = 1.5$, L/D dropped to 10.34 from 10.84 for the bare airfoil; a drop of 4.6%. At $u_c/U_o = 1.0$, L/D dropped to 10.03, or 7.5%. For $u_c/U_o = 0.5$ and 0.25, the decrease from the bare airfoil continues, data is presented in Table 8.1.

$C_L^{3/2}/C_D$, shown in Figure 8.4, shows that in all cases the endurance parameter is less for

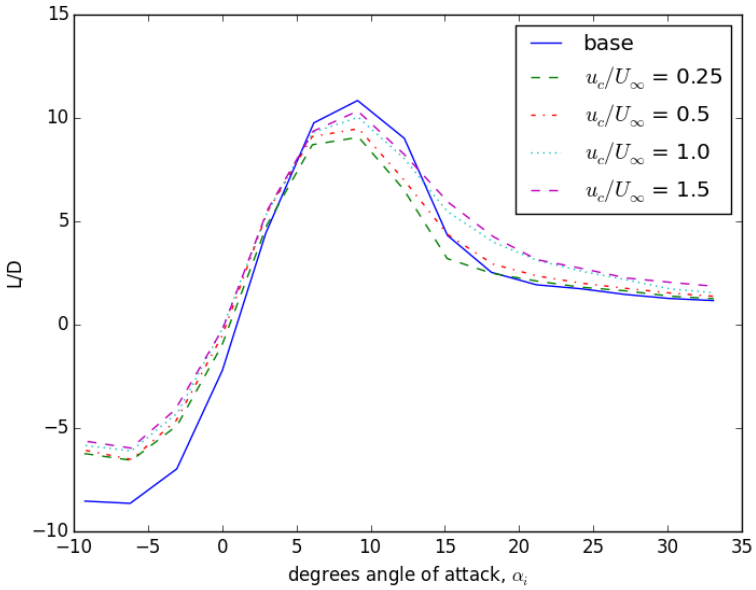

Figure 8.3: Leading Edge Cylinders, L/D, $q = 1$

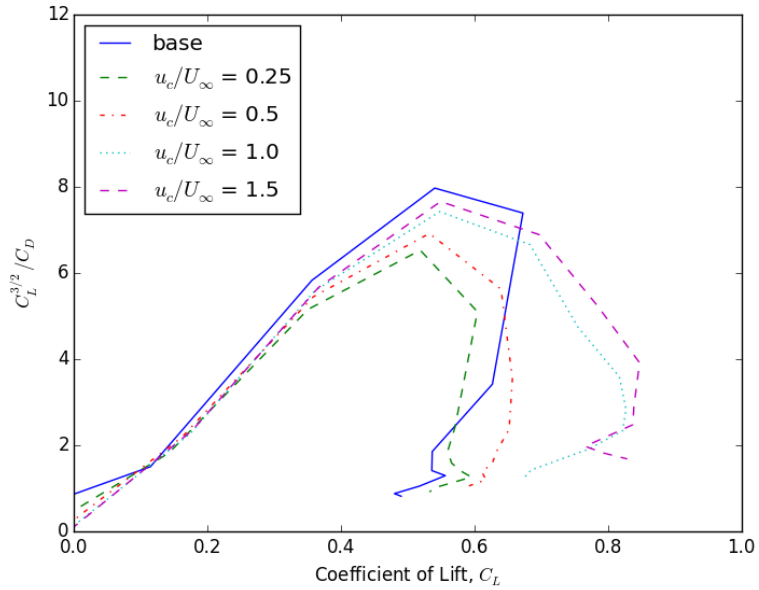

Figure 8.4: Leading Edge Cylinders, Endurance Parameter, $q = 1$

Cylinders, AR-5, q=5			
u_b/U_∞	C_L	$C_L^{3/2}/C_D$	L/D
0.0	0.734	9.94	13.40
0.1	0.594	7.03	10.77
0.25	0.626	7.34	11.04
0.5	0.668	7.85	11.47

Table 8.2: Leading Edge Cylinders, $q = 5$

the activated leading edge cylinders than for the bare airfoil, even $u_c/U_o = 1.5$ showed drop. In general all L/D and $C_L^{3/2}/C_D$ data was demonstrably worse than the bare airfoil and C_L improvement was only observed at $u_c/U_o = 1.0$ and above.

8.2 Leading Edge Cylinders at $q = 5$

With increasing airspeed it was not possible to test u_c/U_o at 1.0 or above with the rotational speed of the motors, hence the leading edge cylinders, limited to roughly 14,000 rpm. Figure 8.5 shows C_L data for $q = 5$, corresponding to a Reynolds number of 4.3×10^5, with a maximum $u_c/U_o = 0.5$. The shift in the slope of C_L in the linear region is apparent, shifting from $C_L$per degree angle of attack of 0.063 to 0.057. The same trend was observed in the $q = 1$ data. The peak C_L for the $u_c/U_o = 0.5$ case dropped 9% to 0.668 at 15-degrees angle of attack, from 0.734 at 12-degrees angle of attack for the bare wing, considerably more than the 2.3% drop observed for the euquivalent $q = 1$ case. Data is presented in Table 8.2.

Figure 8.6 shows the peak L/D drop from 13.4 for the bare wing to 11.47, a 14.04% drop for the $u_c/U_o = 0.5$ case; the equivalent q = 1 case showed a 12.5% drop. For $u_c/U_o = 0.25$, L/D dropped 17.8% for $q = 5$ versus 16.3% for the $q = 1$ equivalent case.

For $u_c/U_o = 0.5$, Figure 8.7 shows a 20.9% drop in $C_L^{3/2}/C_D$ at angle of attack of 9-degrees, from 9.94 to 7.85 compared to the bare airfoil. This corresponds, however to an increase of 13.4% from the $q = 1$, $u_c/U_o = 0.5$, peak value for the endurance parameter.

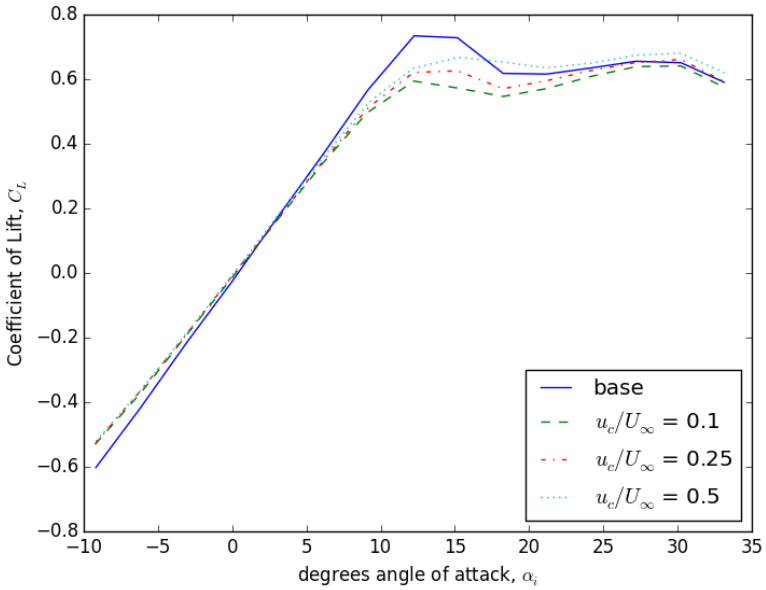

Figure 8.5: Leading Edge Cylinders, Lift Coefficient, $q = 5$

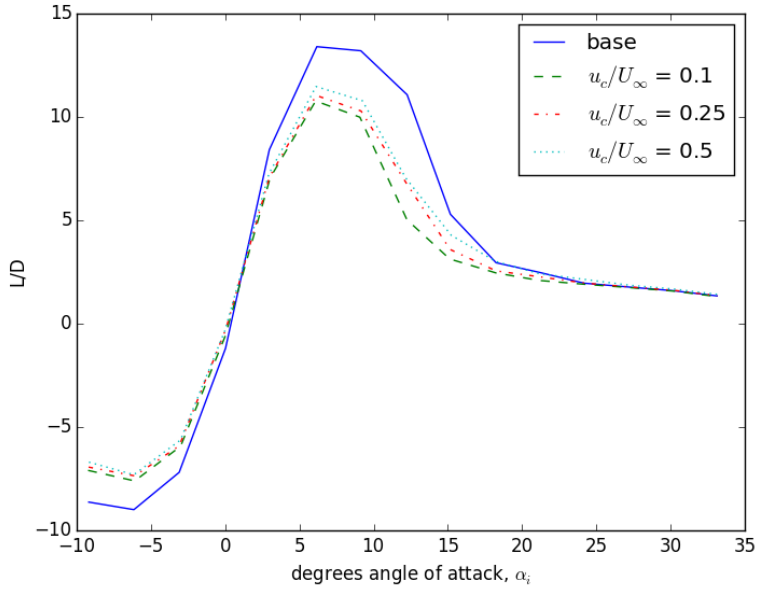

Figure 8.6: Leading Edge Cylinders, L/D, $q = 5$

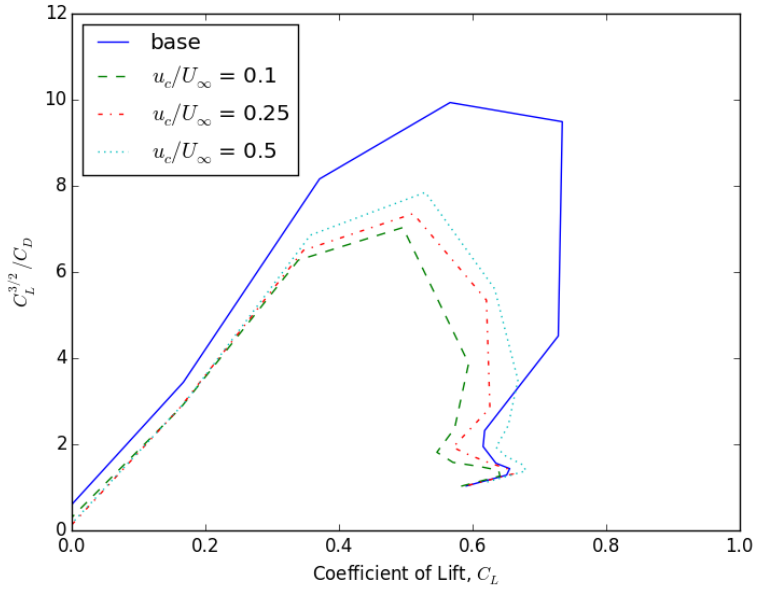

Figure 8.7: Leading Edge Cylinders, Endurance Parameter, $q = 5$

Marginally improved performance is shown with increasing u_c/U_o, although in all cases less than the bare airfoil.

8.3 Leading Edge Cylinders at $q = 10$ and above

Table 8.3 presents summary data for the $q = 10$ test case. Increasing the airspeed further to $q = 10$ and beyond, Reynolds number 6.15×10^5 and greater, the continued trend of dropping peak C_L for u_c/U_o less than unity is observed, with the drops increasing incrementally with increasing q. For $q = 10$ and $u_c/U_o = 0.5$ the drop in peak C_L is 12.7%, versus 9% for the $q = 5$ case and 2.3% for $q = 1$. Figures 8.8, 8.9, and 8.10 show the data for $q = 10$. The data for $q = 20$ is provided in the Appendix and continue to show the same trend, degrading performance as q is further increased.

The data show that the velocity ratio becomes more important at higher dynamic pressure. At $q = 5$, slight, but distinct, improvements with increased u_c/U_o, even below 0.5, are

Cylinders, AR-5, q=10			
u_b/U_∞	C_L	$C_L^{3/2}/C_D$	L/D
0.0	0.765	10.71	15.31
0.1	0.586	6.74	11.53
0.25	0.637	7.53	11.86
0.5	0.667	8.04	12.10

Table 8.3: Leading Edge Cylinders, $q = 10$

observed in all parameters presented. At $q = 10$, the incremental improvement in L/D and $C_L^{3/2}/C_D$ below $u_c/U_o = 0.5$ is diminished and by $q = 20$, there is virtually no difference in L/D and $C_L^{3/2}/C_D$ for the lower values. At high dynamic pressure, the momentum injection, to borrow a term from Modi, that the cylinders can provide is insufficient to provide any meaningful effect for such low velocity ratios. The unsealed gap behind the drive cylinder certainly would be a liability to the system and the $u_c/U_o = 0.1$ can be viewed as representative of $u_c/U_o = 0$ data with open gaps, especially at the higher dynamic pressures. To develop a unity velocity ratio at $q = 10$, the cylinders would need to rotate at 28,750 rpm, where notable improvements that have been published for velocity ratios of four would require over 110,000 rpm. Although the data collected here is not complete a change in the overall physics is it suggested at higher dynamic pressures where the Reynolds number at $q = 10$ is generally regarded as just beyond the critical Reynolds number.

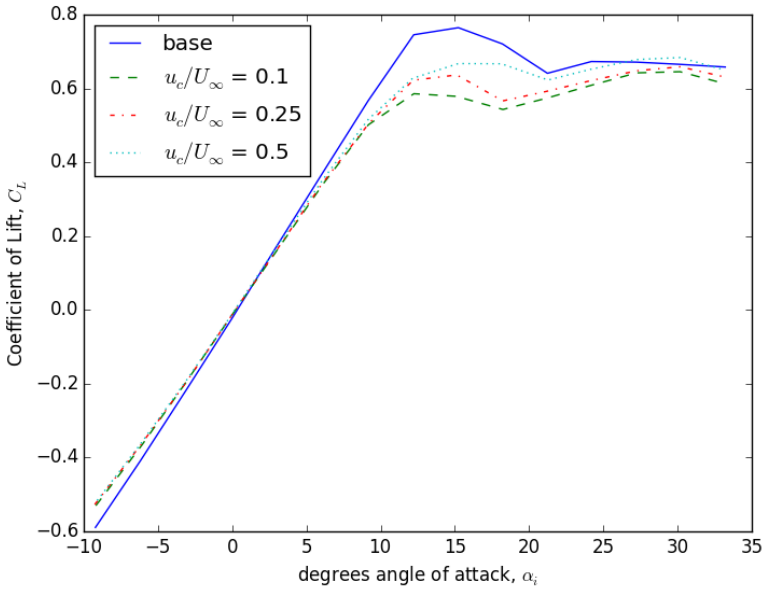

Figure 8.8: Leading Edge Cylinders, Lift Coefficient, $q = 10$

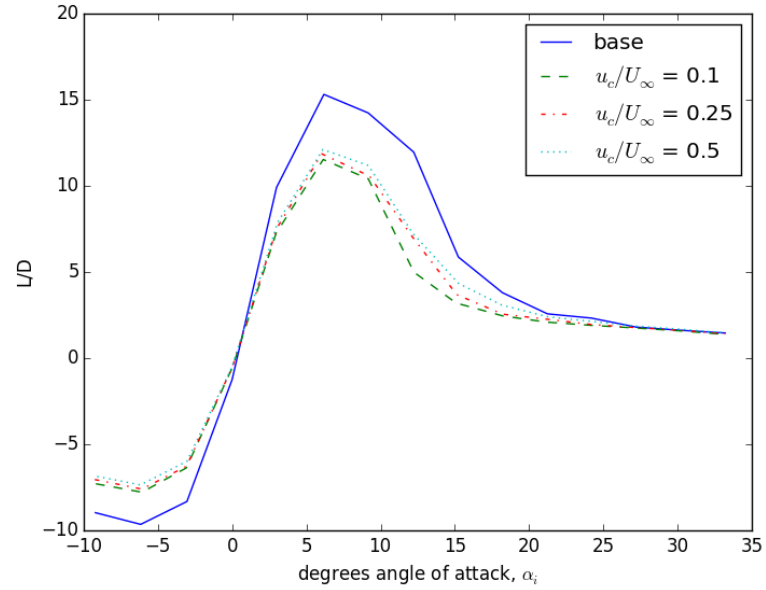

Figure 8.9: Leading Edge Cylinders, L/D, $q = 10$

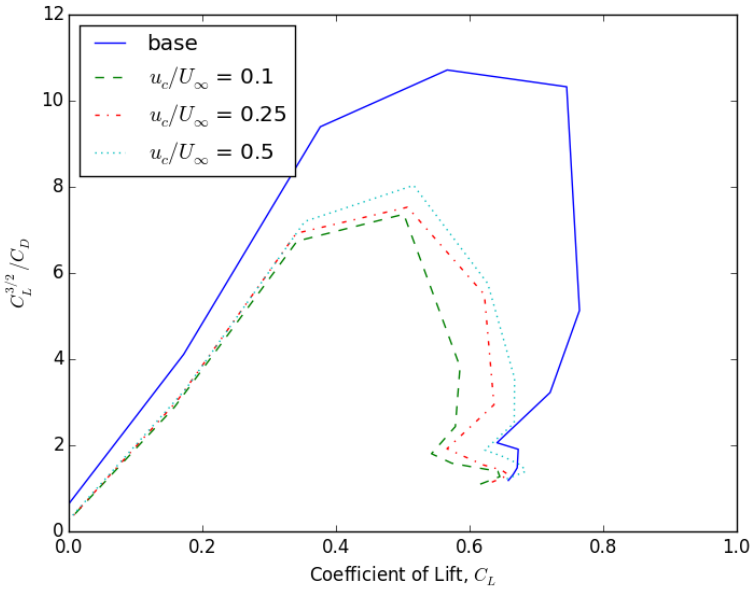

Figure 8.10: Leading Edge Cylinders, Endurance Parameter, $q = 10$

Chapter 9

ASPECT RATIO 5, MOVING SURFACE TESTS

9.1 Aspect Ratio 5, Static Belts, $u_s/U_o = 0$

A set of tests were run with the belts installed but not moving, $u_s/U_o = 0$, with leading edge and trailing edge cylinders operable. Figure 9.1 shows the C_L curves for this AR-5 configuration at dynamic pressures of 1, 5, 10, and 20 psf. The date is presented in Table 9.1.

Through the linear portion of the lift curve, up to 12-degrees angle of attack, the data overlay well with a C_L/α slope between 0.0629 and 0.0640 with $C_L = 0$ crossing very near to the zero degree angle of; the $q = 1$ case being slightly negative. Compared to the bare wing configuration, the peak C_L values all shift toward higher angles of attack, from 12 and 15-degrees for the bare configuration to 18 and 21-degrees for the static belts, with higher dynamic pressures showing the higher angles of attack. In all cases, the belts appear to produce a slight flattening of the lift curve in the stalled region. At $q = 10$ and 20 psf, the C_L peaks at angle of attack of 21-degrees, are a bit jagged compared with the rest of the data,

AR-5, $u_b/U_\infty = 0$			
q	C_L	$C_L^{3/2}/C_D$	L/D
1	0.714	7.16	9.66
5	0.745	7.89	10.67
10	0.807	8.23	11.82
20	0.796	6.71	10.12

Table 9.1: Aspect Ratio 5, Stationary Belts

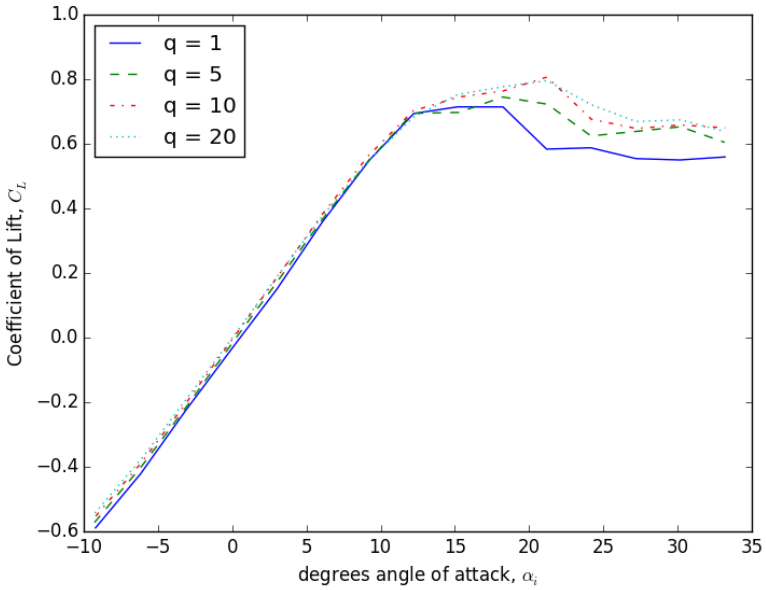

Figure 9.1: Aspect Ratio 5, Lift Coefficient, $u_s/U_o = 0$

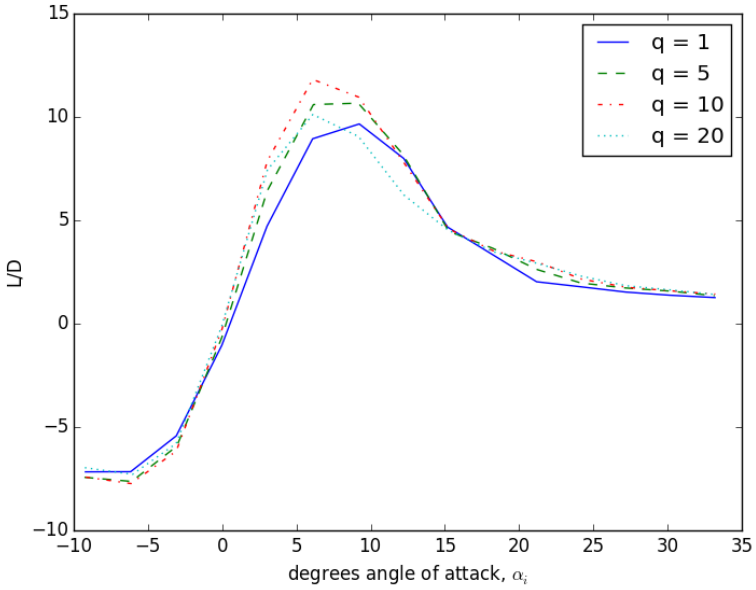

Figure 9.2: Aspect Ratio 5, L/D, $u_s/U_o = 0$

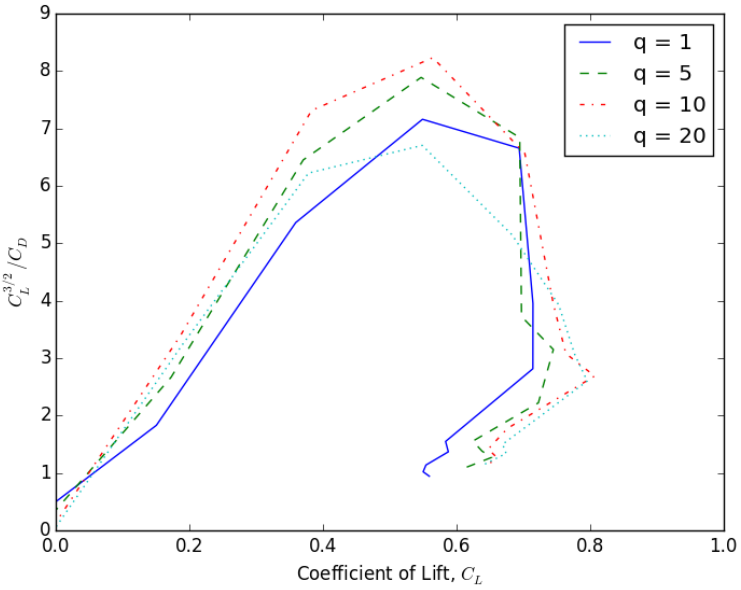

Figure 9.3: Aspect Ratio 5, Endurance Parameter, $u_s/U_o = 0$

this is almost certainly due to billowing, or parachuting of the belts, that was observed at the at the high angles of attack. Compared to the bare wing case, at lower dynamic pressure, $q = 1$ and 5, the data for the static belts show a modest increase in C_L , roughly 6% and 1.4% respectively. If the 21-degree angle of attack peak is disregarded for the $q = 10$ case, the C_L values is nearly identical, where for the $q = 20$ case, the peak C_L is lower overall.

The L/D data shown in Figure 9.2 shows that the aerodynamic efficiency and stall characteristics of the AR-5 wing have been generally maintained by the addition of the static belts. In particular the peak L/D for $q = 1$ remains at 9-degrees with a flatter peak for $q = 5$ and shifted peaks to 6-degrees angle of attack for the higher dynamic pressures. Overall peak L/D values are less than the bare wing case; for $q = 1$ roughly 11% less, 20% less for $q = 5$ and 23% less for $q = 10$. The data also shows a considerable drop of 32% in peak L/D for the $q = 20$ case; the observed billowing of the belts increasing drag as indicated at the

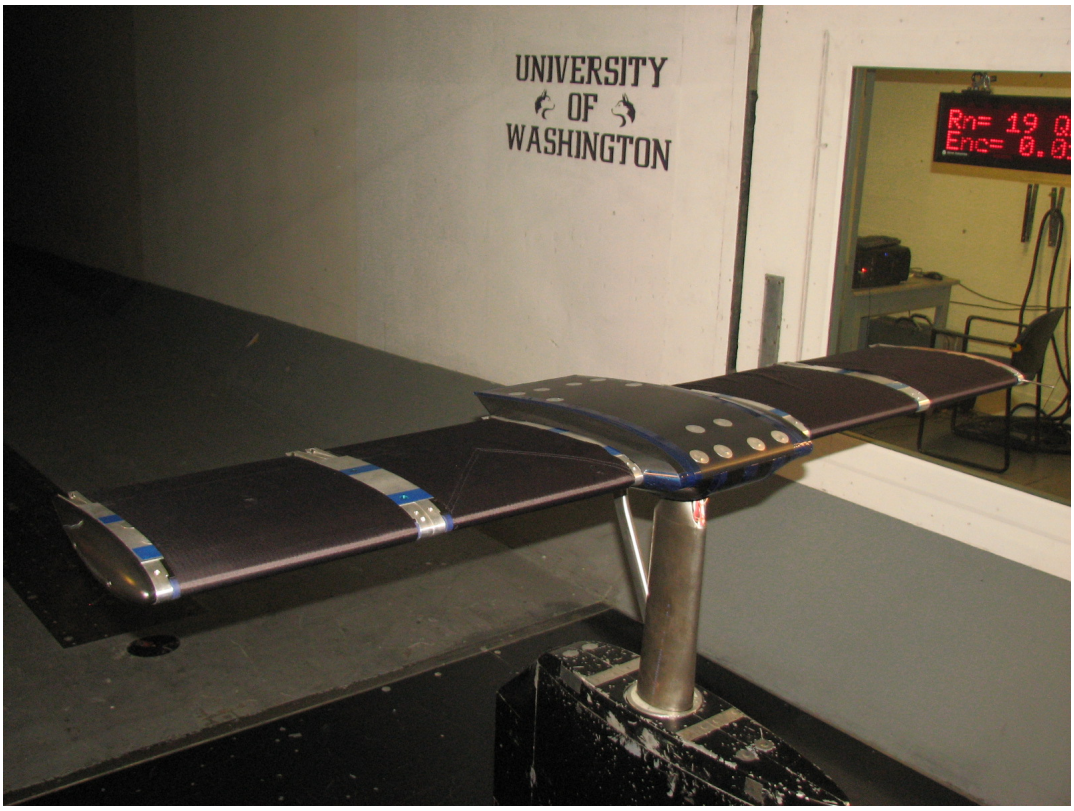

Figure 9.4: AR-5 Wing, with Moving Surface Belts

AR-5, q = 1			
u_b/U_∞	C_L	$C_L^{3/2}/C_D$	L/D
0	0.714	7.16	9.66
0.25	0.799	7.53	9.79
0.5	0.940	8.13	9.89
1	1.078	8.37	9.37
1.5	1.158	8.06	8.37

Table 9.2: Aspect Ratio 5, $q = 1$

higher angles of attack.[1]

The endurance parameter data, Figure 9.3, also show notably different performance for the $q = 20$ case. Unlike the leading edge cylinders, however, the $q = 10$ case does not show adverse effects.

9.2 Aspect Ratio 5, Moving Surface

This section presents the results of the AR-5 with the moving surface system activated for different velocity ratios u_s/U_o at a dynamic pressure of $q = 1$ psf, corresponding to a Reynolds number of 1.9×10^5. The peak data is presented in Table 9.2.

Figure 9.5 presents C_L data for the series of moving surface test runs, along with the $q = 1$ bare wing test data as a reference.[2] The moving surface velocity ratio increased from $u_s/U_o = 0.25$ to 0.5, 1.0, and 1.5. The data show a general increase of the lift curves with increasing velocity ratio, the curves shifting upward from a near zero C_L at 0-degrees angle of attack to 0.321 for $u_s/U_o = 1.5$. The linear portion of the lift curves are observed to

[1] As a comparison, $q = 10$ psf is roughly 60 mph and $q = 20$ just under 90 mph. Although these are not Reynolds number effects as fluid dynamics would assess them, the corresponding high dynamic pressure notably affects the physical.

[2] Table 9.2 only shows values for data collected with belts, as opposed to the figures in this section which include bare airfoil data as a reference.

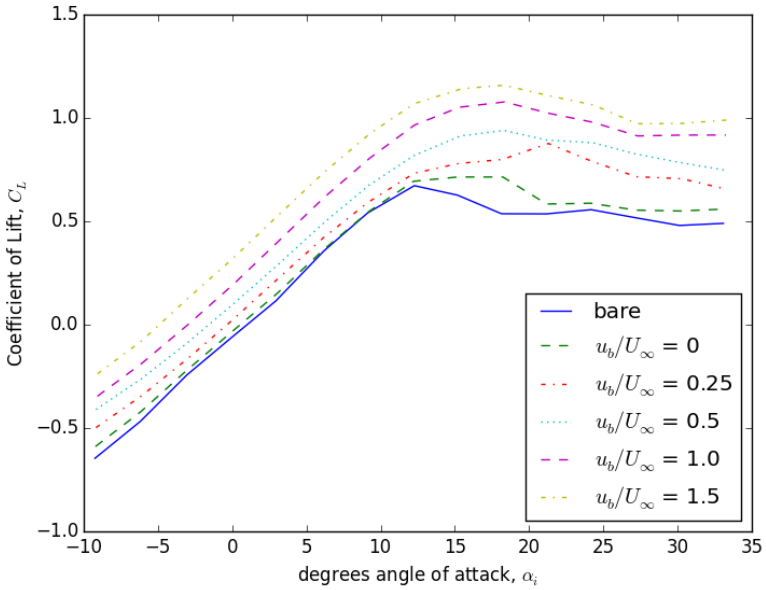

Figure 9.5: Aspect Ratio 5, Lift Coefficient, $q = 1$

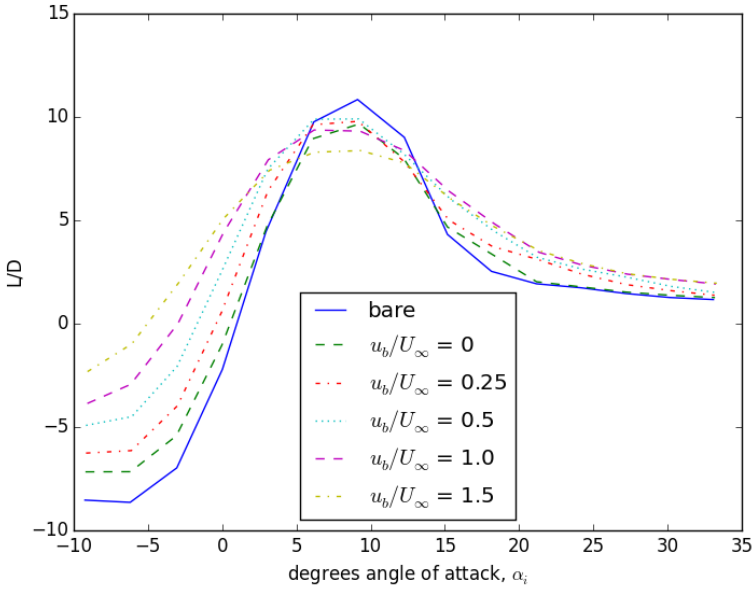

Figure 9.6: Aspect Ratio 5, L/D, $q = 1$

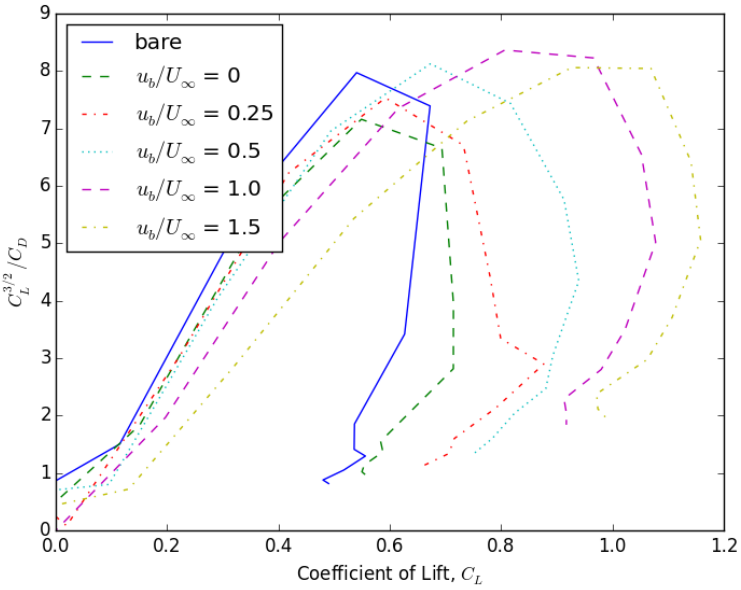

Figure 9.7: Aspect Ratio 5, Endurance Parameter, $q = 1$

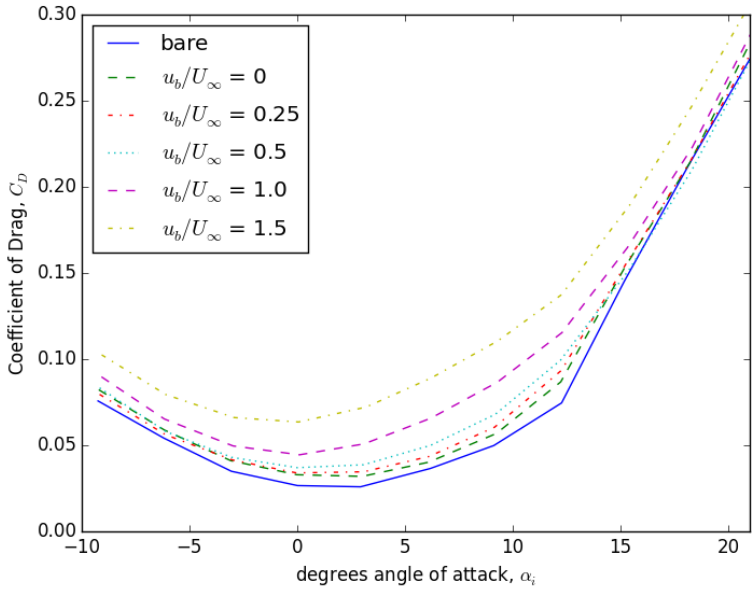

Figure 9.8: Aspect Ratio 5, Drag Coefficient, $q = 1$

decrease in slope compared to the bare wing configuration.

Disregarding the spike in C_L at 21-degrees angle of attack for the $u_s/U_o = 0.25$, the data show an 18.9% increase in C_L at 18-degrees angle of attack compared to the bare wing, increasing from 0.672 to 0.793. The spike in the $u_s/U_o = 0.25$, C_L data at 21-degrees to 0.877 represents a 30% increase in C_L; likely due to billowing as previously noted. Compared with the the $u_s/U_o = 0$ data, CL at $u_s/U_o = 0.25$ is 12% higher for the non-spiked data, and 22.7% for that reported in the table above. The remainder of the C_L data for the moving belts performed well, with out similar spikes that are suspect. At $u_s/U_o = 0.5$, the peak C_L increases to 0.940; a 39.7% increase from the bare airfoil, and 31.5% from the static belt case. At $u_s/U_o = 1.0$, the peak C_L increases to 1.078, a 60.3% increase. At $u_s/U_o = 1.5$, peak C_L is 72.3% greater than the bare wing at 1.158; compared to the static belt case this is a 62.2% increase. All of the moving surface data show shallower stall behavior, with flatter C_L curves, than either the bare wing or static belt tests.

The L/D data shown in Figure 9.6 illustrates the shallower stall behavior and a decreasing, peak L/D at 9-degrees angle of attack for increasing velocity ratio where both the bare wing and static belt configurations are less than 2% apart. This indicates an increase in drag with increasing belt speed, particularly for the $u_s/U_o = 1.5$ test case. Figure 9.8 shows data for the C_D over a narrower range of angle of attack. Due to the action of the belts, shifting the lift curves upward, the increase in drag due to the action of the belts can not be directly evaluated at any particular angle of attack. However, the offset of the drag curves remain qualitatively similar between zero and 12-degrees angle of attack. The data show roughly a 20% increase in drag from the bare wing to static belt cases, ΔC_D of nearly 0.006. The increase in drag is most notable for the $u_s/U_o = 1.0$ and $u_s/U_o = 1.5$ cases, with increase larger for the higher velocity ratio.

Figure 9.7 shows the positive impact of the moving surface on the endurance parameter for $u_s/U_o = 0.5$ and above. Compared to the bare wing configuration for $u_s/U_o = 0.5$, a 1.9% increase in $C_L^{3/2}/C_D$ is observed with a 24.6% increase in C_L at 9-degrees angle of attack. At $u_s/U_o = 1.0$, C_L increases 49.3%, to 0.807 with a 4.9% increase in $C_L^{3/2}/C_D$ at 9-degrees angle

of attack. At 12-degrees angle of attack, this increases to an 11.3% increase in endurance parameter with a 43.6 increase in C_L. At $u_s/U_o = 1.5$, the moving surface increases C_L further to 0.927, for an increase of 71.5% over the bare wing configuration with a nominal 1.1% increase in $C_L^{3/2}/C_D$ at 9-degrees angle of attack. At 12-degrees angle of attack the increase in endurance parameter is 8.8% with 59% increase in C_L. Compared to the static belt case, the increase in C_L is largely the same. A substantial increase in $C_L^{3/2}/C_D$ is shown for $u_s/U_o \geq 1.0$ when compared to the static belt case with at more than 12% at 9-degrees angle of attack and more than 20% at 12-degrees angle of attack. Beyond $u_s/U_o = 1$ the incremental improvement of the moving surface system starts to fall off suggesting that an optimal value for the system exists for a velocity ratio between 1.0 and 1.5.

9.3 Aspect Ratio 5, Moving Surface, Alternate Trailing Edge

Table 9.3 presents the data collected for an alternate trailing edge configuration that was tested with a larger diameter trailing edge cylinder, 12.6 mm (0.5-inch) versus 6.3 mm (0.25-inch). The belts used were constructed from different materials, than other tests, and produced in-situ on the wing, providing a tighter fit to the wing. Additionally, the trailing edge were different mechanical assemblies. It was only possible to operate the system up to a velocity ratio of 0.5.

Figure 9.9 shows an increase in C_L with velocity ratio without the spike observed with the smaller diameter trailing edge and less form fitting belts. The peak C_L for the static belt case was nearly 5% less for the larger diameter trailing edge than the smaller trailing edge at $C_L = 0.679$, which was approximately the same for the bare wing configuration. The increase in C_L for the two alternate trailing edge cases are roughly a third less than the increased observed for the equivalent the smaller trailing edge cases. Endurance parameter data shown in Figure 9.10 shows the general pattern as that for the smaller trailing edge, although at $u_s/U_o = 0.5$, $C_L^{3/2}/C_D$ broadens at 12-degrees angle of attack, as previously observed. The data shows generally lower C_L and $C_L^{3/2}/C_D$ values for the larger trailing edge. Although coefficient of lift and endurance parameter data indicate poorer overall performance for the

AR-5, q = 1			
u_b/U_∞	C_L	$C_L^{3/2}/C_D$	L/D
0	0.679	7.48	9.98
0.25	0.805	7.39	9.79
0.5	0.818	8.07	10.42

Table 9.3: Aspect Ratio 5, Alternate Trailing Edge

larger trailing edge, the leak L/D for the $u_S/U_o = 0.5$ case is better for the larger diameter case; likely the result of a tighter fitting belt.

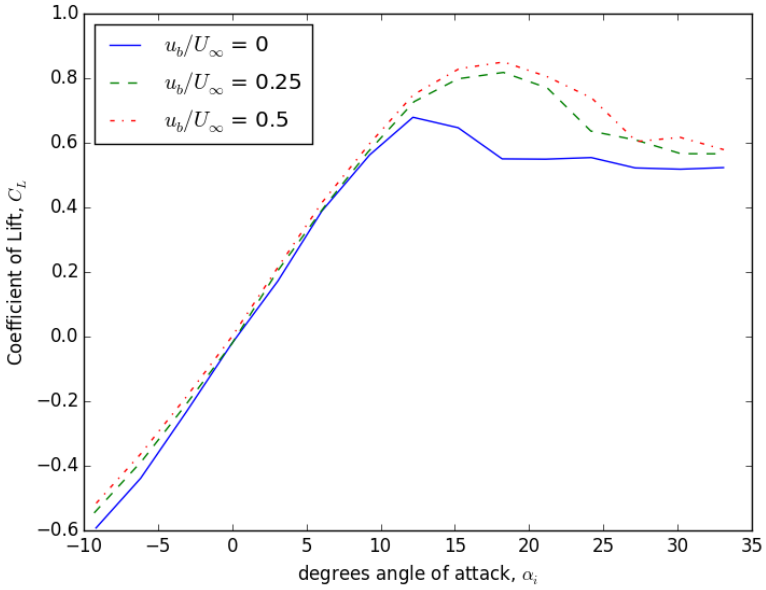

Figure 9.9: Aspect Ratio 5, Lift Coefficient, Alternate Trailing Edge

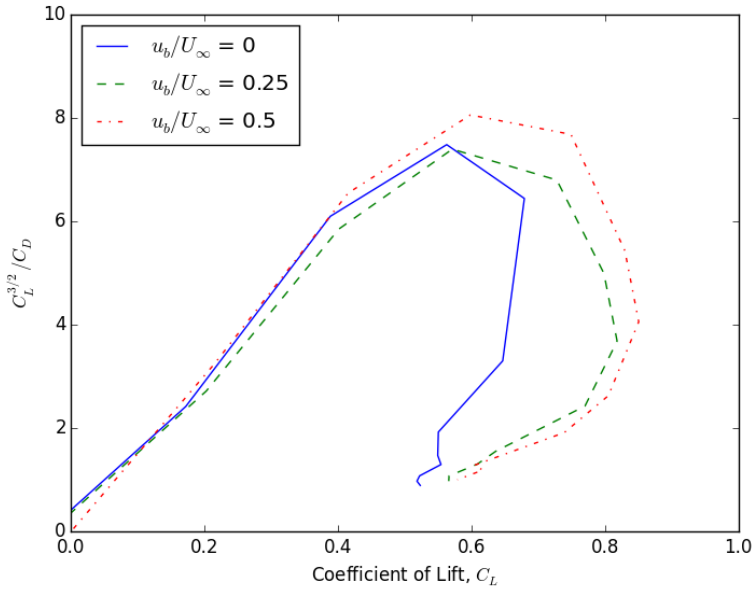

Figure 9.10: Aspect Ratio 5, Endurance Parameter, Alternate Trailing Edge

Chapter 10

ASPECT RATIOS 7 AND 9

10.1 Aspect Ratio 7

AR-7 configuration tests were conducted at $q = 1$ psf for velocity ratios of $u_s/U_o = 0.25$ and 0.5.

All tests were conducted with the 6.3 mm (0.25-inch) trailing edge. Table 10.1 presents the maximum values for the data in these tests. Figure 10.2 shows the C_L data where an upward shift and general increase in C_L curves occur smoothly for increasing velocity ratio. The stall characteristic of the static belt is replaced with a more gradual loss of lift with without the plateau observed in some of the AR-5 data. For the static belts, $u_s/U_o = 0$, the maximum C_L of 0.703 is observed at 12-degrees angle of attack, similar to the AR-5 case of 0.714. Activating the moving surface to $u_s/U_o = 0.25$, the maximum C_L rose to 0.829 while the peak shifted to 15-degrees, which is still a lower angle of attack than the AR-5. This maximum C_L value is higher than the AR-5 at 18-degrees angle of attack, but less than the spiked C_L value at 21-degrees that was attributed to billowing of the belts. Neglecting that data point, the AR-7 sees a modest 3.6% increase in C_L. At $u_s/U_o = 0.5$, the AR-5 configuration shows slightly better C_L at 0.940 versus 0.915 for the AR-7.

The L/D data shown in Figure 10.3 shows increases for both velocity ratio tests above the static belt case, a condition that was not observed in the AR-5 configurations. The peaks in the L/D data appear as a plateau, suggesting the actual peaks may be in between the test points taken at six and nine degrees angle of attack. Values of peak L/D are notably higher than the AR-5 equivalent cases. The endurance parameter, shown in Figure 10.4, similarly shows an increased improvement over the AR-5 configuration, an 18% increase in $C_L^{3/2}/C_D$ at $u_s/U_o = 0.5$ for the AR-7 configuration compared to static belts, compared to a

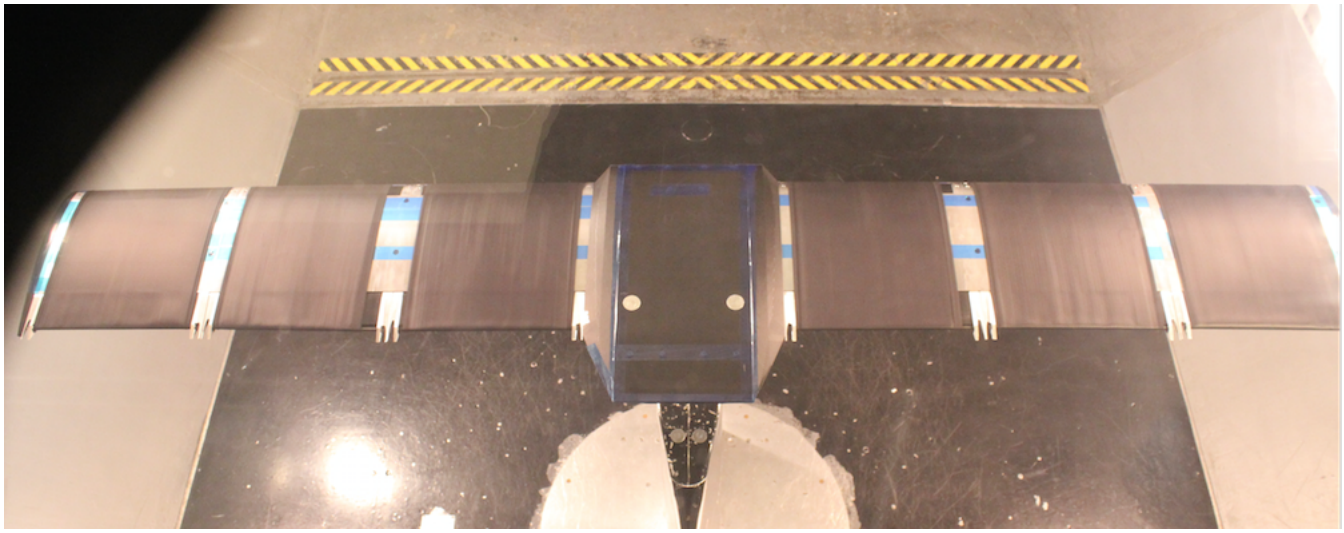

Figure 10.1: AR-7 Wing

AR-7, q = 1			
u_b/U_∞	C_L	$C_L^{3/2}/C_D$	L/D
0	0.703	7.85	10.32
0.25	0.829	9.13	11.26
0.5	0.915	9.59	11.42

Table 10.1: Aspect Ratio 7, $q = 1$

13% increase for the equivalent AR-5 data.

10.2 Aspect Ratio 9

Two configurations were tested for the AR-9 wing. The first had only the inner half of each wing fitted with moving surfaces, essentially the AR-5 configuration with wing extensions installed, with the outer leading edge cylinders rendered in-operable and gaps sealed in the same manner as the bare wing tests. Tests were conducted at a q of one psf with a velocity ratio up to 1.5. The velocity ratio was limited to 0.5 for tests at $q = 5$ psf. The second AR-9

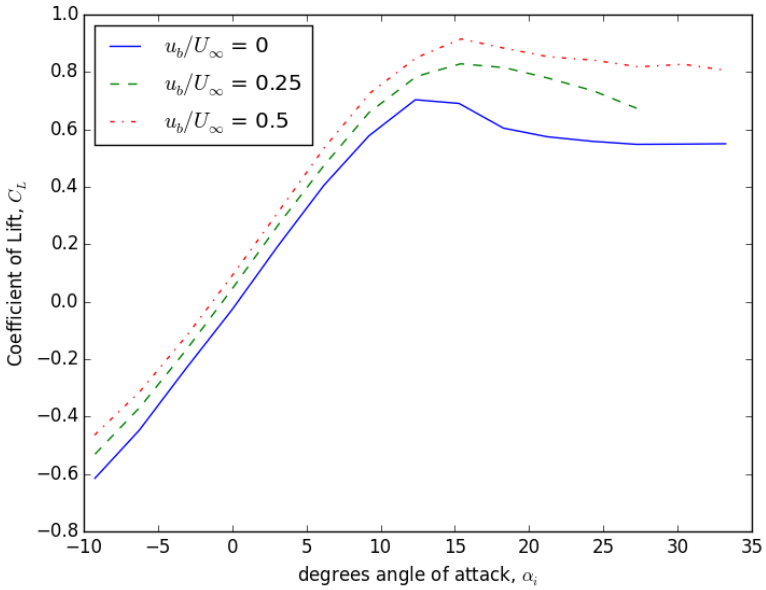

Figure 10.2: Aspect Ratio 7, Lift Coefficient, $q = 1$

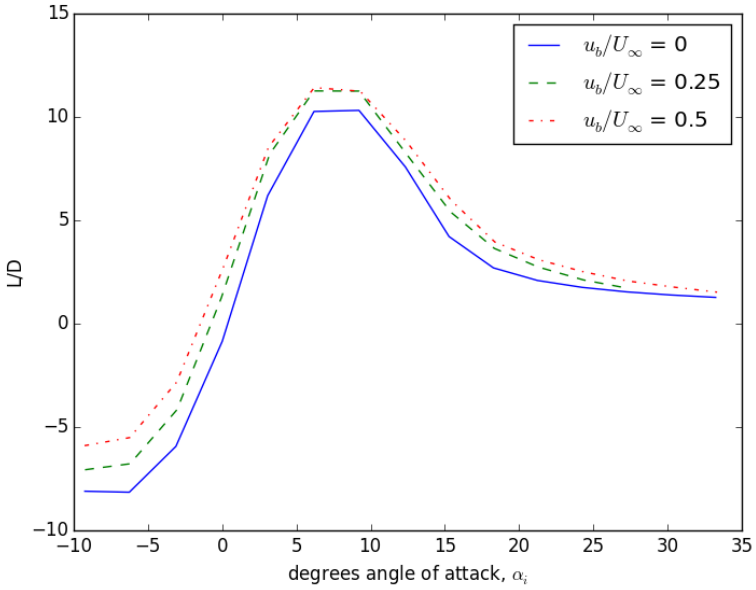

Figure 10.3: Aspect Ratio 7, L/D, $q = 1$

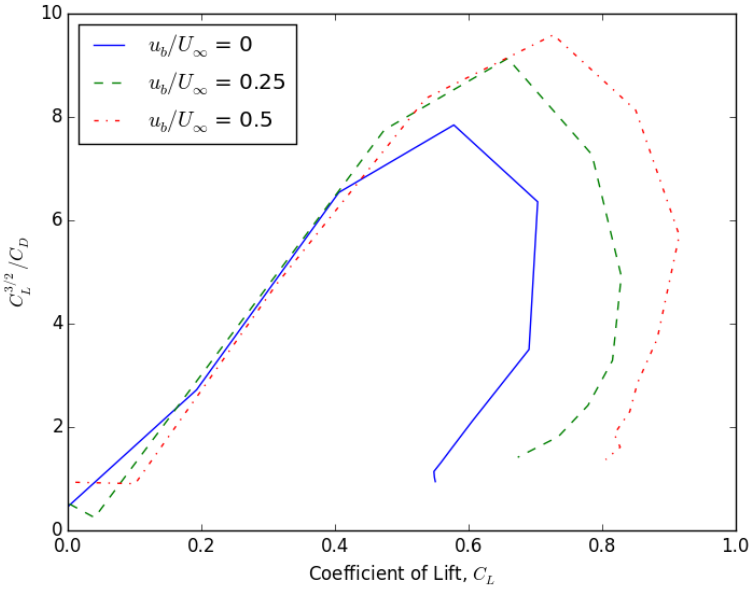

Figure 10.4: Aspect Ratio 7, Endurance Parameter, $q = 1$

configuration had the full span fitted with moving surface belts, where one moving surface test was conducted at $q = 1$ psf. Table 10.2 lists the peak values for the AR-9 inner belts at $q = 1$, Table 10.3 for $q = 5$, and Table 10.4 provides the results for the AR-9 full-belt configuration.

Figure 10.7 shows C_L data for the inner belt configuration at $q = 1$ with increasing belt velocity ratio u_s/U_o. The maximum C_L remains consistently at 12-degrees angle of attack. For $u_s/U_o = 1.5$, C_L remains essentially constant at 1.13, from 12 to 15-degrees before a stalling with in a manner typical of the non-moving surface wing configurations. At this velocity ratio, C_L has increased 44.6% over the static belts. At $u_s/U_o = 1.0$, a 31.5% increase in C_L is observed. C_L increased 19.4% at $u_s/U_o = 0.5$ and 9.6% at $u_s/U_o = 0.25$.

Figure 10.8 shows a general increase in L/D for increasing velocity ratio with the exception $u_s/U_o = 1.5$ case, which shows a sharp drop of 8.2% compared to the static surface case. This drop is accompanied with a flatter and broader L/D curve profile, most noticeably at

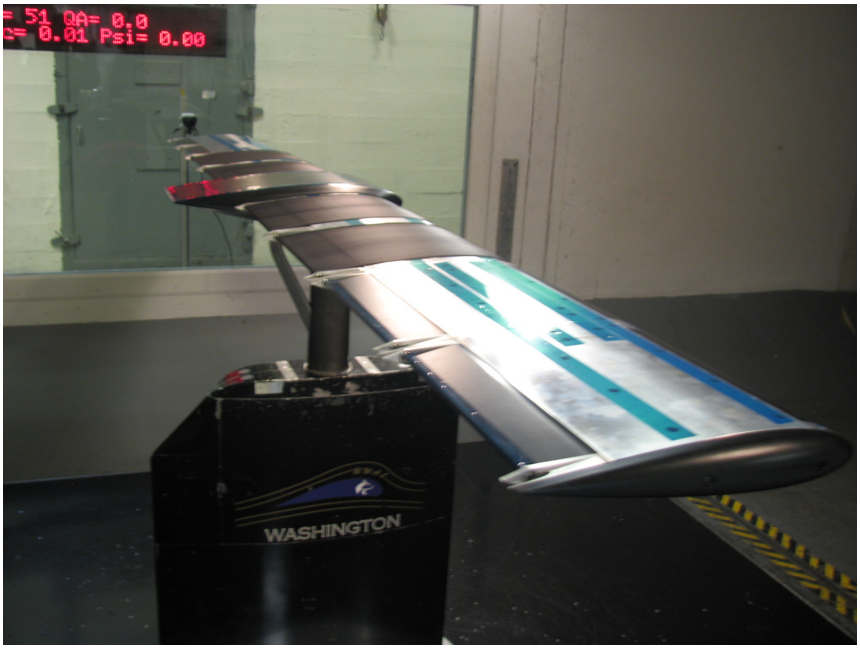

Figure 10.5: AR-9 Wing, Inner Belts

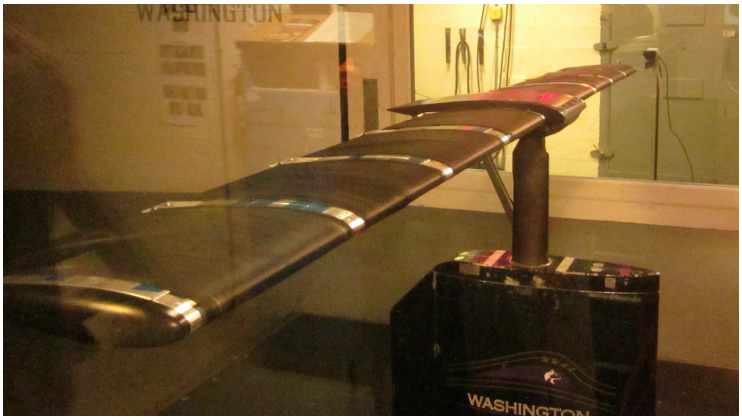

Figure 10.6: AR-9 Wing

AR-9, q = 1			
u_b/U_∞	C_L	$C_L^{3/2}/C_D$	L/D
0	0.782	10.33	13.26
0.25	0.856	11.60	13.98
0.5	0.899	12.27	14.26
1	1.028	12.77	13.49
1.5	1.130	12.18	12.17

Table 10.2: Aspect Ratio 9, Inner Belts, Activated $q = 1$

AR-9, q = 5			
u_b/U_∞	C_L	$C_L^{3/2}/C_D$	L/D
0	0.847	11.39	14.15
0.1	0.834	11.45	14.31
0.25	0.858	11.76	14.84
0.5	0.891	12.55	15.83

Table 10.3: Aspect Ratio 9, Inner Belts, Activated $q = 5$

the lower, and negative, angles-of-attack compared to the rest of the data. The remainder of the data maintains the general shape of the static surface case, with relatively normal stall characteristics unlike the AR-5 and AR-7 cases. The peak L/D value observed was 14.26 at $u_s/U_o = 0.5$; this was the highest observed L/D at $q = 1$ psf through out the test program.

The endurance parameter, shown in Figure 10.9, demonstrates the the same trend as that observed with the AR-5 configuration: $C_L^{3/2}/C_D$ improving along with increased C_L as velocity ratio increases to an apparent maximum at $u_s/U_o = 1$, beyond which the incremental improvement begins to taper. For $u_s/U_o = 1$, a 23.6% increase in $C_L^{3/2}/C_D$ is accompanied by a 35.2% increase in C_L over the static belt case. At $u_s/U_o = 1.5$, $C_L^{3/2}/C_D$ is 22.6% improved

AR-9, q = 1			
u_b/U_∞	C_L	$C_L^{3/2}/C_D$	L/D
0.25	0.928	10.835	13.30

Table 10.4: Aspect Ratio 9, Full Wing

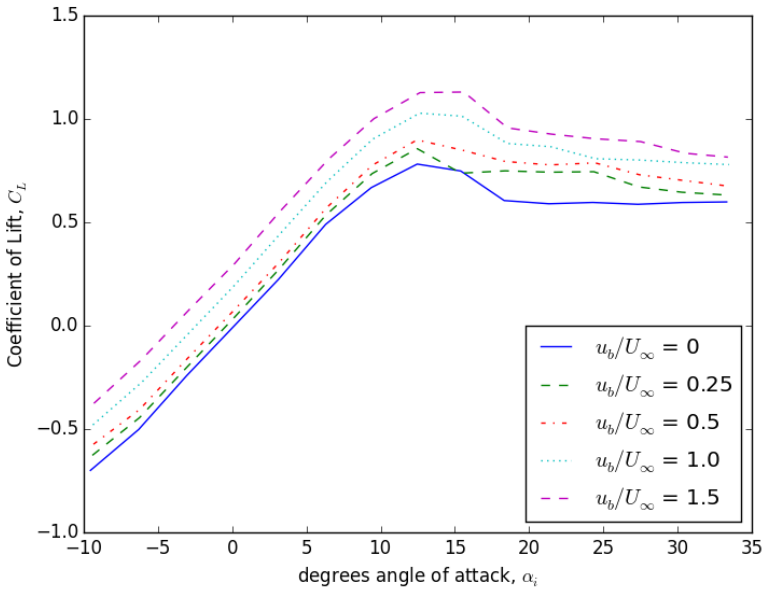

Figure 10.7: Aspect Ratio 9, Inner Belts, Lift Coefficient, $q = 1$

over the $u_s/U_o = 0$ case, but with a further increase of 49.9% in C_L. For $u_s/U_o = 0.5$, only a 19% increase in $C_L^{3/2}/C_D$ over the static case, with a 16% improvement in C_L, is observed.

C_L data for the inner-belt configuration at $q = 5$ is shown in Figure 10.10, where all maximum values were all delayed to 15-degrees angle-of-attack. The apparent stall behavior remains, again, consistent with that of the static belt case, which is also seen in the L/D data, Figure 10.11. Endurance parameter data, Figure 10.12, shows slight improvement of $C_L^{3/2}/C_D$ vs. C_L at $u_s/U_o = 0.25$. At the maximum relative velocity for this dynamic pres-

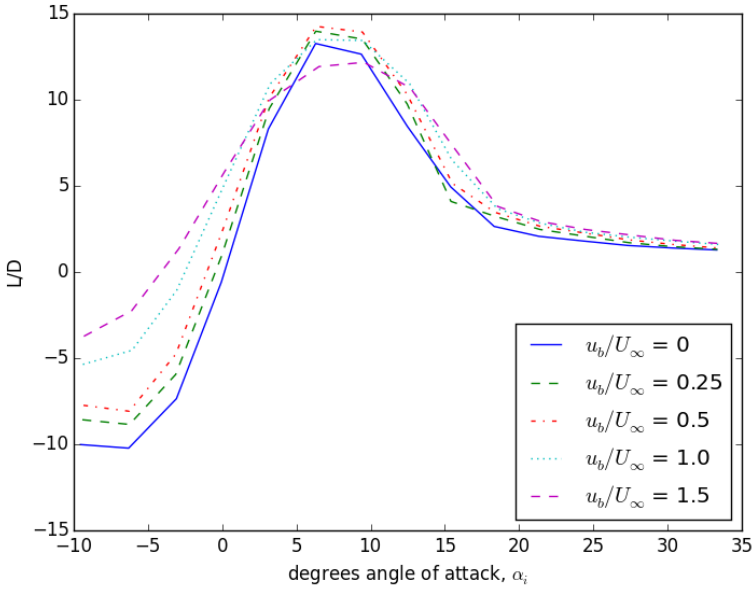

Figure 10.8: Aspect Ratio 9, Inner Belts, L/D, $q = 1$

sure, a 10.1% increase in $C_L^{3/2}/C_D$ is observed along with a 12.2% increase in C_L, less of an improvement than was observed for the equivalent velocity ratios at the lower dynamic pressure but with higher overall values. C_L, for all but the static case, was consistent between the two dynamic pressures and L/D for the $q = 5$ psf case was higher in all cases.

Figure 10.13 shows C_L data for the full set of moving surfaces belts on each wing compared to the static inner-belt configuration at $q = 1$. The velocity ratio of $u_s/U_o = 0.1$ provides a comparative parameter of for these tests; it is noted that data was not collected at this low value of velocity ratio for AR-5 and AR-7 configurations. The C_L curve shows the expected upward shift but with the flatter stall profile observed with the AR-5 and AR-7 configurations, which also had moving belts installed over the full span. The endurance parameter data, Figure 10.15, shows that the full set of belts were roughly one third as effective in increasing $C_L^{3/2}/C_D$ as the inner-belts with a nominal increase in C_L.

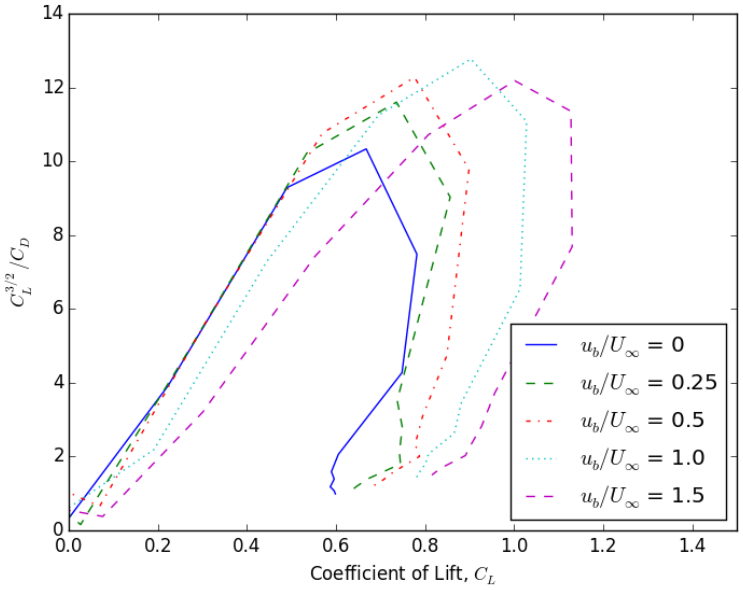

Figure 10.9: Aspect Ratio 9, Inner Belts, Endurance Parameter, $q = 1$

The full set of belts were difficult to fully synchronize and a differential in the surface speeds across the wing was observed during the testing suggesting that the data is not representative of the physics had the system been operating as desired. Even with the inconsistent behavior of the system, the data showed evidence of the positive trends resulting from the moving surfaces observed through out the test program.

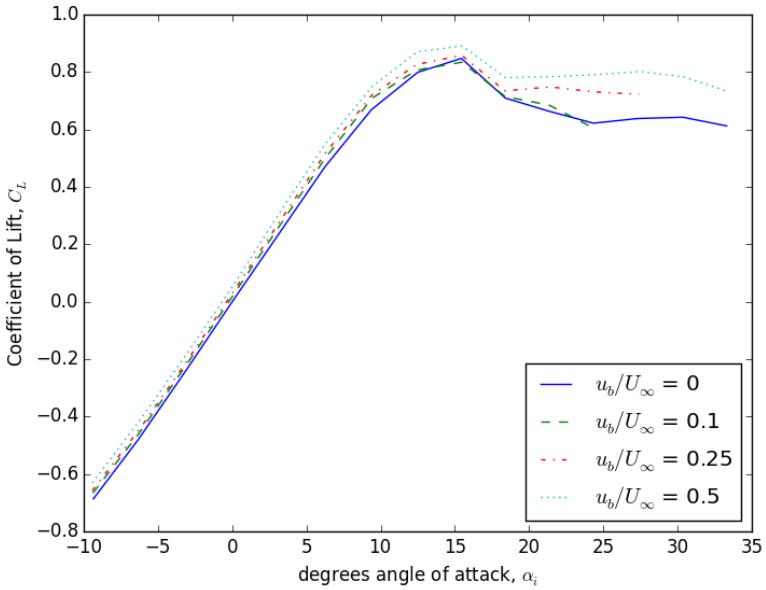

Figure 10.10: Aspect Ratio 9, Inner Belts, Lift Coefficient, $q = 5$

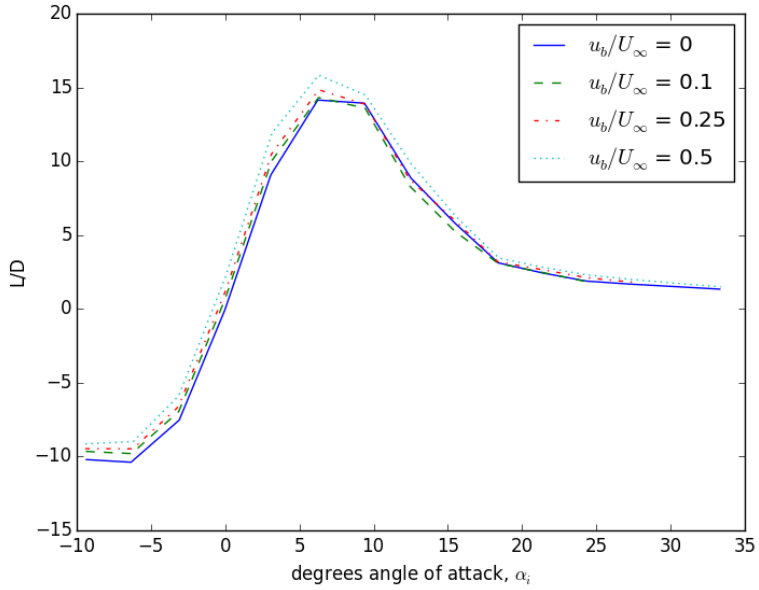

Figure 10.11: Aspect Ratio 9, Inner Belts, L/D, $q = 5$

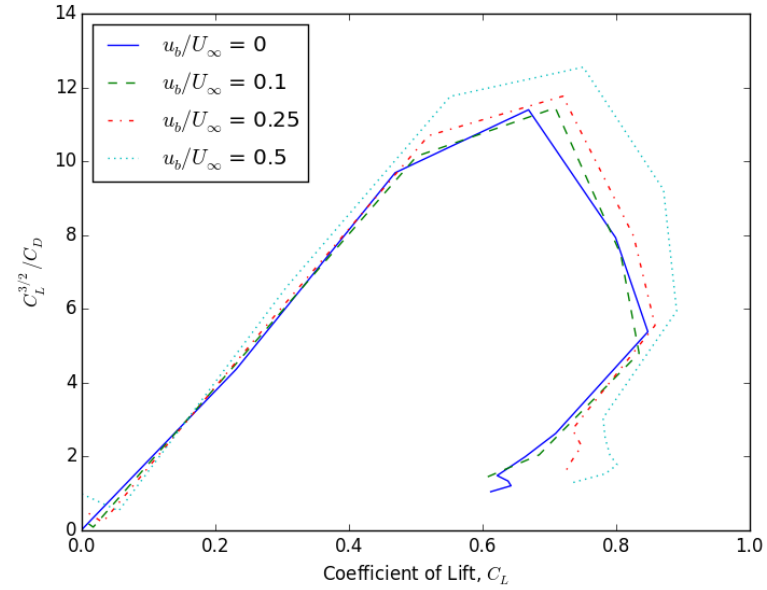

Figure 10.12: Aspect Ratio 9, Inner Belts, Endurance Parameter, $q = 5$

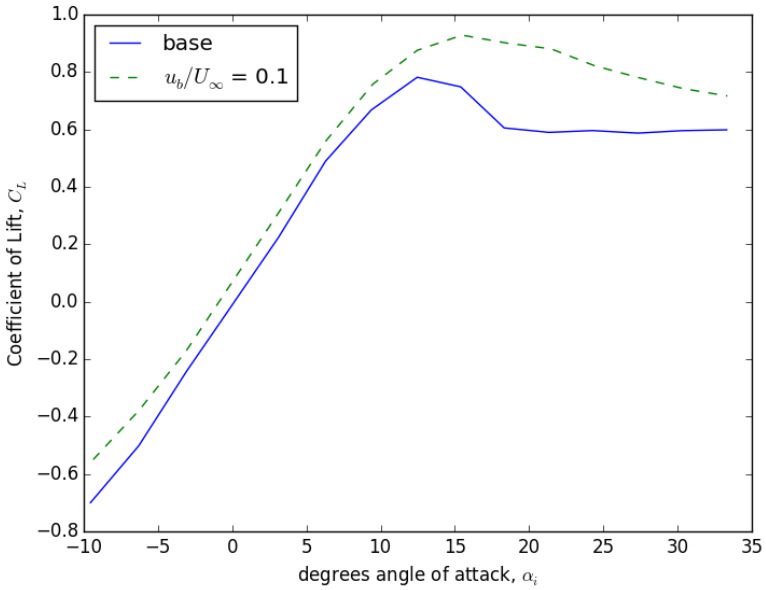

Figure 10.13: Aspect Ratio 9, Full Wing, Lift Coefficient

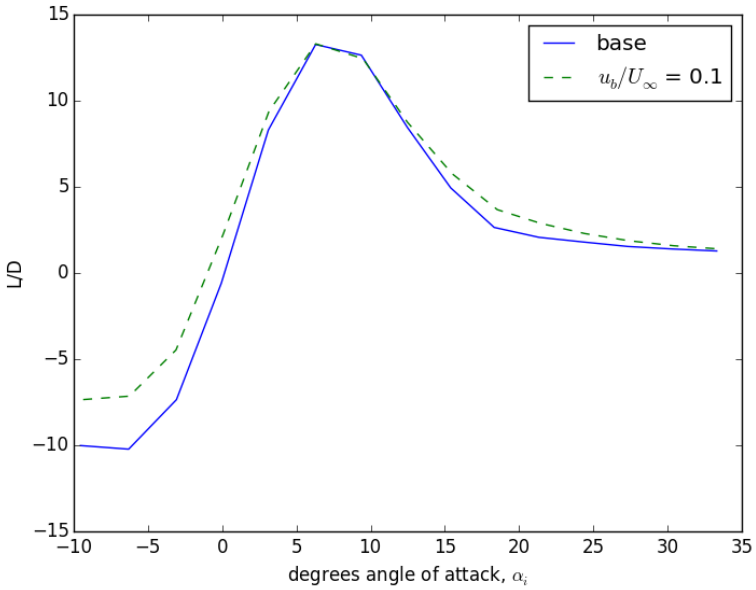

Figure 10.14: Aspect Ratio 9, Full Wing, L/D

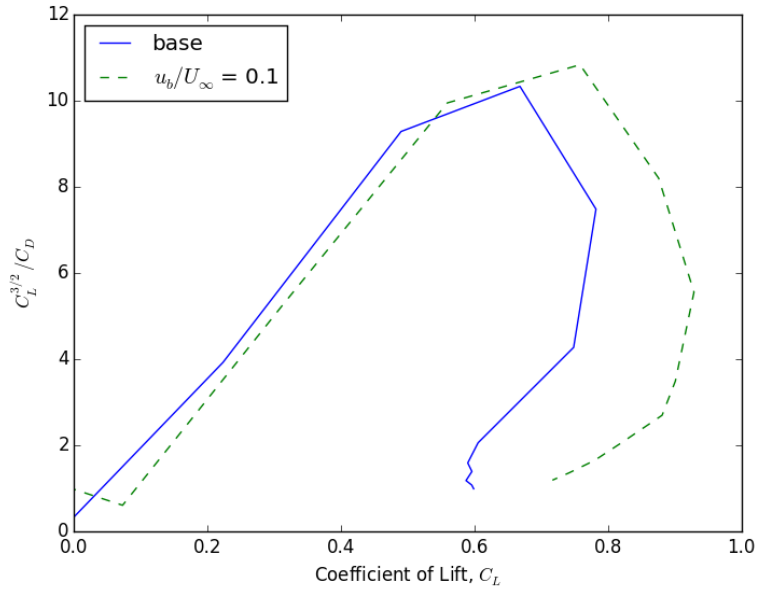

Figure 10.15: Aspect Ratio 9, Full Wing, Endurance Parameter

Chapter 11

CIRCULATION AND INDUCED DRAG

Viewed in terms of the Kutta-Joukowski theorem ($L = \rho_\infty V_\infty \Gamma$), the additional lift observed by the activated moving surfaces is a direct measure of the contribution to the total circulation due to the system. Using the data from the AR-5 and the AR-9 inner belt configurations, Figures 9.5 and 10.7, subtracting the C_L values for the static belt, $u_s/U_o = 0$, from each velocity ratio data set, the net additional circulation due the moving surfaces can be evaluated. This is shown in Figures 11.1 and 11.2. In both figures, the increase in circulation due to the belts is seen to remain consistent through the linear portion of the lift curve. For the AR-5 configuration, the moving surface develops additional circulation in the extended lift region, where the stall has been delayed. For the AR-9 configuration, the increased circulation remains nearly constant through the stall. In both cases, once the wing has stalled, the contribution to circulation of the moving surface begins to wane; more so for the lower velocity ratios.

Similarly, subtracting the static belt C_D data from circulation test run data, the net change in drag due to the belts can be observed. For the two sets of data this is shown in Figures 11.3 and 11.4. For the AR-5 configuration, the presence of the belts, in the $u_s/U_o = 0$ state, increases C_D from 24% at zero degrees angle of attack to 16% at twelve. With the moving surfaces activated, drag can be observed to increases with both velocity ratio and angle of attack through the linear region of the lift curve; suggesting an increase in induced drag. For the AR-9 configuration, the increase in drag due to the moving surfaces, limited to the inner belts, is only with velocity ratio and remains generally flat and consistent with the low angle of attack AR-5 data.

To investigate the increase of drag at higher angles of attack for the AR-5 configuration,

an additional set of tests were conducted with the wing tips replaced with flat plates. The size and shape of the plates corresponded to a 2.5× maximum thickness of the airfoil section. Figure 11.7 show the endplates installed on the model in the wind tunnel. Only data for $u_s/U_o = 0.5$ and $u_s/U_o = 1.0$ was collected. Figure 11.5 shows that the C_L data for both with and with out the end plates is nearly identical, especially for the $u_s/U_o = 0.5$ case. In particular, increasing surface velocity ratio produces the same increase in circulation, or lift, for both cases, with and without the endplates.

Figure 11.6 compares the net drag for both the end plate and non-endplate configurations. The end plates reduced the increase of drag at moderate angles of attack, six to 12 degrees, by nearly 30% for the higher velocity ratio, $u_s/U_o = 1$. The same trend is evident, albeit barely, at the lower velocity ratio.

The net effect of this is an incremental induced drag increase with velocity ratio and angle of attack for the non-endplate wing; suggesting flow around the wing-tip. With the moving surfaces confined to the inner portion of AR-9 wing, the flatter drag profile suggests the extra static span diffuses the additional vorticity shed at the wing tips.

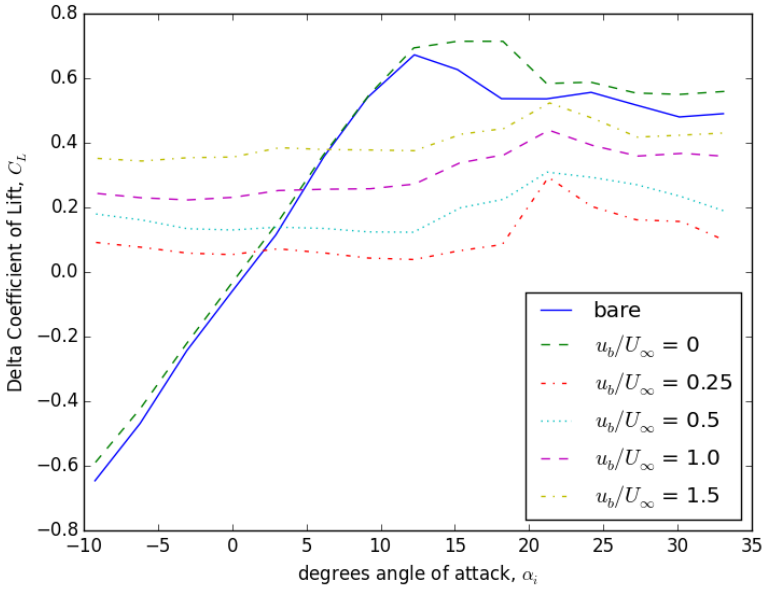

Figure 11.1: Net Circulation, AR-5

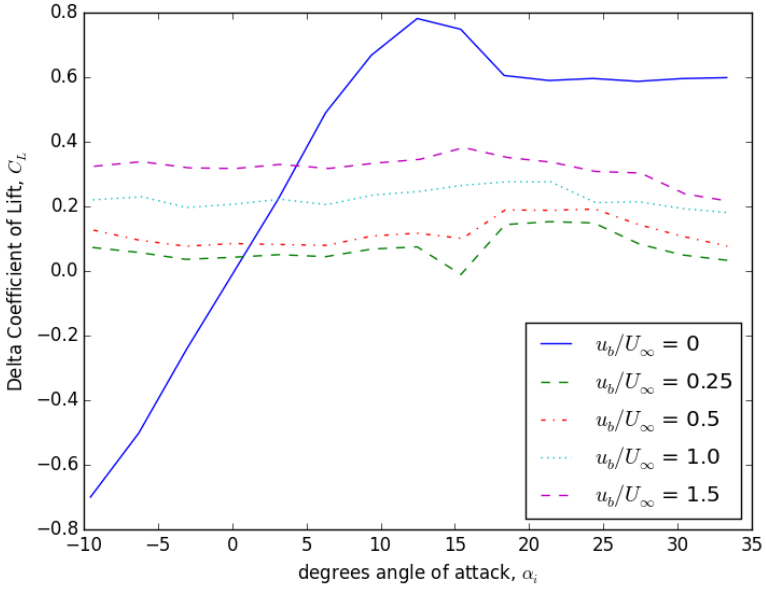

Figure 11.2: Net Circulation, AR-9

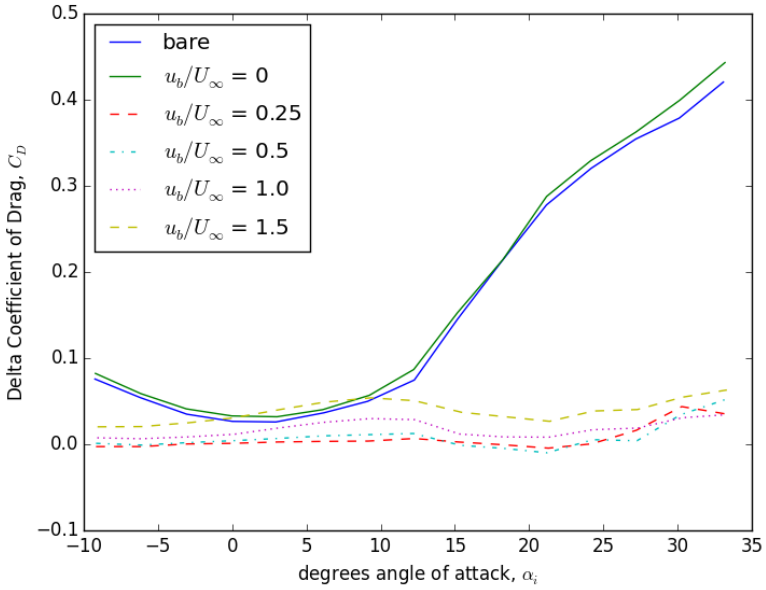

Figure 11.3: Net Induced Drag, AR-5

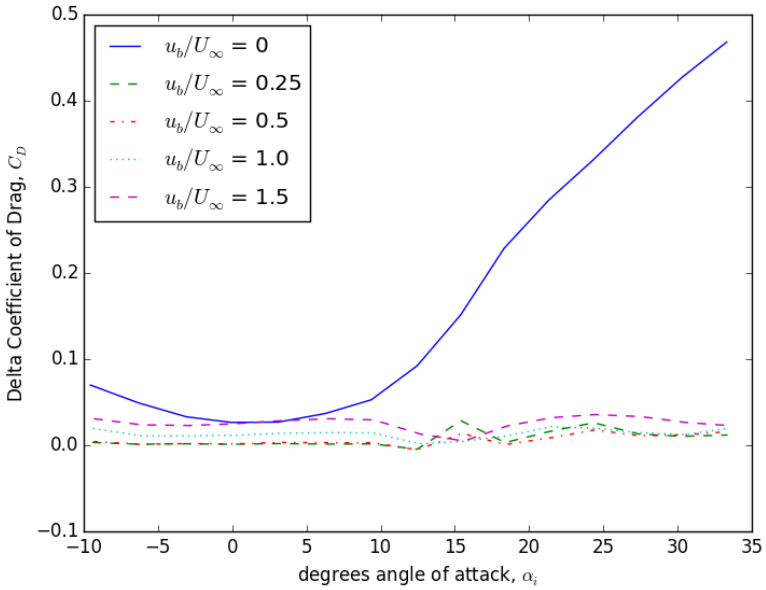

Figure 11.4: Net Induced Drag, AR-9

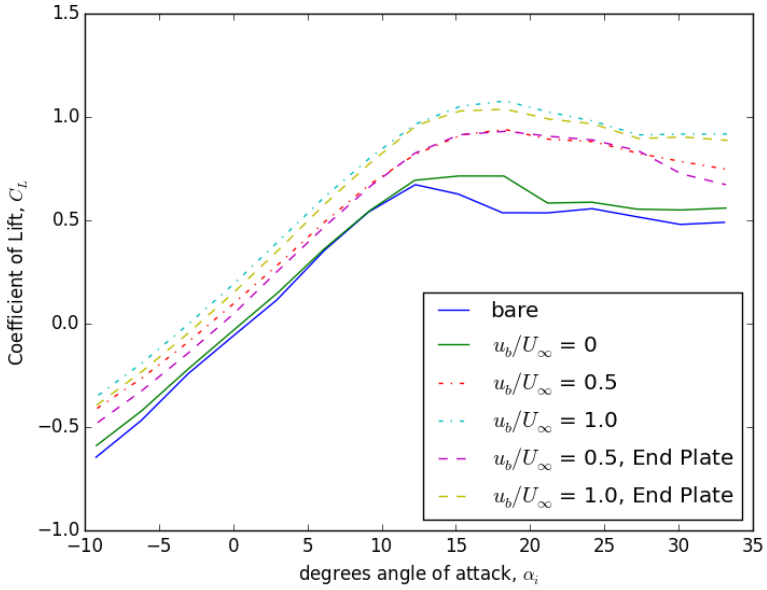

Figure 11.5: End Plates, Lift

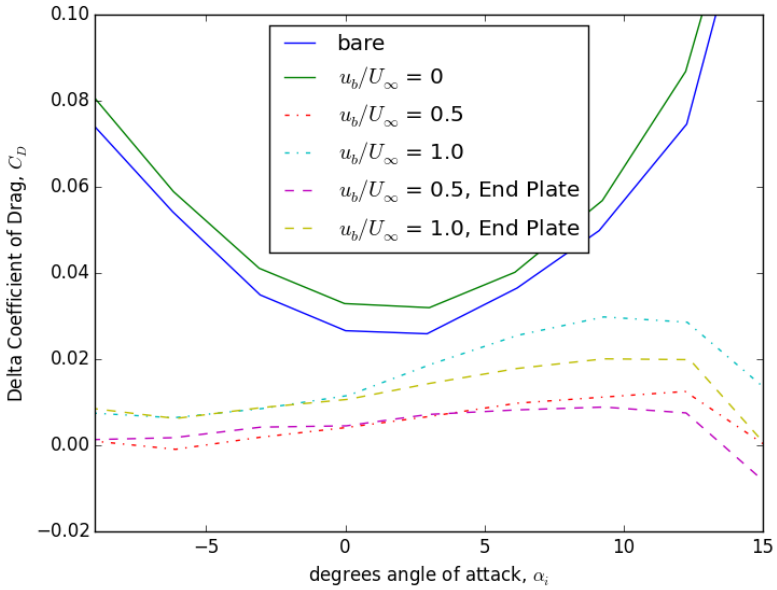

Figure 11.6: End Plate, Net Induced Drag

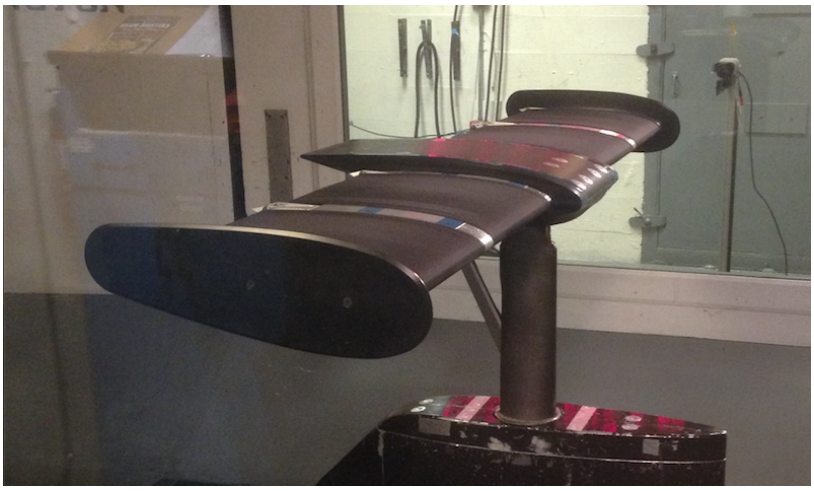

Figure 11.7: AR-5 with End Plates

Chapter 12

RESULTS AND CONCLUSIONS

12.1 Summary of Results

Water tunnel visualization studies and wind tunnel testing provided valuable insights into the fluid mechanics, aerodynamics, and efficacy of moving surface boundary layer and circulation control surfaces for finite wings at moderate Reynolds number. A brief summary of the key results from these test are outlined below:

- The moving surfaces were effective in increasing both C_L and endurance parameter $C_L^{3/2}/C_D$. Increased lift, created by the moving surfaces, remained essentially constant with angle-of-attack up to stall.

- The maximum improvement in endurance parameter was observed at a velocity ratio of $u_s/U_o = 1$. Incremental improvement in the endurance parameter begins to decline after a velocity ratio of one, although C_L continues to increase, suggesting an optimal system effectiveness between $u_s/U_o = 1$ and 1.5.

- Drag increased incrementally with velocity ratio. For full span moving surfaces induced drag also increases with angle of attack.

- The moving surface changes the stall characteristics of the wings when they cover the full span. On the half span tests, the stall profiles of the base wing were maintained.

- Water tunnel images show an apparent stagnation point established at the nadir of the trailing edge cylinder at velocity ratios at and above one. Once established at this

point, further increases in the velocity ratio did not appear to affect the stagnation point's location.

- Downwash was observed to increase slowly up to a velocity ratio $u_s/U_o = 1$ then became more pronounced.

- An observable change was noted it the effectiveness of the leading edge cylinders at Reynolds number of 5×10^5 and above. Despite the low surface velocity ratios tested this suggests that a critical Reynolds number exists for the effectiveness of the leading edge cylinders.[1]

- Leading edge cylinder tests support previous investigations that found surface velocity ratios need to be several times greater than the free stream, requiring high rotation rates, to appreciably influence the aerodynamics of the wing.

- Wind tunnel data for the larger diameter trailing edge cylinder was inconclusive resulting from too many changes to the system: belts, trailing edge axles, and the rear cylinder diameter.

12.2 System and Testing Notes

- Design, materials, and fabrication of the belts are the limiting elements for this type of system and a positive drive system for the belts, opposed to a friction drive, is essential for repeatability, reliability, and any possibility of actual system control.

- The wind tunnel test program executed was overly aggressive in scope. It would have been more effective to have initiated testing with fewer objectives and include more cases of repeated test runs. Having planned for a second set of wind tunnel tests would have been useful.

---

[1]This roughly, or coincidentally, corresponds to the critical Reynolds number for the transition of drag on a sphere 5×10^5. [53]

12.3 Conclusions

- The moving surface system is capable of providing utility for smaller Tier-1 UAVs, operating below a Reynolds Number of 3×10^5. It is especially encouraging for configurations that includes only the inner half of the wing's span, as demonstrated with the AR-9 tests.

- For the moving surface concept tested, it is likely that application of the system to only the pressure recovery side of the upper surface would be sufficient to provide the bulk of the lift and endurance benefits observed. Energizing the boundary layer in this region is all that would be required to delay separation and enhance high-lift performance.

- Practical applications for the moving surface concept, either with belts or cylinders, are not likely for high speed or large systems due to Reynolds number effects and the underlying mechanics required to support the kinematics for surfaces to be effective.

BIBLIOGRAPHY

[1] *Airplane Flying Handbook*. Number FAA-H-8083-3. Federal Aviation Administration, 1999.

[2] *World Unmanned Aerial Vehicle Systems*. Teal Group, 2014.

[3] Ira H. Abbot, Albert E. Von Doenhoff, and Louis S. Silvers Jr. Summary of airfoil data. Technical Report 824, NACA, 1945.

[4] Ira H. Abbot and Albert Edward Von Doenhoff. *Theory of Wing Sections: Including a Summary of Airfoil Data*. Dover, 1949.

[5] Federal Aviation Administration. Integration of civil Unmanned Aircraft Systems (UAS) in the National Airspace System (NAS) roadmap, 2013.

[6] Ahmed Z. Al-Garni, Abdullah M. Al-Garni, Saad A. Ahmed, and Ahmet Z. Sahin. Flow control for an airfoil with leading-edge rotation: An experimental study. *Journal of Aircraft*, 37(4):617, July - August 2000.

[7] John D Anderson. *Introduction to Flight*. McGraw Hill, 1951.

[8] John D Anderson. Ludwig prandtl's boundary layer. *Physics Today*, December 2005.

[9] K. P. Angele and B. Muhammad-Klingmann. The effect of stream-wise vortices on the turbulence structure of a separating layer. *European Journal of Fluid Mechanics B/Fluids*, 24:539–554, 2005.

[10] H. Atik, C. Y. Kim, L. L. van Dommelen, and J. D. A. Walker. Boundary-layer separation control on a thin airfoil using local suction. *Journal of Fluid Mechanics*, 535:415–443, 2005.

[11] Giulio Avanzini and Fabrizio Giulietti. Maximum range for battery aircraft. *Journal of Aircraft*, 50(1), 2013.

[12] David Bloor. *The Enigma of the Airfoil*. The University of Chicago Press, 2011.

[13] M. S. H. Boutilier and S. Yarusevych. Parametric study of separation and transition characteristics over an airfoil at low Reynolds numbers. *Experiments in Fluids*, 52:1491–1503, 2012.

[14] John A. Burns and Yuh-Roung Ou. Effect of rotation rate on the forces of a rotating cylinder: simulation and control. Contractor Report 191442, NASA, 1993.

[15] D. R. Cichy, J. W. Harris, and J. K. MacKay. Flight tests of a rotating cylinder flap on a North American Rockwell YOV-10 aircraft. Technical Report NASA CR-2135, NASA, 1972.

[16] John M. Cimbala, Hassan M. Nagib, and Anatol Roshko. Large structure in the far wakes of two-dimensional bluff bodies. *Journal of Fluid Mechanics*, 190:265–298, 1988.

[17] Martin E. Dempsey. U.S. Army Unmanned Aircraft Systems Roadmap 2010-2035, 2010.

[18] Les Dorr. F faa approves first commercial uas flights over land. Press Release, June 2014.

[19] J. Driver and D. W. Zingg. Optimized natural-laminar-flow airfoils. *Collection of Technical Papers - 44th AIAA Aerospace Sciences Meeting*, 5, 2006.

[20] Daniel Favier, Christian Maresca, Wolfgang Geisser, Marcellin Nsi Mba, and Patrick Sainton. Boundary-layer control by hydrophilic surfaces. *Journal of Aircraft*, 45(4), July - August 2008.

[21] Alexandre Favre. *Contribution a l'etude experimentale des mouvements hydrodynamiques a deux dimensions*. PhD thesis, L'Universite de Paris, November 1938.

[22] Robert W. Fox and Alan T. McDonald. *Introduction to Fluid Mechanics*. John Wiley and Sons, 3 edition, 1985.

[23] George Gerhab and Charles Eastlake. Boundary layer control on airfoils. *The Physics Teacher*, 29(150), 1991.

[24] M. B. Glauret. The flow past a rapidly rotating circular cylinder. *Proceedings of the Royal Society of London. Series A, Mathematical and Physical Sciences*, 242(1228):108–115, Oct 1957.

[25] John E. Green. Laminar flow control - Back to the future? *38th Fluid Dynamics Conference and Exhibit*, (AIAA 2008-3738), 2008.

[26] Frederick G. Harmon, Andrew A. Frank, and Jean-Jacques Chattot. Conceptual design and simulation of a small hybrid-electric unmanned aerial vehicle. *Journal of Aircraft*, 43(5), September-October 2006.

[27] Eastman N. Jacobs, Kenneth E. Ward, and Robert M. Pinkerton. The characteristics of 78 related airfoil sections from test in the variable-density wind tunnel. Technical Report 460, NACA, 1933.

[28] Forrester T. Johnson, Edward N. Tinoco, and N. Jong Yu. Thirty years of development and application of CFD at Boeing Commercial Airplanes. *19th AIAA Computational Fluid Dynamics Conference*, (AIAA 2003-3439), June 2003.

[29] Robert T. Jones and Milton B. Ames. Wind-tunnel investigation of control-surface characteristics V - the use of a beveled trailing edge to reduce the hinge moment of a control surface. War Report L-464, NACA, 1942.

[30] Ronald D. Joslin. Aircraft laminar flow control. *Annual Review of Fluid Mechanics*, 30, 1998.

[31] Ronald D. Joslin. Overview of laminar flow control. Technical Report NASA/TP-1998-208705, NASA, October 1998.

[32] H. Page Hoggard Jr. Wind-tunnel investigation of control-surface characteristics X - 30-percent-chord plain flap with straight contour on the NACA 0015 airfoil. War Report L-366, NACA, September 1942.

[33] H. Page Hoggard Jr. Wind-tunnnel investigation of control-surface characteristics XII - various cover-plate alignments on the NACA 0015 airfoil with a 30-percent-chord flap and large sealed internal balance. War Report L-511, NACA, January 1943.

[34] Arnold M. Kuethe and Chuen-Yen Chow. *Foundations of Aerodynamics*. John Wiley and Sons, 4 edition, 1985.

[35] D. Lengani, D. Simoni, M. Ubaldi, and P. Zunino. Turbulent boundary layer separation control and loss evaluation of low profile vortex generators. *Experimental Thermal and Fluid Sciences*, 35:1505–1513, 2011.

[36] R. Martinez-Val and E. Perez. Aeronautics and astronautics: recent progress and future trends. *Proc. IMechE., Part C: Mechanical Engineering Science*, 223, 2009.

[37] K. W. McAlister and R. K. Takahashi. NACA 0015 wing pressure and trailing vortex measurements. Techincal Paper 3151, NASA, November 1991.

[38] Richard Von Mises. *Theory of Flight*. Dover, 1945.

[39] V. J. Modi. Moving surface boundary-layer control: A review. *Journal of Fluids and Structures*, (11), 1997.

[40] V. J. Modi, M. S. U. K. Fernando, and T. Yokomizo. Moving surface boundary-layer control as applied to two-dimensional and three-dimensional bluff bodies. *Journal of Wind Engineering and Industrial Aerodynamics*, 38, 1991.

[41] V. J. Modi, S. R. Munshi, and G. Bandyopadhyay. High-performance airfoil with moving surface boundary-layer control. *Journal of Aircraft*, 35(4), July - August 1998.

[42] V. J. Modi, S. R. Munshi, G. Bandyopadhyay, and T. Yokomizo. Multielement systems with moving surface boundary-layer control: Analysis and validation. *Fourteenth International Conference on Numerical Methods in Fluid Dynamics*, 453, 1995.

[43] V. J. Modi, J. L. C. Sun, T. Akutsu, P. Lake, K. McMilan, P. G. Swinton, and D. Mullins. Moving-surface boundary-layer control for aircraft operations at high incidence. *Journal of Aircraft*, 18(11):963, 1981.

[44] V. J. Modi and T. Yokomizo. On the boundary-layer control through momentum injection: Studies and applications. *Sadhana*, 19, 1994.

[45] Farzad Mokhtarian. *Fluid dynamics of airfoils with moving surface boundary-layer control*. PhD thesis, Univeristy of British Columbia, 1988.

[46] Farzad Mokhtarian and V. J. Modi. Fluid dynamics of airfoils with moving surface boundary-layer control. Technical Report 86-2184, AIAA, 1988.

[47] S. R. Munshi, V. J. Modi, and T. Yokomizo. Fluid dynamics of flat plates and rectangular prisms in the presence of moving surface boundary-layer control. *Journal of Wind Engineering and Industrial Aerodynamics*, 79, 1999.

[48] Jack N. Nielsen, editor. *Proceedings of the Circulation Control Workshop 1986*, number 2432. NASA, February 1986.

[49] Ludwig Prandtl. *Essentials of fluid dynamics*. Blackie and Son, 1952.

[50] Ludwig Prandtl and O. G. Tietjens. *Applied Hydro- and Aeromechanics*. Dover, 1934.

[51] Ludwig Prandtl and O. G. Tietjens. *Fundamentals of Hydro and Aeromechanics*. Dover, 1934.

[52] Lord Rayleigh. On the irregular flight of a tennis ball. *Messenger of Mathematics*, 7, 1877.

[53] Anatol Roshko. Experiments on the flow past a circular cylinder at very high Reynolds number. *Journal of Fluid Mechanics*, page 345, 1960.

[54] Hermann L. Schlicting. *Boundary Layer Theory*. McGraw Hill, 7 edition, 1951, 1979.

[55] Richard I. Sears and Clarence L. Gillis. Wind-tunnel investigation of control-surface characteristics VIII - a large aerodynamic balance of two nose shapes used with a 30-percent-chord flap on a NACA 0015 airfoil. War Report L-378, NACA, 1942.

[56] Richard I. Sears and H. Page Hoggard Jr. Wind-tunnel investigation of control-surface characteristics VII - medium aerodynamic balance of two nose shapes used with a 30-percent-chord flap on an NACA 0015 airfoil. War Report L-448, NACA, 1942.

[57] Richard I. Sears and H. Page Hoggard Jr. Wind-tunnel investigation of control-surface characteristics XI - various large overhang and internal-type aerodynamic balances for a straight-contour flap on the NACA 0015 airfoil. War Report L-447, NACA, January 1943.

[58] Richard I. Sears and Robert B. Liddell. Wind-tunnel investigation of control-surface characteristics VI - 30-percent-chord plain flap on the NACA 0015 airfoil. War Report L-454, NACA, 1942.

[59] Jost Seifrert. A review of the magnus effect in aeronautics. *Progress in Aerospace Sciences*, 55:17–45, 2012.

[60] S. N. Singh, L. Rai, P. Puri, and A. Bhatnagar. Effect of moving surface on aerodynamic drag of road vehicles. *Proceedings of the Institution of Mechanical Engineers, Part D: Journal of Automobile Engineering*, 219, 2005.

[61] W. M. Swanson. The magnus effect: A summary of investigations to date. *Journal of Basic Engineering*, September 1961.

[62] Itiro Tani. History of boundary layer theory. *Ann. Rev. Fluid Mech.*, 9:87–111, 1977.

[63] J. S. Tennant, W. S. Johnson, and A. Korthapalli. Rotating cylinder for circulation control on an airfoil. *AIAA Journal of Hydronautics*, 1976.

[64] Theodore Theodorsen. Theory of wing wections of arbitrary shape. Report 411, NACA, October 1931.

[65] Theodore Theodorsen and I. E. Garrick. General potential theory of arbitrary wing sections. Technical Report 452, NACA.

[66] A. Thom. Experiments on the flow past a rotating cylinder. Report and Memoranda 1410, Aeronautical Research Committee, March 1931.

[67] A. Thom. Effect of discs on the air forces on a rotating cylinder. Report and Memoranda 1623, Aeronautical Research Committee, 1934.

[68] Brian Thwaites. *Incompressible Aerodynamics*. Oxford Universtiy Press, 1960.

[69] P.T. Tokumaru and P.E. Dimotakis. The lift of a cylinder executing rotary motions in a uniform flow. *Journal of Fluid Mechanics*, 255:1–10, 1993.

[70] Lance W. Traub. Range and endurance estimates for battery-powered aircraft. *Journal of Aircraft*, 48(2):703–707, 2015/08/12 2011.

[71] Univesity of Washington Aeronautical Laboratory. *Techincal Guide for the Kirsten Wind Tunnel*, 2002.

[72] Alexander Vorobiev, R. M. Rennie, and Eric J. Jumper. Lift enhancement by plasma actuators at low reynolds number. *Journal of Aircraft*, 50(1), 2013.

[73] Ira J. Walker. Active boundary-layer separation control on a multi-element airfoil. *Journal of Aircraft*, 43(5):1579, September-October 2006.

[74] James A. Weiberg and Stanley O. Dickinson. Large-scale wind-tunnel tests of an airplane model with four propellers and rotating cylinder flaps. Technical Note NASA TN D-5742, NASA, April 1970.

[75] James A. Weiberg and Berl Gamse. Large-scale wind-tunnel tests of an airplane model with two propellers and rotating cylinder flaps. Technical Note NASA TN D-4489, NASA, March 1968.

[76] E. B. Wolff. Preliminary investigation of the effect of a rotating cylinder in a wing. Technical Memorandum 307, NACA, March 1925.

[77] E. B. Wolff and C. Koning. Test for determining the effect of a rotating cylinder fitted into the leading edge of an airplane wing. Technical Memorandum 354, NACA, 1926.

[78] E.B. Wolff and C. Koning. Discussion of the results of the boundary layer tests of an airfoil fitted with a rotary cylinder. Technical Memorandum 424, NACA, January 1927.

[79] S. Yarusevych, P. E. Sullivan, and J. G. Kawaii. Airfoil boundary-separation and control at low Reynolds number. *Experiments in Fluids*, 38:545–547, 2005.

Appendix A
WIND TUNNEL DATA

This Appendix provides wind tunnel data in tabular form for all tests discussed in this dissertation and several others that were not. In total 104 test runs were executed. Not all the data was valid data due to issues associated with the test model, those test runs have been excluded from the data provided here and within the discussion.

A.1 Definitions

The definitions for the data column headers are provided below:

RUN The sequential number of the test run as executed

TP The test point for collection of force data with the balance

ALPHAC The angle of attack of the model for the test point

QC The dynamic pressure, q, in psf

RE Reynolds number based upon chord

CLSA Coefficient of Lift in the Stability Axis

CDSA Coefficient of Drag in the Stability Axis

CYSA Coefficient of Yaw in the Stability Axis

CMSA25 Pitching Moment Coefficient

CNSA25 Yawing Moment Coefficient

CRSA25 Rolling Moment Coefficient

CL32CD The Endurance Parameter $C_L^{3/2}/C_D$.

VRATIO Surface velocity ratio, u_s/U_o or u_c/U_o

A.2 AR-5, Bare Airfoil

RUN	TP	ALPHAC	QC	RE	CLSA	CDSA	CYSA	CMSA25	CNSA25	CRSA25	CLSA32	CL32CD	VRATIO
2	2	-9.244	1.0167	186826	-0.64634	0.07573	0.00568	-0.00824	-0.00102	-0.00049	0.51963	6.8612	N/A
2	3	-6.197	1.0238	187501	-0.46843	0.0542	0.00512	-0.00684	-0.00116	-0.00039	0.3206	5.9156	N/A
2	4	-3.057	1.0157	186779	-0.24349	0.03491	0.00379	-0.01294	-0.00121	-0.00157	0.12015	3.4416	N/A
2	5	0.011	1.0142	186663	-0.05888	0.0266	0.00343	-0.00311	-0.00127	0.00068	0.01429	0.53705	N/A
2	6	2.938	1.009	186209	0.11477	0.02589	0.0054	0.00716	-0.00139	0.0004	0.03888	1.5018	N/A
2	7	6.173	0.99936	185334	0.35647	0.03651	0.0043	0.00507	-0.00142	-0.00105	0.21283	5.829	N/A
2	8	9.121	0.99365	184821	0.54041	0.04984	0.00038	0.01001	-0.00147	-0.00093	0.39727	7.9716	N/A
2	9	12.268	0.99121	184617	0.6724	0.07459	0.001	0.02093	-0.00149	-0.0002	0.55137	7.3918	N/A
2	10	15.174	1.0075	186146	0.62668	0.14513	-0.00415	-0.0133	0.00504	0.02199	0.49609	3.4184	N/A
2	11	18.139	1.0148	186840	0.53663	0.21209	-0.00037	-0.04566	-0.00123	0.00298	0.39311	1.8536	N/A
2	12	21.174	1.0255	187836	0.53603	0.27792	0.00184	-0.06016	-0.00227	0.00044	0.39245	1.4121	N/A
2	13	24.179	1.0221	187539	0.55621	0.32037	-0.00003	-0.06125	-0.00184	-0.00014	0.41482	1.2948	N/A
2	14	27.173	1.0295	188237	0.51735	0.35426	-0.00429	-0.06929	-0.00122	-0.00693	0.37211	1.0504	N/A
2	15	30.122	1.0421	189396	0.47998	0.37876	-0.00447	-0.0686	-0.00214	0.00082	0.33253	0.87794	N/A
2	16	33.087	1.0513	190248	0.49015	0.42053	0.00096	-0.07822	-0.00168	-0.0004	0.34316	0.81601	N/A

RUN	TP	ALPHAC	QC	RE	CLSA	CDSA	CYSA	CMSA25	CNSA25	CRSA25	CLSA32	CL32CD	VRATIO
3	1	-9.188	4.9967	415562	-0.60256	0.06981	-0.0112	-0.00772	-0.00004	0.00222	0.46774	6.7001	N/A
3	2	-6.15	5.0125	416265	-0.41571	0.04621	-0.01129	-0.00875	0.00001	0.00386	0.26803	5.8002	N/A
3	3	-3.1	5.0222	416699	-0.21764	0.03026	-0.00984	-0.00565	-0.00007	0.00278	0.10153	3.3549	N/A
3	4	0.023	5.0516	417979	-0.02441	0.02048	0.00944	0.00163	-0.00016	0.00134	0.00381	0.18629	N/A
3	5	2.974	5.0583	418291	0.16706	0.01985	0.00823	0.00744	-0.00025	0.00103	0.06828	3.4402	N/A
3	6	6.172	5.0598	418402	0.37092	0.02768	0.00883	0.01658	-0.00039	0.00189	0.22591	8.1608	N/A
3	7	9.137	5.0448	417822	0.56635	0.0429	0.00892	0.02028	-0.00043	0.00106	0.42622	9.93497	N/A
3	8	12.255	5.048	417986	0.73428	0.0663	0.00923	0.02608	-0.00039	0.00046	0.6292	9.49005	N/A
3	9	15.171	5.0376	417591	0.72832	0.13765	0.0074	-0.00869	0.00639	0.01905	0.62157	4.5154	N/A
3	10	18.249	5.0305	417330	0.61805	0.20965	0.00655	-0.0423	0.00093	0.00911	0.48588	2.3176	N/A
3	11	21.17	5.1192	421028	0.61576	0.24817	0.00706	-0.04682	0.00026	0.00194	0.48319	1.9471	N/A
3	12	24.175	5.1794	423530	0.63488	0.32414	0.00213	-0.06647	-0.00052	0.00029	0.50587	1.5606	N/A
3	13	27.193	5.1391	421897	0.65555	0.36989	0.00563	-0.07318	-0.00085	-0.00075	0.53078	1.435	N/A
3	14	30.234	5.1909	424042	0.65097	0.409	0.00733	-0.07875	0.00002	-0.00215	0.52521	1.2842	N/A
3	15	33.136	5.3071	428786	0.5905	0.43973	-0.00023	-0.0807	-0.00204	0.00542	0.45376	1.0319	N/A

RUN	TP	ALPHAC	QC	RE	CLSA	CDSA	CYSA	CMSA25	CNSA25	CRSA25	CLSA32	CL32CD	VRATIO
4	1	-9.213	10.16	593799	-0.58926	0.06568	0.00795	-0.00291	0.00034	0.00236	0.45234	6.8867	N/A
4	2	-6.163	10.017	589615	-0.40743	0.04222	0.01044	-0.00328	0.00033	0.00283	0.26006	6.1598	N/A
4	3	-3.048	10.065	591043	-0.21386	0.0257	0.00908	-0.0002	0.00012	0.00229	0.0989	3.8477	N/A
4	4	-0.005	10.138	593235	-0.02237	0.01793	0.0064	0.00428	0	0.00177	0.00335	0.18658	N/A
4	5	2.988	10.14	593296	0.17199	0.01735	0.00528	0.00972	-0.00005	0.00133	0.07133	4.11	N/A
4	6	6.177	10.137	593234	0.37662	0.0246	0.0061	0.01875	-0.00018	0.00109	0.23113	9.39588	N/A
4	7	9.158	10.114	592579	0.56658	0.0398	0.00044	0.02492	-0.0002	0.00093	0.42647	10.714	N/A
4	8	12.227	10.131	593083	0.74536	0.06233	-0.00125	0.02958	-0.00018	0.00074	0.6435	10.324	N/A
4	9	15.236	10.149	593634	0.76455	0.13031	0.00434	-0.00207	0.0049	0.01579	0.66851	5.1303	N/A
4	10	18.205	10.146	593554	0.72054	0.1897	0.00248	-0.02722	0.00492	0.02848	0.61163	3.2241	N/A
4	11	21.235	10.095	592071	0.641	0.24933	0.00447	-0.0462	-0.00039	-0.00008	0.5132	2.0583	N/A
4	12	24.192	10.339	599195	0.67286	0.28943	0.00509	-0.0514	-0.00061	-0.00103	0.55194	1.907	N/A
4	13	27.214	10.403	601054	0.6713	0.37254	0.00356	-0.07301	0.00041	-0.00133	0.55002	1.4764	N/A
4	14	30.17	10.349	599502	0.66523	0.41088	0.00098	-0.07836	0.00031	-0.0023	0.54257	1.3205	N/A
4	15	33.213	10.414	601379	0.65802	0.4514	0.00213	-0.0871	0.00029	-0.00174	0.53377	1.1825	N/A

RUN	TP	ALPHAC	QC	RE	CLSA	CDSA	CYSA	CMSA25	CNSA25	CRSA25	CLSA32	CL32CD	VRATIO
5	1	-9.188	20.122	835815	-0.56867	0.06985	0.00552	-0.00452	0.00124	0.00186	0.42884	6.1398	N/A
5	2	-6.131	20.158	836553	-0.39112	0.04676	0.0068	-0.00265	0.00093	0.00248	0.2446	5.2311	N/A
5	3	-3.126	20.106	835451	-0.20628	0.0293	0.00751	-0.00026	0.00076	0.0014	0.09369	3.1979	N/A
5	4	0.031	20.063	834552	-0.0123	0.0197	0.00507	0.00374	0.00038	0.00134	0.00136	0.06929	N/A
5	5	2.962	20.243	838282	0.17559	0.01896	0.00404	0.00953	0.00022	0.0012	0.07358	3.8796	N/A
5	6	6.188	20.308	839617	0.38288	0.02589	0.00551	0.01845	0.00007	0.00134	0.23692	9.14921	N/A
5	7	9.199	20.203	837412	0.56871	0.03973	0.00703	0.02694	-0.00011	0.00097	0.42889	10.796	N/A
5	8	12.227	20.314	839722	0.74418	0.06076	0.00625	0.03349	-0.00019	0.00116	0.64197	10.566	N/A
5	9	15.254	20.264	838676	0.8308	0.11799	0.00003	0.00933	-0.00038	-0.00137	0.75726	6.4177	N/A
5	10	18.243	20.178	836869	0.75067	0.18958	0.00647	-0.02431	-0.00549	-0.02823	0.65039	3.4307	N/A
5	11	21.209	20.211	837526	0.64455	0.25017	0.00535	-0.04351	-0.00054	0.00009	0.51747	2.0685	N/A
5	12	24.199	20.76	848795	0.68287	0.29354	0.00501	-0.05144	-0.0007	-0.00068	0.5643	1.9224	N/A
5	13	27.14	20.755	848666	0.69881	0.35498	0.01586	-0.06598	-0.00772	-0.00754	0.58417	1.6457	N/A
5	14	30.224	20.735	848235	0.66302	0.40886	0.00342	-0.07531	0.00056	-0.00178	0.53987	1.3204	N/A
5	15	33.216	20.777	849080	0.63889	0.44551	0.0007	-0.08095	-0.00033	0.00003	0.51067	1.1463	N/A

RUN	TP	ALPHAC	QC	RE	CLSA	CDSA	CYSA	CMSA25	CNSA25	CRSA25	CLSA32	CL32CD	VRATIO
6	2	-9.262	40.93	1189473	-0.56876	0.07411	0.00552	-0.00377	0.00183	0.00163	0.42893	5.7876	N/A
6	3	-6.087	40.743	1186706	-0.38618	0.04992	0.00524	-0.00082	0.00149	0.0015	0.23998	4.8071	N/A
6	4	-3.083	40.75	1186775	-0.19999	0.0329	0.00635	0.00145	0.00119	0.00116	0.08944	2.7181	N/A
6	5	0.023	40.647	1185240	-0.00899	0.02307	0.00517	0.00453	0.00086	0.00108	0.00085	0.03695	N/A
6	6	2.982	40.75	1186682	0.17952	0.02107	0.00284	0.00992	0.00052	0.00099	0.07606	3.6096	N/A
6	7	6.148	40.357	1180891	0.38332	0.02794	0.00398	0.01832	0.00027	0.00116	0.23733	8.4956	N/A
6	8	9.206	40.754	1186642	0.57127	0.04164	-0.00027	0.0278	0.00009	0.00107	0.43177	10.369	N/A
6	9	12.259	40.709	1185933	0.74205	0.06242	0.00249	0.03629	-0.00029	0.00129	0.63922	10.241	N/A
6	10	15.254	40.633	1184720	0.81857	0.1207	0.00366	0.01165	-0.00058	0.00083	0.7406	6.1358	N/A
6	11	18.192	40.357	1180598	0.75822	0.1898	0.00127	-0.01894	0.00459	0.0261	0.66023	3.4785	N/A
6	12	21.22	40.555	1183376	0.64915	0.25143	0.00242	-0.03918	-0.00023	-0.00109	0.52302	2.0801	N/A
6	13	24.167	41.049	1190501	0.67977	0.29258	0.00395	-0.0463	-0.00045	-0.00119	0.56045	1.9156	N/A
6	14	27.224	41.379	1195168	0.70201	0.35389	0.01158	-0.05972	-0.00745	-0.00542	0.58819	1.662	N/A
6	15	30.259	41.436	1195880	0.66097	0.40888	0.00008	-0.06963	-0.00091	0.002	0.53736	1.3143	N/A
6	16	33.13	41.92	1202769	0.62753	0.44086	-0.00006	-0.07258	-0.00057	-0.00033	0.49711	1.1276	N/A

A.3 AR-5, Leading Edge Cylinders

RUN	TP	ALPHAC	QC	RE	CLSA	CDSA	CYSA	CMSA25	CNSA25	CRSA25	CLSA32	CL32CD	VRATIO
7	1	-9.28	1.0015	185353	-0.52605	0.08438	0.0047	-0.01505	-0.00021	0.00335	0.38154	4.5217	0.25
7	2	-6.103	1.0069	185861	-0.40381	0.06154	0.00415	-0.00477	-0.00022	0.0005	0.2566	4.17	0.25
7	3	-3.04	1.0145	186586	-0.19831	0.04064	0.00267	-0.01345	-0.00016	-0.00064	0.08831	2.1728	0.25
7	4	-0.037	1.0157	186711	-0.03172	0.03087	0.00225	-0.00342	-0.00006	0.00167	0.00565	0.18296	0.25
7	5	3.012	1.0074	185965	0.14232	0.02951	0.00161	0.00974	-0.00006	-0.00109	0.05369	1.8195	0.25
7	6	6.074	1.0048	185750	0.35079	0.0403	-0.00049	0.01022	-0.00024	-0.00046	0.20776	5.1559	0.25
7	7	9.193	1.0037	185659	0.51872	0.05722	-0.00135	0.01558	-0.00008	-0.00184	0.37359	6.5288	0.25
7	8	12.202	1.0058	185881	0.60425	0.09208	-0.0022	0.01297	0	-0.0029	0.4697	5.101	0.25
7	9	15.155	1.0128	186539	0.57063	0.17837	-0.00298	-0.04208	-0.00039	0.00073	0.43105	2.4166	0.25
7	10	18.137	1.0181	187052	0.55972	0.22475	-0.00479	-0.05305	-0.00511	0.00002	0.41875	1.8632	0.25
7	11	21.228	1.0232	187522	0.56572	0.26872	-0.00086	-0.05672	-0.00623	-0.00485	0.4255	1.5834	0.25
7	12	24.123	1.0301	188168	0.58123	0.31981	0.00334	-0.06327	-0.00089	-0.00363	0.44312	1.3856	0.25
7	13	27.188	1.0352	188655	0.59524	0.36423	-0.00357	-0.07048	-0.00112	-0.00485	0.45923	1.2608	0.25
7	14	30.22	1.0401	189115	0.53999	0.3921	-0.0042	-0.07278	-0.00097	-0.00401	0.39681	1.012	0.25
7	15	33.109	1.0451	189584	0.5327	0.42418	0.00361	-0.07985	0.00224	-0.00795	0.3888	0.91658	0.25

RUN	TP	ALPHAC	QC	RE	CLSA	CDSA	CYSA	CMSA25	CNSA25	CRSA25	CLSA32	CL32CD	VRATIO
8	1	-9.187	1.0058	186139	-0.52095	0.08565	0.00488	-0.01831	-0.00037	0.00277	0.37601	4.39	0.5
8	2	-6.103	1.0089	186437	-0.39789	0.06101	0.00513	-0.01135	-0.00028	0.00047	0.25098	4.1138	0.5
8	3	-3.098	1.0147	186980	-0.19669	0.04245	0.00342	-0.01549	-0.00016	-0.00144	0.08723	2.0549	0.5
8	4	0.01	1.0068	186260	-0.01664	0.03225	0.00337	-0.00711	-0.00022	0.00191	0.00215	0.06654	0.5
8	5	3.038	1.0094	186503	0.16248	0.02982	0.00321	0.00381	-0.00023	0.00023	0.0655	2.1967	0.5
8	6	6.062	1.0037	185984	0.35848	0.0394	-0.00051	0.00956	-0.00013	-0.00023	0.21464	5.447	0.5
8	7	9.195	1.0044	186059	0.53225	0.05614	-0.00171	0.01463	0.00001	-0.00155	0.38831	6.9166	0.5
8	8	12.211	1.0054	186157	0.6396	0.09094	-0.00281	0.00828	0.00045	-0.00159	0.51152	5.6247	0.5
8	9	15.183	1.0099	186577	0.65665	0.15046	-0.00319	-0.02106	-0.00037	0.00129	0.53211	3.5366	0.5
8	10	18.228	1.018	187336	0.65167	0.22215	-0.00294	-0.05032	-0.00142	-0.00156	0.52607	2.3681	0.5
8	11	21.183	1.0307	188509	0.63384	0.26822	-0.00202	-0.0609	-0.0059	-0.00378	0.50463	1.8814	0.5
8	12	24.168	1.0349	188899	0.62667	0.31184	0.00132	-0.06275	-0.00677	-0.00257	0.49608	1.5908	0.5
8	13	27.197	1.0404	189401	0.61097	0.34769	0.01541	-0.0698	-0.003	-0.01988	0.47756	1.3735	0.5
8	14	30.205	1.0336	188785	0.61727	0.40429	-0.00268	-0.07703	0.00001	-0.00968	0.48497	1.1996	0.5
8	15	33.121	1.0454	189934	0.5916	0.43068	0.0002	-0.07898	0.00112	-0.00529	0.45504	1.0566	0.5

RUN	TP	ALPHAC	QC	RE	CLSA	CDSA	CYSA	CMSA25	CNSA25	CRSA25	CLSA32	CL32CD	VRATIO
9	1	-9.199	1.0041	186155	-0.52255	0.08934	0.00495	-0.01513	-0.00058	0.00231	0.37774	4.2282	1
9	2	-6.126	1.0122	186899	-0.38311	0.06275	0.00512	-0.00924	-0.00025	0.00151	0.23713	3.7788	1
9	3	-3.009	1.0138	187050	-0.18228	0.0427	0.00388	-0.01492	-0.00017	-0.00108	0.07782	1.8223	1
9	4	-0.038	1.0049	186240	-0.00872	0.03362	0.00292	-0.00606	-0.00012	0.00072	0.00081	0.02423	1
9	5	3.033	1.0036	186118	0.17402	0.03203	0.00102	0.00432	-0.00023	-0.00107	0.07259	2.2661	1
9	6	6.107	1.0036	186132	0.36068	0.03878	-0.00079	0.0117	-0.00012	-0.00046	0.21661	5.5859	1
9	7	9.159	1.0082	186549	0.5478	0.05461	-0.00176	0.01479	-0.00001	-0.00157	0.40545	7.4246	1
9	8	12.236	1.0104	186758	0.6829	0.08475	-0.00348	0.01728	0.00036	-0.00179	0.56434	6.6589	1
9	9	15.175	1.0105	186776	0.75448	0.138	-0.0041	-0.00659	-0.00058	-0.00208	0.65535	4.7489	1
9	10	18.33	1.0123	186950	0.81673	0.20561	-0.00313	-0.0343	-0.00341	-0.00238	0.7381	3.5899	1
9	11	21.215	1.0201	187668	0.82672	0.26566	-0.00088	-0.05712	-0.00113	0.00026	0.75168	2.8295	1
9	12	24.283	1.0264	188245	0.82145	0.31889	-0.00282	-0.06646	-0.00157	-0.00011	0.74452	2.3347	1
9	13	27.179	1.0332	188875	0.7707	0.35403	-0.0019	-0.07173	-0.00246	-0.00482	0.67659	1.9111	1
9	14	30.245	1.0404	189534	0.68445	0.39747	-0.0047	-0.07918	-0.00176	0.00142	0.56626	1.4247	1
9	15	33.194	1.0422	189810	0.67566	0.43735	0.00005	-0.08312	-0.00063	0.0005	0.55538	1.2699	1

RUN	TP	ALPHAC	QC	RE	CLSA	CDSA	CYSA	CMSA25	CNSA25	CRSA25	CLSA32	CL32CD	VRATIO
10	1	-9.078	1.0043	186261	-0.50875	0.09003	0.00451	-0.01462	-0.00079	0.00171	0.36287	4.0306	1.5
10	2	-6.129	1.0142	187174	-0.37197	0.06229	0.00472	-0.0133	-0.00035	0.00091	0.22686	3.6421	1.5
10	3	-3.16	1.0129	187061	-0.18172	0.04426	0.00376	-0.01379	-0.00018	-0.0011	0.07747	1.7504	1.5
10	4	0.034	1.011	186883	-0.00675	0.03376	0.00316	-0.00433	-0.00014	0.00093	0.00055	0.01642	1.5
10	5	3.062	1.0045	186287	0.1775	0.03186	0.00148	0.005	-0.00014	-0.00073	0.07478	2.3475	1.5
10	6	6.123	0.99859	185738	0.36622	0.03914	-0.00072	0.01388	-0.00018	-0.00018	0.22163	5.6618	1.5
10	7	9.132	0.99796	185682	0.54912	0.05313	-0.0021	0.01803	0.00005	-0.00184	0.40691	7.6589	1.5
10	8	12.242	1.0102	186819	0.6969	0.08444	-0.00387	0.01619	0.00054	0.00006	0.58177	6.8895	1.5
10	9	15.261	1.0147	187246	0.78455	0.13298	-0.00368	-0.00064	0.00011	-0.0001	0.69492	5.2259	1.5
10	10	18.263	1.0153	187301	0.84698	0.19904	-0.00309	-0.02815	-0.00049	-0.0006	0.77948	3.9163	1.5
10	11	21.213	1.016	187364	0.83837	0.2668	-0.00249	-0.0568	-0.00079	0.00035	0.76763	2.8772	1.5
10	12	24.303	1.0229	188013	0.83697	0.3091	-0.00263	-0.06383	-0.00075	-0.00083	0.76571	2.4772	1.5
10	13	27.231	1.0356	189171	0.76558	0.3391	-0.00169	-0.06556	-0.00026	-0.00219	0.66986	1.9754	1.5
10	14	30.2	1.0379	189382	0.79234	0.38702	-0.00116	-0.07283	-0.00126	-0.0012	0.70528	1.8223	1.5
10	15	33.278	1.0375	189346	0.82858	0.44822	0.00204	-0.08932	-0.00114	-0.00708	0.75423	1.6827	1.5

RUN	TP	ALPHAC	QC	RE	CLSA	CDSA	CYSA	CMSA25	CNSA25	CRSA25	CLSA32	CL32CD	VRATIO
11	1	-9.237	5.0083	416445	-0.53062	0.07477	0.00875	-0.01019	-0.00028	0.0026	0.38653	5.1699	0.1
11	2	-6.096	5.023	417062	-0.36763	0.04833	0.01086	-0.01042	0.00008	0.0029	0.2229	4.6124	0.1
11	3	-3.005	5.0204	416971	-0.18793	0.03168	0.01021	-0.00486	0.00011	0.00207	0.08147	2.5719	0.1
11	4	-0.01	5.0742	419208	-0.01447	0.02323	0.0085	0.00224	0.00007	0.00118	0.00174	0.07495	0.1
11	5	3.031	5.0401	417811	0.16346	0.02315	0.00743	0.01024	0	-0.0005	0.06609	2.8543	0.1
11	6	6.095	4.9914	415804	0.33916	0.03148	0.00601	0.01971	-0.00005	-0.00015	0.19752	6.2754	0.1
11	7	9.075	4.9788	415276	0.49563	0.04962	0.0022	0.02622	0.00003	0.00003	0.34893	7.0324	0.1
11	8	12.24	5.0745	419267	0.59409	0.11811	0.00094	-0.00604	-0.00016	-0.00097	0.45791	3.8769	0.1
11	9	15.124	5.0674	418985	0.5731	0.18313	0.00063	-0.03966	-0.00343	-0.00242	0.43386	2.3691	0.1
11	10	18.244	5.0819	419598	0.54657	0.2227	-0.00094	-0.04434	-0.00503	-0.00383	0.40408	1.8145	0.1
11	11	21.154	5.0986	420288	0.57068	0.27292	0.00848	-0.05289	-0.00167	-0.00256	0.43111	1.5796	0.1
11	12	24.128	5.2093	424834	0.60815	0.31837	0.00197	-0.06079	-0.00166	-0.00121	0.47426	1.4896	0.1
11	13	27.224	5.2249	425475	0.63895	0.36577	0.00555	-0.06942	-0.00012	-0.005	0.51073	1.3963	0.1
11	14	30.213	5.1776	423550	0.641	0.40679	0.00771	-0.07635	0.0009	-0.00618	0.5132	1.2616	0.1
11	15	33.135	5.1978	424378	0.57526	0.43837	0.00388	-0.08008	-0.00074	-0.00097	0.43631	0.99529	0.1

RUN	TP	ALPHAC	QC	RE	CLSA	CDSA	CYSA	CMSA25	CNSA25	CRSA25	CLSA32	CL32CD	VRATIO
12	1	-9.2	4.996	416117	-0.52699	0.07595	0.01018	-0.01197	-0.0004	0.0028	0.38256	5.0369	0.25
12	2	-6.103	5.0045	416465	-0.36049	0.04898	0.01064	-0.01136	0.00001	0.00335	0.21644	4.419	0.25
12	3	-3.1	5.0549	418567	-0.19146	0.03238	0.01068	-0.00598	0.00009	0.0023	0.08378	2.5873	0.25
12	4	0.043	5.0607	418808	-0.00644	0.02417	0.00853	0.00132	-0.00001	0.00119	0.00052	0.02141	0.25
12	5	2.971	5.0621	418875	0.16189	0.02287	0.007	0.0099	0.00008	-0.00017	0.06514	2.8484	0.25
12	6	6.128	5.0153	416942	0.34671	0.0314	0.00829	0.01965	-0.00004	-0.0007	0.20415	6.5015	0.25
12	7	9.15	4.9863	415737	0.51111	0.04968	0.00226	0.02488	-0.00008	-0.00107	0.3654	7.3549	0.25
12	8	12.211	5.0221	417229	0.6207	0.09145	0.00169	0.01627	-0.00028	-0.00307	0.48901	5.3476	0.25
12	9	15.152	5.0551	418598	0.62595	0.17437	0.00094	-0.03363	-0.0003	0.00228	0.49524	2.8402	0.25
12	10	18.247	5.0885	419988	0.57064	0.22349	-0.00077	-0.0467	-0.00487	-0.0012	0.43107	1.9288	0.25
12	11	21.158	5.1016	420527	0.59509	0.26218	0.00675	-0.05064	-0.00643	-0.00417	0.45906	1.7509	0.25
12	12	24.2	5.1437	422263	0.62702	0.3192	0.00555	-0.06246	-0.00141	-0.00212	0.4965	1.5554	0.25
12	13	27.173	5.1827	423863	0.65124	0.36578	0.00854	-0.07125	-0.00023	-0.00555	0.52554	1.4368	0.25
12	14	30.224	5.1844	423939	0.66112	0.40939	0.00693	-0.07852	0.00065	-0.00716	0.53755	1.3131	0.25
12	15	33.132	5.2113	425038	0.59263	0.4377	0.00932	-0.07936	0.00012	-0.00548	0.45622	1.0423	0.25

RUN	TP	ALPHAC	QC	RE	CLSA	CDSA	CYSA	CMSA25	CNSA25	CRSA25	CLSA32	CL32CD	VRATIO
13	1	-9.177	5.0345	417809	-0.52061	0.07772	0.00914	-0.0113	-0.00056	0.00291	0.37564	4.8335	0.5
13	2	-6.154	5.0239	417362	-0.36267	0.04964	0.01009	-0.01234	-0.00009	0.00291	0.21841	4.4001	0.5
13	3	-3.014	5.0651	419066	-0.18225	0.03238	0.01003	-0.00534	0.00008	0.00251	0.0778	2.4024	0.5
13	4	-0.009	5.067	419156	-0.00789	0.02471	0.00793	0.00168	0.00012	0.00153	0.0007	0.02837	0.5
13	5	2.95	5.0092	416762	0.17121	0.02359	0.00585	0.00964	0.0001	0.00051	0.07084	3.0034	0.5
13	6	6.119	4.9989	416337	0.35723	0.03114	0.00848	0.01877	0.00018	-0.00057	0.21351	6.8557	0.5
13	7	9.237	5.0245	417400	0.52927	0.04906	0.00902	0.02482	-0.00009	-0.00022	0.38505	7.8491	0.5
13	8	12.158	5.0216	417284	0.63303	0.08979	0.00134	0.01039	-0.0001	-0.00201	0.50366	5.6096	0.5
13	9	15.226	5.0063	416650	0.66784	0.15616	0.00067	-0.02277	-0.00051	-0.0018	0.54577	3.4949	0.5
13	10	18.198	5.0562	418726	0.65352	0.2165	0.00046	-0.04442	-0.00148	0.00294	0.5283	2.4402	0.5
13	11	21.139	5.0906	420142	0.63524	0.26244	-0.00013	-0.05196	-0.00518	-0.00203	0.5063	1.9292	0.5
13	12	24.229	5.0891	420082	0.64978	0.30364	0.00401	-0.05651	-0.00713	-0.00294	0.52378	1.725	0.5
13	13	27.252	5.2234	425592	0.67456	0.36287	0.0097	-0.07077	-0.00125	-0.00398	0.55403	1.5268	0.5
13	14	30.186	5.2101	425052	0.68007	0.40529	0.00634	-0.07856	-0.00024	-0.00753	0.56083	1.3838	0.5
13	15	33.18	5.211	425093	0.61945	0.43772	0.00752	-0.08092	0.00145	-0.01146	0.48753	1.1138	0.5

RUN	TP	ALPHAC	QC	RE	CLSA	CDSA	CYSA	CMSA25	CNSA25	CRSA25	CLSA32	CL32CD	VRATIO
14	2	-9.185	9.97305	587866	-0.53023	0.07269	0.00723	-0.01083	-0.00015	0.00409	0.3861	5.3117	0.1
14	3	-6.074	10.021	589280	-0.36568	0.04698	0.00873	-0.00871	0.00047	0.00396	0.22114	4.707	0.1
14	4	-3.091	10.085	591176	-0.19471	0.03055	0.00795	-0.00274	0.00041	0.00275	0.08592	2.8126	0.1
14	5	0.021	10.152	593180	-0.01166	0.0221	0.00649	0.00311	0.00025	0.00118	0.00126	0.05699	0.1
14	6	2.958	9.94039	586982	0.15806	0.0218	0.00407	0.01085	0.0002	-0.00018	0.06284	2.8823	0.1
14	7	6.132	9.95065	587304	0.34176	0.02964	0.00693	0.02177	0.00013	-0.00076	0.19979	6.7396	0.1
14	8	9.172	10.016	589237	0.50148	0.04822	0.00114	0.02984	0.00011	0.00001	0.35512	7.3652	0.1
14	9	12.239	10.033	589762	0.58571	0.11734	-0.00055	-0.00472	0	0.00064	0.44825	3.8201	0.1
14	10	15.082	10.161	593523	0.57869	0.18086	-0.00155	-0.03599	-0.00399	-0.00116	0.44022	2.434	0.1
14	11	18.236	10.126	592501	0.54298	0.22177	-0.00002	-0.04318	-0.0055	-0.00243	0.4001	1.8042	0.1
14	12	21.157	10.25	596112	0.57329	0.27402	0.00583	-0.05258	-0.00153	-0.00377	0.43408	1.5841	0.1
14	13	24.165	10.261	596439	0.60825	0.31943	0.0062	-0.0603	-0.00081	-0.00331	0.47438	1.4851	0.1
14	14	27.25	10.302	597658	0.64219	0.36806	0.00475	-0.06996	-0.00051	-0.0044	0.51463	1.3982	0.1
14	15	30.168	10.41	600777	0.6453	0.40764	0.00124	-0.0765	0.00037	-0.00585	0.51837	1.2717	0.1
14	16	33.132	10.437	601566	0.61341	0.4442	0.00126	-0.0811	-0.00049	-0.00189	0.48042	1.0815	0.1

RUN	TP	ALPHAC	QC	RE	CLSA	CDSA	CYSA	CMSA25	CNSA25	CRSA25	CLSA32	CL32CD	VRATIO
15	1	-9.256	10.07	590945	-0.52701	0.07477	0.00821	-0.01125	-0.00032	0.00372	0.38259	5.1166	0.25
15	2	-6.082	10.067	590836	-0.36161	0.04756	0.00855	-0.0096	0.00034	0.00398	0.21745	4.5726	0.25
15	3	-3.074	10.109	592080	-0.19431	0.03098	0.00807	-0.00273	0.00042	0.0033	0.08565	2.7649	0.25
15	4	0.019	10.102	591875	-0.01146	0.02281	0.00676	0.00315	0.00025	0.00171	0.00123	0.05375	0.25
15	5	3.006	9.9812	588335	0.16273	0.02159	0.00435	0.01083	0.00026	0.00066	0.06565	3.0401	0.25
15	6	6.032	10.063	590754	0.34059	0.02872	0.00517	0.02084	0.00016	-0.00025	0.19877	6.9215	0.25
15	7	9.246	10.054	590499	0.50713	0.04797	0.00102	0.0278	0.0001	-0.00034	0.36114	7.5282	0.25
15	8	12.195	10.03	589806	0.62216	0.08924	-0.00093	0.0202	-0.00032	-0.00155	0.49074	5.4993	0.25
15	9	15.125	10.052	590447	0.63656	0.17269	-0.00178	-0.02866	-0.00104	0.00224	0.50788	2.941	0.25
15	10	18.226	10.105	591993	0.56621	0.22198	-0.00486	-0.04442	-0.00509	-0.00109	0.42605	1.9193	0.25
15	11	21.166	10.214	595173	0.59199	0.2618	0.00326	-0.0491	-0.00671	-0.00425	0.45548	1.7398	0.25
15	12	24.152	10.241	595942	0.62103	0.31755	0.00737	-0.06087	-0.00168	-0.0019	0.48941	1.5412	0.25
15	13	27.257	10.417	601072	0.64793	0.3665	0.00746	-0.06965	-0.00088	-0.00414	0.52155	1.4231	0.25
15	14	30.179	10.458	602232	0.65859	0.40781	0.00163	-0.07737	-0.00041	-0.00518	0.53447	1.3106	0.25
15	15	33.189	10.367	599606	0.63087	0.44505	0.00249	-0.08123	0.00064	-0.0058	0.50108	1.1259	0.25

RUN	TP	ALPHAC	QC	RE	CLSA	CDSA	CYSA	CMSA25	CNSA25	CRSA25	CLSA32	CL32CD	VRATIO
16	1	-9.095	10.012	589251	-0.51617	0.07516	0.00737	-0.01134	-0.00041	0.00393	0.37085	4.9343	0.5
16	2	-6.18	10.033	589872	-0.3634	0.04938	0.00853	-0.00918	0.00021	0.00357	0.21907	4.4362	0.5
16	3	-3.043	10.106	591998	-0.18837	0.03149	0.00845	-0.00289	0.00041	0.00337	0.08176	2.5962	0.5
16	4	-0.025	10.103	591920	-0.01223	0.02314	0.00656	0.00287	0.00027	0.00173	0.00135	0.05844	0.5
16	5	3.067	10.101	591868	0.17497	0.02217	0.00437	0.00998	0.00027	0.00047	0.07319	3.3009	0.5
16	6	6.114	10.138	592957	0.35346	0.02919	0.00621	0.01956	0.00037	-0.00059	0.21014	7.1984	0.5
16	7	9.171	10.064	590779	0.51624	0.04616	0.00046	0.02715	0.00012	-0.00087	0.37091	8.0346	0.5
16	8	12.148	10.071	590996	0.62723	0.08632	-0.00122	0.01409	-0.00004	-0.00107	0.49676	5.7545	0.5
16	9	15.231	10.075	591090	0.66737	0.15345	-0.00252	-0.01737	-0.00099	-0.00151	0.54519	3.5529	0.5
16	10	18.138	10.048	590319	0.66681	0.21603	0.00158	-0.04183	-0.00195	0.00184	0.5445	2.5205	0.5
16	11	21.278	10.206	594951	0.62276	0.26007	0.00133	-0.04904	-0.00553	-0.00175	0.49146	1.8897	0.5
16	12	24.127	10.238	595860	0.65168	0.30446	0.00535	-0.0575	-0.00717	-0.0028	0.52608	1.7279	0.5
16	13	27.245	10.329	598512	0.67825	0.36571	0.00927	-0.07208	-0.00143	-0.00289	0.55858	1.5274	0.5
16	14	30.182	10.367	599608	0.68366	0.40648	0.00463	-0.07876	0.00025	-0.00716	0.56528	1.3907	0.5
16	15	33.169	10.434	601547	0.64986	0.44253	-0.0013	-0.08227	0.00008	-0.00746	0.52388	1.1838	0.5

RUN	TP	ALPHAC	QC	RE	CLSA	CDSA	CYSA	CMSA25	CNSA25	CRSA25	CLSA32	CL32CD	VRATIO
17	2	-9.154	20.08	833141	-0.52362	0.07341	0.0064	-0.0115	0.00022	0.00494	0.3789	5.1612	0.1
17	3	-6.128	20.087	833357	-0.36643	0.04843	0.00721	-0.00753	0.00084	0.0049	0.22181	4.5799	0.1
17	4	-3.108	20.051	832655	-0.19723	0.03215	0.00782	-0.00125	0.00064	0.00261	0.08759	2.7241	0.1
17	5	-0.004	20.121	834178	-0.01217	0.02284	0.0063	0.00351	0.00041	0.00091	0.00134	0.05878	0.1
17	6	3.014	20.242	836718	0.16431	0.02225	0.00394	0.0118	0.00008	0.00048	0.0666	2.9932	0.1
17	7	6.15	20.189	835678	0.34522	0.03026	0.00555	0.02275	-0.00015	0.0003	0.20284	6.7042	0.1
17	8	9.109	20.252	837017	0.4952	0.04718	0.00597	0.03215	-0.00029	0.00058	0.34847	7.3858	0.1
17	9	12.182	20.023	832294	0.57791	0.11549	-0.00066	-0.00016	-0.00048	0.00113	0.43933	3.8039	0.1
17	10	15.215	20.16	835149	0.57032	0.18261	-0.00304	-0.0328	-0.00467	0.00211	0.43071	2.3586	0.1
17	11	18.168	20.163	835231	0.53339	0.22006	0.00297	-0.03875	-0.00616	-0.00176	0.38955	1.7702	0.1
17	12	21.154	20.45	841157	0.56142	0.27037	0.00725	-0.04726	-0.00265	-0.00304	0.42066	1.5559	0.1
17	13	24.132	20.527	842747	0.59935	0.31721	0.0077	-0.05535	-0.00137	-0.00272	0.464	1.4628	0.1
17	14	27.216	20.706	846435	0.63171	0.36486	0.00652	-0.06499	-0.00056	-0.00461	0.50208	1.3761	0.1
17	15	30.198	20.701	846321	0.64179	0.4079	0.00425	-0.07329	-0.00062	-0.00434	0.51414	1.2605	0.1
17	16	33.202	21.04	853205	0.62531	0.44695	-0.00007	-0.08079	-0.00161	-0.00163	0.49447	1.1063	0.1

RUN	TP	ALPHAC	QC	RE	CLSA	CDSA	CYSA	CMSA25	CNSA25	CRSA25	CLSA32	CL32CD	VRATIO
18	1	-9.259	19.966	831097	-0.52073	0.07711	0.0059	-0.01013	0.00004	0.0052	0.37577	4.873	0.25
18	2	-6.098	20.247	836904	-0.36032	0.04955	0.00604	-0.00744	0.00068	0.00471	0.21629	4.3648	0.25
18	3	-3.04	20.273	837434	-0.19046	0.03303	0.00725	-0.00113	0.00058	0.00249	0.08312	2.5165	0.25
18	4	-0.035	20.193	835784	-0.01205	0.02401	0.00563	0.00373	0.00033	0.00157	0.00132	0.0551	0.25
18	5	3.068	20.218	836297	0.1703	0.0226	0.00308	0.0112	0.00007	0.00066	0.07028	3.11	0.25
18	6	6.067	20.17	835292	0.34711	0.03005	0.00539	0.02147	-0.00022	0.00032	0.20451	6.8047	0.25
18	7	9.209	20.232	836579	0.49842	0.04762	0.00644	0.03057	-0.00027	0.00007	0.35188	7.3897	0.25
18	8	12.188	20.045	832702	0.6035	0.09713	0.00663	0.01746	-0.00101	0.00001	0.46883	4.827	0.25
18	9	15.112	20.097	833767	0.61657	0.17295	0.00446	-0.02482	-0.00187	0.00332	0.48414	2.7992	0.25
18	10	18.167	20.342	838854	0.55332	0.22	-0.00423	-0.03866	-0.00614	0.0004	0.41159	1.8708	0.25
18	11	21.207	20.424	840525	0.58273	0.26122	0.00378	-0.04468	-0.00724	-0.00422	0.44483	1.7029	0.25
18	12	24.206	20.472	841471	0.6158	0.31994	0.00913	-0.05742	-0.00186	-0.00239	0.48324	1.5104	0.25
18	13	27.202	20.808	848334	0.64391	0.36624	0.00798	-0.06567	-0.00064	-0.00502	0.5167	1.4108	0.25
18	14	30.176	20.859	849355	0.65173	0.40657	0.00452	-0.07331	-0.00063	-0.00506	0.52614	1.2941	0.25
18	15	33.186	21.047	853150	0.63233	0.4435	0.00087	-0.07926	-0.00095	-0.00364	0.50283	1.1338	0.25

A.4 AR-5, Moving Surfaces

RUN	TP	ALPHAC	QC	RE	CLSA	CDSA	CYSA	CMSA25	CNSA25	CRSA25	CLSA32	CL32CD	VRATIO
19	2	-9.173	1.0153	186627	-0.49788	0.07953	0.0033	-0.02655	-0.00012	-0.00004	0.3513	4.417	0.25
19	3	-6.118	1.0116	186306	-0.34486	0.05617	0.00428	-0.02493	-0.00003	0.00104	0.20252	3.6052	0.25
19	4	-3.008	1.0117	186323	-0.16449	0.04147	0.00246	-0.01912	-0.00005	-0.00067	0.06671	1.6085	0.25
19	5	-0.031	1.003	185539	0.01946	0.03395	0.00202	-0.01679	-0.00018	0.00049	0.00271	0.07995	0.25
19	6	3.084	1.0037	185626	0.22247	0.03461	0.00159	-0.01203	-0.00023	-0.00066	0.10493	3.0319	0.25
19	7	6.116	1.0058	185839	0.41866	0.0435	0.00107	-0.00402	-0.00029	-0.00033	0.27089	6.2273	0.25
19	8	9.16	1.0055	185820	0.59227	0.06051	-0.0012	0.00455	-0.00016	-0.00147	0.4558	7.5323	0.25
19	9	12.256	1.0058	185868	0.73237	0.09346	-0.00398	0.00485	0.00003	-0.00162	0.62675	6.7063	0.25
19	10	15.261	1.0122	186476	0.77988	0.15541	-0.00322	-0.0222	-0.00368	-0.00829	0.68871	4.4315	0.25
19	11	18.193	1.0176	186983	0.7993	0.21389	-0.00364	-0.04056	-0.0022	-0.01225	0.7146	3.3409	0.25
19	12	21.301	1.0287	188022	0.8766	0.28325	0.00172	-0.06545	-0.00186	-0.0127	0.82073	2.8976	0.25
19	13	24.221	1.0332	188445	0.79045	0.32971	0.00044	-0.0673	0.0004	-0.00202	0.70277	2.1315	0.25
19	14	27.219	1.0316	188307	0.71586	0.37866	0.00057	-0.0774	0.00106	-0.00565	0.60568	1.5995	0.25
19	15	30.277	1.0457	189613	0.70611	0.44328	-0.00556	-0.09004	0	-0.00313	0.59334	1.3385	0.25
19	16	33.166	1.0548	190447	0.65749	0.47859	-0.0048	-0.09761	-0.00032	-0.00066	0.53313	1.114	0.25

RUN	TP	ALPHAC	QC	RE	CLSA	CDSA	CYSA	CMSA25	CNSA25	CRSA25	CLSA32	CL32CD	VRATIO
20	1	-9.171	1.0052	186032	-0.40988	0.08329	0.00375	-0.03449	-0.00027	-0.00329	0.26241	3.1507	0.5
20	2	-6.094	1.0092	186406	-0.26057	0.05793	0.00377	-0.03867	-0.00021	-0.00151	0.13301	2.296	0.5
20	3	-3.036	1.011	186579	-0.08881	0.04297	0.00286	-0.0371	-0.00017	-0.00172	0.02647	0.61592	0.5
20	4	0.002	1.0063	186152	0.09567	0.03699	0.00264	-0.0327	-0.0002	-0.00021	0.02959	0.80003	0.5
20	5	3.072	1.0049	186036	0.28943	0.03868	0.00234	-0.02941	-0.00029	-0.00119	0.15571	4.0258	0.5
20	6	6.189	1.0071	186241	0.49408	0.04994	-0.00129	-0.02311	-0.00026	-0.00097	0.34729	6.9547	0.5
20	7	9.19	0.99954	185553	0.67315	0.06797	-0.00347	-0.0149	-0.00015	-0.00192	0.55229	8.1259	0.5
20	8	12.211	1.0065	186208	0.81688	0.09929	-0.00561	-0.00808	0.00031	0.00012	0.73831	7.4362	0.5
20	9	15.379	1.0112	186642	0.91316	0.15157	-0.00509	-0.02055	0.00007	0.00314	0.87261	5.7572	0.5
20	10	18.305	1.0122	186750	0.93955	0.2096	-0.00105	-0.03778	-0.00177	0.00018	0.91071	4.3449	0.5
20	11	21.209	1.0227	187718	0.89271	0.27785	-0.00215	-0.06742	-0.00242	-0.00882	0.84346	3.0356	0.5
20	12	24.294	1.0305	188437	0.88025	0.33451	-0.00233	-0.07398	-0.00239	-0.0016	0.82587	2.4689	0.5
20	13	27.267	1.0402	189338	0.82416	0.36654	-0.00082	-0.07419	-0.00152	-0.0008	0.74819	2.0412	0.5
20	14	30.204	1.0457	189837	0.78406	0.4338	-0.01516	-0.08881	0.00396	-0.00084	0.69426	1.6004	0.5
20	15	33.23	1.0443	189706	0.74685	0.49516	-0.00964	-0.10371	0.00021	0.00137	0.64543	1.3035	0.5

RUN	TP	ALPHAC	QC	RE	CLSA	CDSA	CYSA	CMSA25	CNSA25	CRSA25	CLSA32	CL32CD	VRATIO
21	1	-9.084	1.0194	187498	-0.34623	0.08971	0.00338	-0.04187	0.0002	-0.00242	0.20373	2.2708	1
21	2	-6.166	1.0021	185903	-0.19156	0.06526	0.00314	-0.05015	-0.00042	-0.00129	0.08384	1.2847	1
21	3	-2.98	1.0087	186519	0.00025	0.04962	0.00215	-0.05341	-0.00047	-0.00146	0	0.00008	1
21	4	0.106	1.0089	186538	0.19688	0.04446	0.0021	-0.05343	-0.00059	0.00148	0.08736	1.965	1
21	5	3.105	1.0037	186061	0.40287	0.05081	0.00118	-0.0551	-0.00043	-0.00252	0.25571	5.0323	1
21	6	6.194	1.0048	186168	0.61547	0.06569	-0.00396	-0.05372	-0.00078	0.00005	0.48285	7.3508	1
21	7	9.287	1.0022	185926	0.80677	0.08662	-0.00462	-0.04848	-0.0013	0.00169	0.72465	8.3656	1
21	8	12.284	1.0034	186040	0.96586	0.11537	-0.00658	-0.03653	-0.0021	0.0048	0.94924	8.2279	1
21	9	15.318	1.0056	186255	1.0519	0.16468	-0.00589	-0.04443	-0.00186	0.00596	1.0789	6.5514	1
21	10	18.329	1.0239	187942	1.0776	0.22291	-0.0038	-0.05874	-0.00214	0.0076	1.1186	5.0179	1
21	11	21.337	1.0209	187665	1.0225	0.29597	-0.00536	-0.08121	-0.00218	0.00785	1.0339	3.4934	1
21	12	24.264	1.0294	188453	0.97969	0.34607	-0.0025	-0.09032	-0.00272	-0.00761	0.96969	2.802	1
21	13	27.309	1.0418	189586	0.91302	0.38127	-0.00318	-0.08894	-0.00253	0.00284	0.87241	2.2882	1
21	14	30.349	1.0414	189551	0.91731	0.43041	-0.00112	-0.09324	-0.00148	0.00214	0.87857	2.0413	1
21	15	33.259	1.0356	189024	0.91719	0.47744	0.00131	-0.10117	-0.00077	0.00086	0.8784	1.8398	1

RUN	TP	ALPHAC	QC	RE	CLSA	CDSA	CYSA	CMSA25	CNSA25	CRSA25	CLSA32	CL32CD	VRATIO
22	1	-9.073	1.0102	186737	-0.2377	0.10247	0.00223	-0.06346	0.00019	0.0013	0.11589	1.1309	1.5
22	2	-6.093	1.013	187000	-0.07787	0.07939	0.00238	-0.0697	-0.0005	0.00286	0.02173	0.2737	1.5
22	3	-2.926	1.0104	186764	0.13113	0.06608	0.00099	-0.07628	-0.00116	0.00116	0.04748	0.71858	1.5
22	4	0.063	1.0106	186779	0.32145	0.06351	0.00049	-0.0794	-0.00152	0.00356	0.18225	2.8698	1.5
22	5	3.191	1.0022	186001	0.5355	0.07215	-0.00081	-0.08268	-0.00193	0.00333	0.39186	5.4313	1.5
22	6	6.212	1.0022	186005	0.73847	0.08903	0.00075	-0.08433	-0.00249	0.00541	0.63459	7.1282	1.5
22	7	9.322	1.0024	186027	0.9268	0.1107	-0.00472	-0.07585	-0.00273	0.00486	0.89223	8.0598	1.5
22	8	12.267	1.0074	186493	1.0692	0.13744	-0.00517	-0.0603	-0.00303	0.0061	1.1055	8.0437	1.5
22	9	15.455	1.0131	187025	1.1412	0.1899	-0.00495	-0.06482	-0.00264	0.0072	1.219	6.4193	1.5
22	10	18.293	1.0141	187119	1.1584	0.24652	-0.00522	-0.07669	-0.00284	0.00563	1.2468	5.0576	1.5
22	11	21.379	1.0196	187630	1.107	0.3144	-0.0055	-0.09305	-0.00372	0.00178	1.1647	3.7046	1.5
22	12	24.336	1.0317	188747	1.0627	0.36781	-0.00425	-0.10451	-0.00182	-0.00666	1.0955	2.9783	1.5
22	13	27.297	1.0383	189346	0.97169	0.40275	-0.00431	-0.10317	-0.00244	0.00546	0.95784	2.3782	1.5
22	14	30.315	1.0434	189814	0.97379	0.45417	-0.00359	-0.11174	-0.00296	0.00487	0.96095	2.1158	1.5
22	15	33.318	1.0443	189893	0.98998	0.50615	-0.0009	-0.11945	-0.00157	0.00359	0.98501	1.9461	1.5

RUN	TP	ALPHAC	QC	RE	CLSA	CDSA	CYSA	CMSA25	CNSA25	CRSA25	CLSA32	CL32CD	VRATIO
27	4	-9.211	1.0018	185207	-0.58936	0.08223	0.00496	-0.00797	0.00018	0.00079	0.45245	5.5025	0
27	5	-6.167	1.0176	186674	-0.42151	0.05887	0.0052	-0.00832	0.00023	0.00099	0.27366	4.6487	0
27	6	-3.09	1.0195	186873	-0.22289	0.04109	0.00485	-0.00757	-0.00002	-0.00176	0.10523	2.5608	0
27	7	-0.025	1.0039	185457	-0.03442	0.0329	0.0028	-0.00281	-0.00003	0.00035	0.00639	0.19412	0
27	8	3.02	0.99757	184892	0.15064	0.03195	0.00209	0.00596	-0.00001	-0.00269	0.05847	1.8301	0
27	9	6.093	1.0038	185483	0.35922	0.04016	0.00226	0.00957	-0.00011	-0.00046	0.2153	5.3606	0
27	10	9.236	1.0074	185839	0.54901	0.05682	-0.00118	0.01139	-0.00008	-0.00019	0.40679	7.1595	0
27	11	12.229	1.0064	185773	0.6937	0.0868	-0.00439	0.01848	0.00029	0.00063	0.57777	6.656	0
27	12	15.178	1.0106	186170	0.71436	0.1528	-0.00458	-0.01576	-0.00143	0.00283	0.60377	3.9513	0
27	13	18.235	1.0155	186642	0.71422	0.2144	-0.00322	-0.03699	-0.0032	0.00115	0.6036	2.8152	0
27	14	21.179	1.0222	187265	0.58356	0.28775	-0.00709	-0.06634	0.00201	0.00114	0.44579	1.5492	0
27	15	24.15	1.0208	187158	0.58766	0.32922	-0.00776	-0.06878	-0.00053	0.00552	0.45049	1.3684	0
27	16	27.192	1.0271	187747	0.55414	0.36245	-0.00596	-0.0722	-0.00212	0.00906	0.41251	1.1381	0
27	17	30.155	1.0535	190167	0.54996	0.39955	-0.00919	-0.07596	-0.00344	0.0064	0.40784	1.0207	0
27	18	33.194	1.0525	190103	0.55921	0.44315	-0.00423	-0.0838	-0.00337	0.00513	0.41818	0.94365	0

RUN	TP	ALPHAC	QC	RE	CLSA	CDSA	CYSA	CMSA25	CNSA25	CRSA25	CLSA32	CL32CD	VRATIO
28	1	-9.279	4.9706	413641	-0.57261	0.07704	-0.01357	-0.00941	0.00026	0.00196	0.4333	5.6247	0
28	2	-6.097	5.0153	415535	-0.39809	0.05216	-0.01027	-0.00727	0.00019	0.00167	0.25117	4.8153	0
28	3	-3.058	5.0836	418400	-0.21244	0.03585	-0.0094	-0.00492	0.00015	0.00165	0.09792	2.7309	0
28	4	-0.033	5.0578	417372	-0.01912	0.02801	-0.01091	-0.00044	0.00013	0.00214	0.00264	0.09441	0
28	5	3.029	4.9839	414349	0.17272	0.0269	-0.00987	0.00543	0.00009	0.00168	0.07178	2.6681	0
28	6	6.146	5.0217	415966	0.3705	0.03495	-0.0081	0.01439	0.00008	0.00281	0.22552	6.4521	0
28	7	9.167	5.0069	415383	0.54692	0.05127	-0.00853	0.02245	0.00004	0.00247	0.40446	7.8884	0
28	8	12.152	5.0229	416062	0.69453	0.0846	-0.01082	0.02019	0.00004	0.00404	0.57881	6.8419	0
28	9	15.275	5.0252	416189	0.69719	0.15625	-0.01187	-0.01981	-0.00322	0.00157	0.58214	3.7256	0
28	10	18.22	5.0476	417134	0.7449	0.2041	-0.0125	-0.0321	-0.00361	-0.0024	0.6429	3.1499	0
28	11	21.236	5.0706	418115	0.72245	0.27643	-0.01742	-0.05568	0.0057	0.01059	0.61406	2.2214	0
28	12	24.166	5.179	422587	0.62437	0.31738	-0.0232	-0.0658	0.00462	0.00989	0.49336	1.5545	0
28	13	27.169	5.1761	422485	0.63815	0.36932	-0.01627	-0.0767	-0.00061	0.00906	0.50979	1.3803	0
28	14	30.198	5.1848	422863	0.65277	0.41454	-0.00908	-0.08242	0.0008	0.00299	0.5274	1.2723	0
28	15	33.176	5.2581	425864	0.60453	0.44646	-0.00628	-0.08244	0.00049	-0.00047	0.47003	1.0528	0

RUN	TP	ALPHAC	QC	RE	CLSA	CDSA	CYSA	CMSA25	CNSA25	CRSA25	CLSA32	CL32CD	VRATIO
29	1	-9.19	9.98135	586976	-0.55273	0.07447	0.00671	-0.00381	0.00046	-0.00014	0.41093	5.5181	0
29	2	-6.138	9.9666	586575	-0.38862	0.05024	0.0087	-0.00212	0.00056	0.00029	0.24227	4.8223	0
29	3	-3.097	10.069	589588	-0.20192	0.03275	0.00883	-0.00088	0.0007	0.00076	0.09073	2.7703	0
29	4	-0.014	10.136	591575	-0.00658	0.02439	0.00657	0.00333	0.0007	0.0011	0.00053	0.02187	0
29	5	3.032	10.079	589954	0.1871	0.0238	0.00493	0.00833	0.00066	-0.0001	0.08093	3.4001	0
29	6	6.091	10.058	589346	0.38298	0.03241	0.00658	0.01667	0.00064	-0.0001	0.23701	7.3134	0
29	7	9.201	10.021	588287	0.56455	0.05152	0.00718	0.02433	0.00042	0.00061	0.42419	8.2329	0
29	8	12.199	10.029	588520	0.70224	0.08967	0.00641	0.02047	0.00035	0.00116	0.58847	6.563	0
29	9	15.261	10.04	588885	0.74465	0.16253	0.00574	-0.02008	-0.00128	0.00314	0.64259	3.9537	0
29	10	18.249	10.085	590201	0.76353	0.21655	0.00414	-0.04028	-0.00144	-0.00113	0.66718	3.0809	0
29	11	21.21	10.196	593451	0.80673	0.26956	0.00303	-0.05381	-0.00037	-0.004	0.7246	2.6881	0
29	12	24.187	10.307	596704	0.67611	0.31303	0.00619	-0.05828	-0.00258	-0.00513	0.55593	1.776	0
29	13	27.233	10.297	596397	0.64731	0.36801	-0.00004	-0.07144	0.00023	0.00902	0.52079	1.4152	0
29	14	30.179	10.371	598561	0.65839	0.41379	0.0037	-0.07926	0.00049	0.00308	0.53423	1.2911	0
29	15	33.216	10.408	599638	0.64945	0.45398	0.0047	-0.08606	0.00204	-0.00478	0.52339	1.1529	0

RUN	TP	ALPHAC	QC	RE	CLSA	CDSA	CYSA	CMSA25	CNSA25	CRSA25	CLSA32	CL32CD	VRATIO
30	1	-9.249	19.95	830107	-0.54296	0.07794	0.00567	-0.00386	0.00038	-0.00119	0.40008	5.1329	0
30	2	-6.044	20.044	832045	-0.37155	0.05097	0.00736	-0.00138	0.00039	-0.00063	0.22648	4.4437	0
30	3	-3.104	20.288	837072	-0.1912	0.03297	0.00838	-0.00073	0.00063	-0.00168	0.0836	2.5361	0
30	4	-0.029	20.196	835150	-0.00288	0.02418	0.00701	0.00352	0.00087	-0.00127	0.00015	0.0064	0
30	5	3.049	20.18	834804	0.19056	0.02559	0.00501	0.00661	0.00043	-0.00048	0.08319	3.2501	0
30	6	6.108	20.056	832239	0.37828	0.03739	0.00641	0.01442	0.00049	-0.0014	0.23266	6.2218	0
30	7	9.185	20.07	832517	0.54862	0.0606	0.00738	0.02103	0.00018	0.00088	0.40636	6.7055	0
30	8	12.243	20.207	835340	0.6833	0.10981	0.00848	0.00469	-0.0006	0.00294	0.56483	5.1436	0
30	9	15.217	20.085	832798	0.75286	0.1663	0.00869	-0.01879	-0.00191	0.00218	0.65324	3.9281	0
30	10	18.263	20.192	834988	0.77679	0.22331	0.0065	-0.04028	-0.00192	0.00073	0.68462	3.0659	0
30	11	21.219	20.162	834342	0.7956	0.27278	0.00509	-0.05198	-0.00144	-0.00036	0.70964	2.6015	0
30	12	24.219	20.707	845514	0.72045	0.31413	0.00669	-0.05688	0.00085	-0.01593	0.61151	1.9467	0
30	13	27.212	20.569	842667	0.66892	0.36461	-0.00791	-0.07094	0.00358	0.01075	0.54709	1.5005	0
30	14	30.21	20.599	843259	0.67411	0.41295	-0.00075	-0.0797	0.00103	0.00918	0.55347	1.3403	0
30	15	33.166	20.785	847033	0.63804	0.45126	0.00599	-0.08598	0.00149	-0.00446	0.50965	1.1294	0

RUN	TP	ALPHAC	QC	RE	CLSA	CDSA	CYSA	CMSA25	CNSA25	CRSA25	CLSA32	CL32CD	VRATIO
31	2	-9.221	1.0022	185794	-0.52406	0.08089	0.00438	-0.0253	0.00014	-0.00074	0.37938	4.69	0.25
31	3	-6.105	0.99964	185560	-0.37044	0.05814	0.00433	-0.0165	0.00012	0.00016	0.22547	3.8778	0.25
31	4	-3.059	1.0026	185836	-0.19649	0.04195	0.00366	-0.01893	0.00009	-0.00165	0.0871	2.0764	0.25
31	5	-0.035	1.004	185975	0.00157	0.03385	0.00215	-0.0137	-0.00008	0.0002	0.00006	0.00184	0.25
31	6	3.054	1.0046	186037	0.20563	0.03328	0.00049	-0.00889	-0.00018	-0.00002	0.09325	2.8019	0.25
31	7	6.144	1.0037	185957	0.40187	0.04158	0.00013	-0.00415	-0.00026	0.0009	0.25476	6.1273	0.25
31	8	9.123	1.0033	185921	0.58095	0.05809	-0.00192	-0.01065	-0.00028	0.0004	0.4428	7.6221	0.25
31	9	12.231	0.99823	185454	0.73434	0.08907	-0.0042	0.01379	-0.0002	0.00218	0.62928	7.0649	0.25
31	10	15.326	1.0025	185852	0.82192	0.14593	-0.00488	-0.01238	0.00002	0.00257	0.74515	5.1062	0.25
31	11	18.252	1.0127	186804	0.85677	0.21348	-0.00447	-0.03583	-0.00002	-0.00001	0.79304	3.7149	0.25
31	12	21.246	1.0218	187641	0.81416	0.28821	-0.00343	-0.06318	-0.00006	-0.0027	0.73462	2.5489	0.25
31	13	24.235	1.0243	187869	0.76646	0.34838	-0.00227	-0.07427	0.00168	0.00073	0.67101	1.9261	0.25
31	14	27.201	1.0401	189313	0.68139	0.38569	-0.00787	-0.07923	0.00148	-0.00135	0.56247	1.4583	0.25
31	15	30.199	1.048	190028	0.62336	0.42025	-0.01079	-0.0837	-0.00163	0.00815	0.49217	1.1711	0.25
31	16	33.167	1.0414	189437	0.60707	0.45918	-0.00582	-0.08907	-0.00141	0.00424	0.47299	1.0301	0.25

RUN	TP	ALPHAC	QC	RE	CLSA	CDSA	CYSA	CMSA25	CNSA25	CRSA25	CLSA32	CL32CD	VRATIO
32	1	-9.255	4.996	415327	-0.55574	0.078	-0.01391	-0.00962	0.00042	0.0021	0.41429	5.3116	0.1
32	2	-6.13	4.9974	415386	-0.38294	0.05361	-0.01125	-0.00937	0.00041	0.00246	0.23697	4.42	0.1
32	3	-3.03	4.9968	415362	-0.19006	0.03628	-0.00941	-0.00888	0.00027	0.00272	0.08286	2.2839	0.1
32	4	0.014	5.011	415963	0.00053	0.02883	-0.01226	-0.00345	0.00016	0.00234	0.00001	0.00043	0.1
32	5	3.026	5.0122	416012	0.19174	0.02768	-0.00938	-0.0008	0.00005	0.00225	0.08396	3.0334	0.1
32	6	6.098	5.0168	416213	0.3932	0.03634	-0.00916	0.00729	-0.00013	0.00264	0.24656	6.7857	0.1
32	7	9.18	5.0134	416079	0.57033	0.05374	-0.00959	0.01563	-0.00019	0.00249	0.43072	8.0142	0.1
32	8	12.251	5.0298	416762	0.72151	0.08849	-0.01235	0.01381	-0.00027	0.00305	0.61286	6.9255	0.1
32	9	15.261	5.0088	415893	0.79493	0.14519	-0.01384	-0.01203	-0.00044	0.00245	0.70875	4.8815	0.1
32	10	18.199	5.0045	415723	0.80034	0.20561	-0.01535	-0.03495	0.00269	0.00653	0.716	3.4823	0.1
32	11	21.267	5.0871	419140	0.77866	0.26951	-0.01809	-0.05345	-0.00084	0.00319	0.6871	2.5494	0.1
32	12	24.269	5.1347	421101	0.75609	0.32782	-0.01557	-0.06938	-0.00014	-0.00453	0.65744	2.0055	0.1
32	13	27.198	5.1697	422536	0.74631	0.39285	-0.01632	-0.08669	0.00232	-0.00037	0.64474	1.6412	0.1
32	14	30.187	5.2013	423824	0.72316	0.43779	-0.01255	-0.09359	-0.00034	-0.00008	0.61496	1.4047	0.1
32	15	33.211	5.2313	425051	0.64173	0.45906	-0.00573	-0.08722	0.0017	-0.00559	0.51407	1.1198	0.1

RUN	TP	ALPHAC	QC	RE	CLSA	CDSA	CYSA	CMSA25	CNSA25	CRSA25	CLSA32	CL32CD	VRATIO
33	3	-9.146	9.96135	585970	-0.54847	0.07155	0.00685	-0.0051	0.00038	-0.00045	0.4062	5.6767	0.1
33	4	-6.177	9.88171	583658	-0.37947	0.04848	0.0085	-0.00499	0.00031	0.00048	0.23376	4.8214	0.1
33	5	-3.054	9.96502	586149	-0.18572	0.03124	0.00929	-0.00423	0.00021	0.00017	0.08004	2.5622	0.1
33	6	0.018	10.025	587967	0.00637	0.02368	0.0063	0.0001	0.00013	0.00037	0.00051	0.02148	0.1
33	7	2.96	10.036	588289	0.1974	0.02303	0.00415	0.00338	0.00006	0.00024	0.0877	3.808	0.1
33	8	6.217	10.055	588906	0.40694	0.03202	0.00693	0.0104	0.00003	0.00045	0.2596	8.1083	0.1
33	9	9.163	10.048	588696	0.58311	0.04817	0.00611	0.01793	-0.00001	0.00048	0.44527	9.24404	0.1
33	10	12.228	10.113	590615	0.72494	0.08505	0.0053	0.01376	-0.00032	0.00022	0.61723	7.2574	0.1
33	11	15.224	10.05	588816	0.78265	0.14429	-0.0028	-0.01385	-0.00053	-0.00435	0.69239	4.7987	0.1
33	12	18.266	10.017	587855	0.79087	0.20331	0.00129	-0.03224	0.00284	0.00543	0.70333	3.4595	0.1
33	13	21.256	10.164	592238	0.80381	0.26281	0.00101	-0.05037	-0.00071	0.00383	0.72067	2.7421	0.1
33	14	24.258	10.337	597287	0.78172	0.32486	0.0022	-0.06548	0.00246	0.00166	0.69116	2.1276	0.1
33	15	27.181	10.287	595838	0.74081	0.38592	-0.00167	-0.07922	0.00164	-0.00122	0.63762	1.6522	0.1
33	16	30.203	10.378	598483	0.72484	0.43333	0.00036	-0.08891	0.00044	0.00082	0.61711	1.4241	0.1
33	17	33.233	10.47	601134	0.67782	0.46727	-0.00101	-0.09534	-0.00162	0.00227	0.55804	1.1943	0.1

RUN	TP	ALPHAC	QC	RE	CLSA	CDSA	CYSA	CMSA25	CNSA25	CRSA25	CLSA32	CL32CD	VRATIO
34	2	-9.2	20.04	829146	-0.53934	0.07553	0.00427	-0.00372	0.00031	0.00045	0.39609	5.2442	0.1
34	3	-6.141	20.065	829852	-0.37021	0.05034	0.00595	-0.00418	0.00025	0.00123	0.22526	4.475	0.1
34	4	-3.117	20.203	832887	-0.18698	0.03337	0.00737	-0.00166	0.00011	0.00107	0.08086	2.4227	0.1
34	5	-0.015	20.264	834316	0.00294	0.02389	0.00694	0.00141	0	0.00145	0.00016	0.00667	0.1
34	6	3.091	20.139	831896	0.20061	0.02359	0.00463	0.00541	-0.00009	0.00091	0.08985	3.8097	0.1
34	7	6.105	20.047	830081	0.39399	0.03204	0.00463	0.01316	-0.00009	0.00072	0.2473	7.7189	0.1
34	8	9.186	20.042	830090	0.56635	0.05166	0.00622	0.02105	0.00023	0.0004	0.42621	8.2495	0.1
34	9	12.208	20.15	832413	0.66537	0.09689	0.00681	0.00979	0.00228	0.00564	0.54275	5.6017	0.1
34	10	15.187	20.147	832425	0.70126	0.14717	-0.00217	-0.00491	0.00186	0.01758	0.58725	3.9903	0.1
34	11	18.279	20.17	832972	0.71732	0.21709	0.00152	-0.03177	-0.00693	0.0056	0.60753	2.7985	0.1
34	12	21.192	20.583	841509	0.73568	0.27773	0.00514	-0.05085	-0.00439	0.0049	0.631	2.272	0.1
34	13	24.239	20.718	844316	0.75923	0.33027	0.00847	-0.06012	-0.00386	0.00097	0.66155	2.003	0.1
34	14	27.192	20.838	846803	0.72312	0.38019	0.00951	-0.07187	-0.0037	-0.00586	0.61491	1.6174	0.1
34	15	30.218	20.926	848606	0.70323	0.42523	0.00807	-0.07974	-0.00184	-0.00339	0.58972	1.3868	0.1
34	16	33.246	21.021	850559	0.66361	0.45951	0.00671	-0.08283	-0.00019	-0.00506	0.54059	1.1764	0.1

A.5 AR-5, Moving Surfaces with End Plates

RUN	TP	ALPHAC	QC	RE	CLSA	CDSA	CYSA	CMSA25	CNSA25	CRSA25	CLSA32	CL32CD	VRATIO
43	1	-9.132	0.99776	184031	-0.47863	0.08353	0.00366	-0.01827	0.00001	0.00351	0.33113	3.964	0.5
43	2	-6.159	1.0183	185915	-0.32429	0.06063	0.00349	-0.01939	0.00009	0.00332	0.18467	3.046	0.5
43	3	-3.03	1.0162	185727	-0.14195	0.0453	0.00197	-0.01755	0.00008	0.00164	0.05348	1.1807	0.5
43	4	0.036	1.0134	185478	0.048	0.03741	0.0008	-0.01168	-0.00001	0.00404	0.01052	0.28106	0.5
43	5	2.97	1.0031	184540	0.25303	0.0391	0.00162	-0.00847	-0.00023	0.00237	0.12728	3.2553	0.5
43	6	6.125	0.99801	184079	0.4676	0.04836	0.00271	-0.00944	-0.00045	0.00292	0.31975	6.6124	0.5
43	7	9.289	0.99934	184208	0.66787	0.06569	-0.00027	0.00307	-0.00035	0.00411	0.54581	8.3089	0.5
43	8	12.244	1.0059	184813	0.82487	0.09431	-0.00124	0.00797	-0.00006	0.0053	0.74916	7.9434	0.5
43	9	15.247	1.0122	185407	0.914	0.14326	-0.00167	-0.00639	0.00062	0.00778	0.87382	6.0994	0.5
43	10	18.37	1.0162	185773	0.93091	0.21633	-0.0017	-0.03408	-0.00239	0.00107	0.89817	4.1519	0.5
43	11	21.291	1.0208	186198	0.90647	0.28025	-0.00029	-0.06015	-0.00123	-0.00217	0.86304	3.0796	0.5
43	12	24.227	1.0298	187028	0.88855	0.33815	-0.00169	-0.06682	-0.00315	-0.00393	0.83758	2.477	0.5
43	13	27.302	1.0393	187894	0.83598	0.40331	-0.00217	-0.08355	-0.00181	0.00867	0.76435	1.8952	0.5
43	14	30.185	1.0376	187745	0.72467	0.43005	-0.00063	-0.08885	0.00026	0.00077	0.61689	1.4345	0.5
43	15	33.198	1.0468	188578	0.67224	0.46606	0.00209	-0.09644	0.00043	0.00269	0.55117	1.1826	0.5

RUN	TP	ALPHAC	QC	RE	CLSA	CDSA	CYSA	CMSA25	CNSA25	CRSA25	CLSA32	CL32CD	VRATIO
44	1	-9.207	0.99605	183978	-0.39511	0.09088	0.00365	-0.03014	-0.00002	-0.00068	0.24836	2.7328	1
44	2	-6.093	1.0101	185271	-0.22816	0.06509	0.00257	-0.03512	-0.00006	0.00069	0.10898	1.6743	1
44	3	-3.04	1.0108	185337	-0.04654	0.04981	0.00168	-0.03508	-0.00008	-0.00038	0.01004	0.20161	1
44	4	0.11	0.99985	184338	0.15564	0.04357	-0.00159	-0.03733	-0.00013	0.00136	0.0614	1.4092	1
44	5	3.053	0.99742	184118	0.35641	0.04634	-0.00001	-0.03109	-0.00029	0.00002	0.21278	4.592	1
44	6	6.162	1.0013	184477	0.57783	0.05798	0.00163	-0.03016	-0.0005	0.00175	0.43924	7.5756	1
44	7	9.288	1.0054	184866	0.78156	0.07689	-0.00096	-0.02363	-0.00048	0.00191	0.69095	8.986	1
44	8	12.378	1.0015	184505	0.96033	0.10668	-0.00088	-0.01847	-0.00039	0.00367	0.9411	8.8215	1
44	9	15.3	1.0055	184876	1.0291	0.15145	-0.00156	-0.02137	0.00021	0.00844	1.0439	6.8927	1
44	10	18.343	1.0227	186455	1.0371	0.21537	-0.00187	-0.03792	-0.00105	0.00278	1.0561	4.9038	1
44	11	21.287	1.022	186396	0.98938	0.28358	0.00086	-0.06254	0.00134	0.01393	0.98411	3.4703	1
44	12	24.245	1.0273	186876	0.96662	0.3348	-0.00061	-0.07353	-0.00215	0.01133	0.95036	2.8386	1
44	13	27.308	1.039	187946	0.89559	0.37332	-0.00018	-0.07321	-0.00154	-0.00399	0.84754	2.2703	1
44	14	30.286	1.0412	188147	0.90334	0.42703	-0.00045	-0.08033	-0.00201	-0.00274	0.85857	2.0106	1
44	15	33.306	1.0438	188386	0.88674	0.49842	0.0001	-0.10302	-0.00583	0.00028	0.83502	1.6753	1

A.6 AR-9, Base Airfoil

RUN	TP	ALPHAC	QC	RE	CLSA	CDSA	CYSA	CMSA25	CNSA25	CRSA25	CLSA32	CL32CD	VRATIO
46	2	-9.548	1.0023	184504	-0.70009	0.06989	0.00336	0.00347	-0.00004	0.00262	0.58578	8.3813	0
46	3	-6.3	1.0029	184567	-0.50219	0.04911	0.00267	0.00822	-0.0001	0.00368	0.35588	7.2465	0
46	4	-3.082	1.0172	185894	-0.24295	0.03304	0.00166	0.00336	-0.00011	0.00407	0.11975	3.6243	0
46	5	-0.061	1.0093	185185	-0.01581	0.02653	0.00261	0.00949	-0.0002	0.00407	0.00199	0.07491	0
46	6	3.109	1.006	184899	0.22331	0.0269	0.00123	0.01623	-0.00026	0.00295	0.10553	3.9224	0
46	7	6.294	1.0027	184602	0.48998	0.03694	-0.00294	0.02083	-0.00012	0.00215	0.34298	9.2857	0
46	8	9.371	1.0054	184867	0.66791	0.05282	-0.00329	0.02957	-0.00019	0.00066	0.54585	10.334	0
46	9	12.465	1.0029	184642	0.78173	0.09237	-0.00251	0.02085	-0.00058	0.0013	0.69117	7.4829	0
46	10	15.394	1.0178	186022	0.74833	0.15148	-0.00412	0.00011	-0.00046	0.0076	0.64735	4.2735	0
46	11	18.321	1.0369	187769	0.60527	0.2288	-0.0044	-0.03807	-0.00006	0.00828	0.4709	2.0581	0
46	12	21.339	1.0594	189803	0.58977	0.28486	-0.00265	-0.04441	0.00037	0.00363	0.45292	1.59	0
46	13	24.29	1.063	190138	0.59606	0.33088	-0.00558	-0.05333	-0.00079	0.00422	0.46018	1.3908	0
46	14	27.321	1.0592	189803	0.58717	0.38122	-0.00759	-0.06695	-0.00137	0.00568	0.44994	1.1803	0
46	15	30.308	1.0749	191216	0.59577	0.42722	-0.00649	-0.0785	-0.00183	0.00554	0.45985	1.0764	0
46	16	33.312	1.0909	192648	0.59866	0.46822	-0.0051	-0.08368	-0.00217	0.00521	0.4632	0.98928	0

RUN	TP	ALPHAC	QC	RE	CLSA	CDSA	CYSA	CMSA25	CNSA25	CRSA25	CLSA32	CL32CD	VRATIO
47	1	-9.354	4.9662	411576	-0.68685	0.06731	-0.00747	-0.00605	-0.00064	0.00432	0.56923	8.4563	0
47	2	-6.342	5.0297	414220	-0.48128	0.04635	-0.007	-0.00537	-0.00047	0.00576	0.33389	7.2036	0
47	3	-3.096	5.0606	415521	-0.23838	0.03166	-0.00709	-0.00169	-0.00051	0.0048	0.11639	3.6764	0
47	4	-0.009	5.0391	414667	-0.00096	0.02511	-0.00724	0.00189	-0.00054	0.00533	0.00003	0.00119	0
47	5	3.075	5.0689	415928	0.23123	0.02547	-0.00852	0.00957	-0.00051	0.00189	0.11119	4.366	0
47	6	6.236	5.0328	414462	0.4691	0.03316	-0.00904	0.02017	-0.00045	0.00143	0.32129	9.68848	0
47	7	9.378	5.0105	413565	0.66882	0.048	-0.011	0.0313	-0.00021	-0.00139	0.54696	11.395	0
47	8	12.503	5.0234	414122	0.79917	0.09008	-0.00899	0.01695	-0.00053	-0.00036	0.71443	7.9308	0
47	9	15.437	5.0568	415512	0.84747	0.14501	-0.00989	-0.00311	-0.00111	-0.00093	0.78016	5.3802	0
47	10	18.396	5.1365	418794	0.70937	0.22746	-0.00987	-0.04215	-0.00028	-0.00067	0.59747	2.6267	0
47	11	21.353	5.2246	422388	0.66323	0.27167	-0.00902	-0.04934	-0.00126	0.00799	0.54012	1.9881	0
47	12	24.331	5.2583	423767	0.62179	0.32999	-0.00951	-0.0605	-0.00117	-0.0006	0.4903	1.4858	0
47	13	27.331	5.3587	427805	0.63812	0.38091	-0.01104	-0.07177	-0.00024	0.00051	0.50974	1.3382	0
47	14	30.352	5.4065	429718	0.64259	0.42596	-0.01177	-0.08143	0.00188	-0.00442	0.51512	1.2093	0
47	15	33.312	5.4352	430869	0.61221	0.45694	-0.01196	-0.083	-0.00032	0.00024	0.47902	1.0483	0

A.7 AR-9, Inner Wing Moving Surfaces

RUN	TP	ALPHAC	QC	RE	CLSA	CDSA	CYSA	CMSA25	CNSA25	CRSA25	CLSA32	CL32CD	VRATIO
49	1	-9.42	1.0137	186098	-0.62723	0.07313	0.00373	-0.00077	-0.00009	0.00193	0.49675	6.7924	0.25
49	2	-6.245	1.0257	187195	-0.44507	0.0503	0.00335	0.00062	-0.00009	0.00355	0.29692	5.9025	0.25
49	3	-3.132	1.0187	186549	-0.20685	0.03477	0.00194	-0.00192	-0.0001	0.00165	0.09408	2.7056	0.25
49	4	-0.031	1.0095	185708	0.02647	0.02767	0.00115	0.0031	-0.00022	0.00299	0.00431	0.15566	0.25
49	5	3.164	1.0063	185407	0.27381	0.02888	0.00005	0.00861	-0.00028	0.00399	0.14328	4.9619	0.25
49	6	6.304	1.0107	185817	0.5344	0.03823	0.0001	0.01518	-0.00031	0.00237	0.39066	10.219	0.25
49	7	9.43	1.0112	185858	0.73591	0.05442	0.00004	0.0242	-0.00034	0.00174	0.6313	11.601	0.25
49	8	12.46	1.0083	185589	0.85648	0.0878	-0.00126	0.02439	-0.00038	0.00182	0.79264	9.02747	0.25
49	9	15.409	1.0195	186613	0.73752	0.17997	-0.00222	-0.02198	-0.00037	0.00488	0.63338	3.5194	0.25
49	10	18.39	1.0382	188323	0.74896	0.23191	-0.00233	-0.03577	-0.0008	0.00453	0.64817	2.7949	0.25
49	11	21.417	1.0645	190689	0.74245	0.30102	-0.00144	-0.05135	-0.00059	0.00234	0.63974	2.1252	0.25
49	12	24.362	1.0704	191215	0.74486	0.35703	-0.00503	-0.0615	-0.00122	0.00606	0.64286	1.8006	0.25
49	13	27.402	1.072	191357	0.67102	0.39421	-0.00762	-0.06918	-0.00128	0.01023	0.54967	1.3944	0.25
49	14	30.296	1.0768	191776	0.6455	0.43757	-0.0079	-0.0792	-0.00392	0.01289	0.51861	1.1852	0.25
49	15	33.365	1.0923	193154	0.63164	0.48016	-0.00633	-0.08581	-0.0032	0.00775	0.502	1.0455	0.25

RUN	TP	ALPHAC	QC	RE	CLSA	CDSA	CYSA	CMSA25	CNSA25	CRSA25	CLSA32	CL32CD	VRATIO
51	2	-9.343	1.0062	185231	-0.57355	0.0741	0.0033	-0.00437	0.0003	0.00011	0.43437	5.8621	0.5
51	3	-6.259	1.0178	186305	-0.40675	0.05032	0.003	-0.00387	0.00006	0.00131	0.25941	5.1552	0.5
51	4	-3.116	1.0258	187042	-0.16632	0.03496	0.00249	-0.00729	0.00004	0.00093	0.06783	1.9404	0.5
51	5	0.047	1.0055	185186	0.06927	0.02807	0.00128	-0.00123	-0.00001	0.00144	0.01823	0.64951	0.5
51	6	3.159	0.99834	184528	0.30532	0.03019	0.00117	0.00197	-0.00016	0.002	0.16871	5.5891	0.5
51	7	6.338	1.0028	184939	0.56934	0.03993	0.00011	0.0072	-0.00016	0.00152	0.42959	10.759	0.5
51	8	9.443	1.002	184872	0.7764	0.05573	-0.00001	0.01927	-0.00018	0.00135	0.68412	12.275	0.5
51	9	12.452	1.0036	185027	0.89874	0.08711	-0.00183	0.02055	-0.00031	0.00114	0.85202	9.78049	0.5
51	10	15.507	1.0194	186480	0.84899	0.1651	-0.00341	-0.00992	0.00632	0.02607	0.78226	4.7381	0.5
51	11	18.391	1.0331	187730	0.79425	0.22964	-0.00234	-0.03812	-0.00012	0.00206	0.70785	3.0824	0.5
51	12	21.432	1.0488	189150	0.77775	0.29351	-0.00404	-0.04729	-0.00063	0.00382	0.6859	2.3368	0.5
51	13	24.442	1.0574	189931	0.78767	0.34873	-0.00333	-0.05853	0.00064	-0.00172	0.69906	2.0046	0.5
51	14	27.432	1.0796	191916	0.73007	0.39229	-0.00594	-0.06786	-0.00204	0.00652	0.6238	1.5902	0.5
51	15	30.334	1.0917	192998	0.70314	0.43915	-0.00518	-0.07714	-0.00328	0.00808	0.58961	1.3426	0.5
51	16	33.35	1.0971	193474	0.6758	0.48392	-0.00181	-0.08551	-0.0006	0.00114	0.55556	1.148	0.5

RUN	TP	ALPHAC	QC	RE	CLSA	CDSA	CYSA	CMSA25	CNSA25	CRSA25	CLSA32	CL32CD	VRATIO
53	2	-9.381	1.0057	185196	-0.47975	0.08945	0.00272	-0.01154	0.00109	-0.00246	0.33229	3.715	1
53	3	-6.075	1.0082	185425	-0.27266	0.05999	0.00187	-0.01985	0.00078	-0.00244	0.14238	2.3732	1
53	4	-3.061	1.0146	186022	-0.0464	0.04384	0.00079	-0.02635	0.00069	-0.00287	0.00999	0.22794	1
53	5	0.101	1.0123	185814	0.19104	0.03817	-0.00019	-0.02297	0.00055	-0.00227	0.0835	2.1876	1
53	6	3.24	1.0098	185583	0.44549	0.04075	-0.0011	-0.0203	0.00052	-0.00262	0.29734	7.2964	1
53	7	6.371	1.01	185611	0.69544	0.05156	-0.00062	-0.01648	0.0003	-0.00314	0.57995	11.248	1
53	8	9.477	1.0048	185141	0.90304	0.06719	-0.00065	-0.00656	0.00043	-0.00232	0.85814	12.771	1
53	9	12.626	0.99628	184354	1.028	0.09409	-0.00275	0.00633	0.00025	-0.00199	1.0423	11.078	1
53	10	15.477	1.0248	186974	1.0134	0.15589	-0.00245	-0.01235	-0.00361	-0.00831	1.0202	6.544	1
53	11	18.539	1.0477	189060	0.88139	0.2397	-0.00302	-0.04513	0.00055	0.00224	0.82747	3.4522	1
53	12	21.47	1.0589	190072	0.86551	0.30637	-0.0034	-0.05881	0.00099	-0.00194	0.80521	2.6282	1
53	13	24.483	1.0575	189952	0.80761	0.35054	-0.00541	-0.06515	0.00052	-0.0002	0.72577	2.0704	1
53	14	27.415	1.0773	191725	0.80135	0.3958	-0.00757	-0.07593	0.00006	0.00484	0.71735	1.8124	1
53	15	30.437	1.0875	192628	0.78859	0.43957	-0.00776	-0.08439	-0.00213	0.00757	0.70029	1.5931	1
53	16	33.463	1.0924	193065	0.77929	0.48805	-0.00433	-0.09137	-0.00026	0.00082	0.68794	1.4096	1

RUN	TP	ALPHAC	QC	RE	CLSA	CDSA	CYSA	CMSA25	CNSA25	CRSA25	CLSA32	CL32CD	VRATIO
54	3	-9.318	1.0279	187122	-0.37588	0.10073	0.00283	-0.03243	0.00078	-0.00068	0.23045	2.2877	1.5
54	4	-6.097	1.011	185585	-0.16377	0.07283	0.00179	-0.04249	0.0007	-0.00042	0.06628	0.90998	1.5
54	5	-2.91	1.0149	185954	0.07641	0.056	0.00104	-0.04705	0.00051	0.00058	0.02112	0.37723	1.5
54	6	0.176	1.0145	185926	0.30128	0.05152	-0.00087	-0.04546	0.00037	0.00052	0.16537	3.2101	1.5
54	7	3.222	1.0068	185223	0.55316	0.05539	-0.00109	-0.04758	0.00029	0.00143	0.41141	7.4274	1.5
54	8	6.522	1.0161	186077	0.8074	0.0677	-0.00061	-0.04047	0.00023	0.00112	0.7255	10.716	1.5
54	9	9.548	1.0095	185487	1.0015	0.08228	-0.00063	-0.02931	0.00009	0.0003	1.0023	12.181	1.5
54	10	12.657	1.0173	186214	1.1276	0.10544	-0.00294	-0.01152	-0.00002	0.00065	1.1974	11.356	1.5
54	11	15.602	1.0109	185630	1.1303	0.15639	-0.00393	-0.01737	0.00001	0.00425	1.2016	7.6834	1.5
54	12	18.554	1.0492	189116	0.9566	0.25135	-0.00369	-0.05531	0.00042	0.00237	0.93562	3.7224	1.5
54	13	21.479	1.0561	189747	0.9268	0.3168	-0.00576	-0.06823	-0.00007	0.0024	0.89224	2.8164	1.5
54	14	24.469	1.0577	189886	0.90434	0.36656	-0.00706	-0.07812	-0.00003	0.00094	0.86	2.3462	1.5
54	15	27.503	1.0793	191828	0.8906	0.41453	-0.00934	-0.08668	0.00026	0.00489	0.84047	2.0275	1.5
54	16	30.509	1.0902	192800	0.83422	0.45383	-0.00683	-0.09625	-0.00122	0.0073	0.76193	1.6789	1.5
54	17	33.393	1.0894	192728	0.81533	0.49115	-0.00575	-0.09744	-0.00123	0.00689	0.7362	1.4989	1.5

RUN	TP	ALPHAC	QC	RE	CLSA	CDSA	CYSA	CMSA25	CNSA25	CRSA25	CLSA32	CL32CD	VRATIO
55	2	-9.389	5.0021	412698	-0.66662	0.06907	-0.00661	-0.00624	-0.00001	0.00119	0.54427	7.8795	0.1
55	3	-6.299	5.1187	417543	-0.46006	0.04695	-0.00769	-0.00593	-0.00001	0.00255	0.31205	6.6467	0.1
55	4	-3.131	4.9516	410718	-0.22363	0.03218	-0.00866	-0.00344	0	0.00212	0.10575	3.2859	0.1
55	5	-0.003	5.0062	413023	0.01715	0.02541	-0.00829	-0.00079	-0.00006	0.00262	0.00225	0.08836	0.1
55	6	3.125	5.0317	414119	0.25936	0.02588	-0.00766	0.00264	-0.00011	0.00212	0.13208	5.103	0.1
55	7	6.288	5.0436	414647	0.50139	0.03503	-0.00859	0.01121	-0.00023	0.00221	0.35503	10.136	0.1
55	8	9.422	4.9925	412575	0.70892	0.05215	-0.00811	0.02009	-0.00016	0.00113	0.59689	11.446	0.1
55	9	12.438	5.0236	413887	0.80697	0.09707	-0.00894	0.00749	-0.00083	-0.00117	0.72492	7.4678	0.1
55	10	15.476	5.1143	417633	0.83428	0.1588	-0.00977	-0.01559	-0.00405	-0.00872	0.76203	4.7986	0.1
55	11	18.386	5.1721	420015	0.71467	0.23191	-0.01076	-0.04617	-0.00017	-0.00156	0.60417	2.6051	0.1
55	12	21.353	5.2523	423279	0.68458	0.27695	-0.01075	-0.05119	0.00039	-0.00482	0.56641	2.0452	0.1
55	13	24.305	5.2766	424301	0.60616	0.32751	-0.01039	-0.06051	-0.00074	0.00177	0.47194	1.441	0.1

RUN	TP	ALPHAC	QC	RE	CLSA	CDSA	CYSA	CMSA25	CNSA25	CRSA25	CLSA32	CL32CD	VRATIO
56	2	-9.426	5.099	416891	-0.65784	0.06949	-0.00642	-0.00848	-0.00005	0.00187	0.53356	7.6784	0.25
56	3	-6.207	5.0644	415507	-0.44155	0.04661	-0.00824	-0.00791	0.00004	0.00239	0.2934	6.2943	0.25
56	4	-3.148	5.0928	416704	-0.21419	0.03236	-0.00831	-0.00608	-0.00003	0.00279	0.09913	3.0636	0.25
56	5	0.032	5.0653	415615	0.03134	0.02524	-0.00742	-0.00383	-0.00006	0.00257	0.00555	0.21984	0.25
56	6	3.124	5.0377	414508	0.27347	0.02606	-0.00713	0.00115	-0.00014	0.00174	0.14301	5.4869	0.25
56	7	6.299	4.9957	412810	0.51899	0.03497	-0.00847	0.00903	-0.00027	0.00105	0.37389	10.692	0.25
56	8	9.42	5.0392	414631	0.72024	0.05196	-0.00821	0.01767	-0.00022	-0.00038	0.61125	11.763	0.25
56	9	12.428	5.0523	415189	0.82614	0.09422	-0.00844	0.00802	-0.00196	-0.00305	0.7509	7.9696	0.25
56	10	15.461	5.0513	415171	0.85818	0.14316	-0.01005	-0.00383	-0.00218	-0.00683	0.79501	5.5532	0.25
56	11	18.367	5.1661	419885	0.73446	0.23015	-0.00965	-0.04636	-0.0012	-0.00115	0.62943	2.7349	0.25
56	12	21.444	5.2966	425175	0.74817	0.28311	-0.01025	-0.05557	0.00005	-0.00053	0.64714	2.2858	0.25
56	13	24.389	5.3195	426107	0.73046	0.34614	-0.00971	-0.06724	-0.00036	-0.00139	0.6243	1.8036	0.25
56	14	27.411	5.3127	425856	0.72277	0.3987	-0.01497	-0.07934	0.0004	-0.00371	0.61447	1.5412	0.25

RUN	TP	ALPHAC	QC	RE	CLSA	CDSA	CYSA	CMSA25	CNSA25	CRSA25	CLSA32	CL32CD	VRATIO
57	2	-9.423	5.0824	416371	-0.63079	0.06897	0.0053	-0.00833	0.00005	0.00042	0.50099	7.2637	0.5
57	3	-6.183	5.0029	413123	-0.41058	0.04576	0.00436	-0.01017	0.00014	0.00135	0.26308	5.7487	0.5
57	4	-3.131	5.1117	417623	-0.18671	0.03173	0.00338	-0.00794	0.00006	0.00156	0.08068	2.5428	0.5
57	5	0.049	4.9792	412196	0.05532	0.0246	0.00297	-0.00651	0.00003	0.00123	0.01301	0.52894	0.5
57	6	3.148	5.0206	413932	0.30615	0.02572	0.00118	-0.00309	-0.00004	0.00104	0.16939	6.5859	0.5
57	7	6.293	4.9975	413004	0.55161	0.03484	0.00146	0.00438	-0.00009	0.00073	0.40968	11.757	0.5
57	8	9.444	4.9752	412097	0.75068	0.05183	0.00271	0.01435	-0.00007	-0.00257	0.65041	12.549	0.5
57	9	12.482	5.1179	417989	0.87088	0.08809	0.00146	0.01141	-0.00071	-0.00321	0.81271	9.22575	0.5
57	10	15.497	5.0549	415419	0.89053	0.1414	0.0009	-0.00467	-0.00185	-0.00677	0.84038	5.9434	0.5
57	11	18.431	5.1379	418834	0.78035	0.22641	0.00218	-0.04248	-0.00038	0.00356	0.68933	3.0447	0.5
57	12	21.37	5.2072	421666	0.78353	0.27718	0.00232	-0.05418	-0.00071	0.00089	0.69356	2.5022	0.5
57	13	24.435	5.245	423208	0.79064	0.34467	0.00242	-0.07023	-0.00136	0.00047	0.70303	2.0397	0.5
57	14	27.494	5.3953	429235	0.8014	0.40341	-0.00428	-0.08235	-0.00044	0.00017	0.71742	1.7784	0.5
57	15	30.397	5.3765	428498	0.78352	0.45242	-0.008	-0.09121	-0.00063	0.00134	0.69355	1.533	0.5
57	16	33.379	5.5191	434153	0.73231	0.48904	-0.00586	-0.09427	0.00154	-0.00472	0.62668	1.2815	0.5

A.8 AR-9, Full Wing Moving Surfaces

RUN	TP	ALPHAC	QC	RE	CLSA	CDSA	CYSA	CMSA25	CNSA25	CRSA25	CLSA32	CL32CD	VRATIO
58	2	-9.365	1.0156	185346	-0.55003	0.07485	0.00318	-0.01078	0.00024	0.00192	0.40793	5.4502	0.25
58	3	-6.255	1.0094	184819	-0.3771	0.05275	0.0024	-0.00689	0.0002	0.00245	0.23157	4.39	0.25
58	4	-3.113	1.0064	184560	-0.17237	0.03857	0.00114	-0.00693	0.0001	0.00377	0.07156	1.8555	0.25
58	5	0.063	1.0145	185316	0.07313	0.0326	0.00017	-0.00371	0.00006	0.00372	0.01978	0.60671	0.25
58	6	3.15	1.0039	184371	0.31198	0.03324	-0.00104	-0.00133	-0.00003	0.00269	0.17426	5.2418	0.25
58	7	6.302	1.0073	184698	0.55926	0.04204	-0.00145	0.00848	0.00001	0.00253	0.41824	9.94947	0.25
58	8	9.474	1.0062	184620	0.7578	0.06088	-0.00055	0.01761	-0.00013	0.00078	0.65968	10.835	0.25
58	9	12.466	1.0053	184558	0.87555	0.09989	-0.00268	0.00826	-0.00015	0.00201	0.81925	8.2014	0.25
58	10	15.486	1.03	186829	0.92844	0.16105	-0.00277	-0.00788	-0.00088	0	0.8946	5.5547	0.25
58	11	18.531	1.0412	187860	0.90054	0.24491	-0.00237	-0.0463	-0.00017	-0.0007	0.85458	3.4894	0.25
58	12	21.481	1.0429	188024	0.88071	0.30652	-0.0049	-0.0575	-0.00052	0.00148	0.82652	2.6964	0.25
58	13	24.411	1.0741	190829	0.8219	0.3585	-0.00484	-0.06489	-0.002	0.00527	0.74512	2.0785	0.25
58	14	27.425	1.0847	191784	0.77989	0.41732	-0.00362	-0.0795	-0.0009	-0.00005	0.68873	1.6504	0.25
58	15	30.44	1.0852	191848	0.74167	0.46933	-0.00074	-0.09448	0.00124	-0.0039	0.63873	1.3609	0.25
58	16	33.354	1.1006	193218	0.71652	0.50996	-0.00192	-0.09866	0.00056	-0.00234	0.60652	1.1893	0.25

A.9 AR-7

RUN	TP	ALPHAC	QC	RE	CLSA	CDSA	CYSA	CMSA25	CNSA25	CRSA25	CLSA32	CL32CD	VRATIO
61	2	-9.251	0.99719	183669	-0.61517	0.0759	0.00466	-0.00951	0.00016	0.00178	0.4825	6.3573	0
61	3	-6.258	0.9942	183411	-0.44754	0.05489	0.00353	-0.0033	0.00016	0.00237	0.29939	5.4547	0
61	4	-3.118	0.99988	183951	-0.23315	0.03928	0.00229	-0.00365	0.00022	0.00282	0.11258	2.8658	0
61	5	0.003	1.0172	185556	-0.02698	0.03154	0.00161	-0.00061	0.0001	0.00195	0.00443	0.1405	0
61	6	3.063	1.0148	185363	0.19284	0.03114	-0.00052	0.00516	0	0.00187	0.08468	2.7199	0
61	7	6.184	0.99011	183107	0.40582	0.03953	0.00012	0.01284	-0.00006	0.00147	0.25852	6.5393	0
61	8	9.214	0.9975	183806	0.57793	0.05601	0.00037	0.02143	-0.00011	0.00043	0.43936	7.8449	0
61	9	12.341	1.0284	186654	0.70344	0.09279	-0.00206	0.01373	-0.00026	0.00461	0.58999	6.3582	0
61	10	15.282	1.0114	185119	0.6905	0.16386	-0.00357	-0.02266	-0.00366	-0.014	0.57377	3.5016	0
61	11	18.269	1.0312	186943	0.6046	0.22398	-0.00282	-0.04179	-0.00071	-0.00777	0.47012	2.0989	0
61	12	21.241	1.0473	188410	0.57439	0.27486	-0.00294	-0.053	-0.00177	-0.00797	0.43532	1.5838	0
61	13	24.247	1.0475	188442	0.55866	0.31799	0.0023	-0.06036	-0.00045	-0.00297	0.41756	1.3131	0
61	14	27.222	1.0489	188580	0.54812	0.35588	0.00401	-0.07009	0.00032	-0.00276	0.4058	1.1403	0
61	15	30.214	1.0494	188641	0.54885	0.39538	0.00247	-0.07505	0.00012	-0.00495	0.40662	1.0284	0
61	16	33.239	1.0603	189624	0.55023	0.4326	0.0018	-0.08099	0.00133	-0.00724	0.40815	0.94349	0

RUN	TP	ALPHAC	QC	RE	CLSA	CDSA	CYSA	CMSA25	CNSA25	CRSA25	CLSA32	CL32CD	VRATIO
62	1	-9.337	5.0327	413668	-0.5697	0.07246	-0.00917	-0.0208	-0.00042	0.0003	0.43	5.9341	0
62	2	-6.252	5.0588	414768	-0.40756	0.05212	-0.0107	-0.01168	-0.00058	0.00225	0.26019	4.9922	0
62	3	-3.033	5.0729	415386	-0.2032	0.03747	-0.01	-0.00624	-0.00065	0.00309	0.0916	2.4445	0
62	4	0.018	5.0457	414307	0.00269	0.03027	-0.00945	-0.00196	-0.00047	0.00313	0.00014	0.0046	0
62	5	3.048	5.0382	414039	0.20914	0.03036	-0.00888	0.00609	-0.00038	0.00282	0.09565	3.1503	0
62	6	6.192	5.0495	414539	0.42631	0.03945	-0.00974	0.01555	-0.00055	0.00334	0.27835	7.056	0
62	7	9.279	5.0477	414491	0.59008	0.05498	-0.00889	0.03072	-0.00028	0.00105	0.45328	8.2442	0
62	8	12.317	5.0299	413783	0.72103	0.09181	-0.01433	0.02395	0	0.00066	0.61225	6.6688	0
62	9	15.304	5.067	415366	0.73528	0.16551	-0.01502	-0.01655	-0.00013	-0.00073	0.6305	3.8093	0
62	10	18.261	5.1852	420198	0.7094	0.22921	-0.01419	-0.04795	0.001	-0.00353	0.5975	2.6068	0
62	11	21.321	5.1589	419155	0.68094	0.28305	-0.01658	-0.05889	-0.00252	0.01049	0.56191	1.9852	0
62	12	24.308	5.1653	419434	0.66826	0.32832	-0.01287	-0.06675	-0.00348	0.00502	0.54628	1.6639	0
62	13	27.212	5.2705	423703	0.61665	0.36643	-0.00604	-0.07418	-0.00095	-0.00337	0.48424	1.3215	0
62	14	30.252	5.3053	425111	0.59152	0.40327	-0.00439	-0.07664	0.00021	-0.00317	0.45494	1.1281	0
62	15	33.265	5.2904	424529	0.59357	0.44409	-0.00355	-0.08403	-0.00024	-0.001	0.4573	1.0298	0

RUN	TP	ALPHAC	QC	RE	CLSA	CDSA	CYSA	CMSA25	CNSA25	CRSA25	CLSA32	CL32CD	VRATIO
63	1	-9.249	9.9115	581238	-0.55935	0.07039	0.00585	-0.01783	-0.00034	0.00125	0.41834	5.9429	0
63	2	-6.151	9.99602	583728	-0.38416	0.04698	0.00542	-0.01798	-0.00025	0.00119	0.23811	5.0679	0
63	3	-3.16	10.106	586955	-0.19086	0.03304	0.00352	-0.00988	-0.00017	0.0015	0.08338	2.5234	0
63	4	0.081	10.162	588607	0.01865	0.02552	0.00356	-0.00411	0.00005	0.00201	0.00255	0.09981	0
63	5	3.02	10.113	587205	0.21537	0.02702	0.00237	0.00785	0.00005	0.00204	0.09995	3.6989	0
63	6	6.236	10.117	587337	0.42698	0.03636	0.00116	0.02019	-0.00006	0.00276	0.279	7.6739	0
63	7	9.289	10.058	585657	0.59322	0.05398	0.00288	0.03169	0.00019	0.00001	0.45691	8.465	0
63	8	12.345	10.147	588232	0.75057	0.0949	0.0019	0.01713	0.0005	-0.00125	0.65026	6.8518	0
63	9	15.299	10.123	587551	0.75236	0.16536	-0.00332	-0.01743	-0.00079	-0.00249	0.65259	3.9464	0
63	10	18.356	10.161	588676	0.78035	0.22506	0.00019	-0.03897	0.00109	-0.00009	0.68934	3.0629	0
63	11	21.27	10.353	594203	0.71146	0.28155	-0.00152	-0.05802	-0.00119	0.00396	0.6001	2.1314	0
63	12	24.274	10.325	593419	0.61798	0.3178	-0.00388	-0.06296	-0.00224	-0.00478	0.48581	1.5287	0
63	13	27.27	10.443	596792	0.603	0.35789	0.00637	-0.0673	-0.00153	-0.0063	0.46825	1.3084	0
63	14	30.206	10.709	604359	0.60971	0.39986	0.00676	-0.07649	-0.00065	-0.00476	0.47608	1.1906	0
63	15	33.269	10.694	603920	0.60488	0.44373	0.00263	-0.08282	-0.00009	-0.00434	0.47044	1.0602	0

RUN	TP	ALPHAC	QC	RE	CLSA	CDSA	CYSA	CMSA25	CNSA25	CRSA25	CLSA32	CL32CD	VRATIO
64	2	-9.273	1.002	184608	-0.52808	0.07613	0.00398	-0.02291	-0.00017	0.00522	0.38375	5.0407	0.25
64	3	-6.192	1.0087	185231	-0.36211	0.05421	0.00329	-0.01542	-0.00009	0.00326	0.2179	4.0195	0.25
64	4	-3.037	1.0133	185648	-0.16382	0.03988	0.0015	-0.01638	-0.00011	0.00302	0.06631	1.6626	0.25
64	5	-0.035	1.0084	185208	0.04873	0.03363	0.00029	-0.01388	-0.00022	0.00266	0.01076	0.31983	0.25
64	6	3.046	1.0009	184522	0.26761	0.03381	0.00029	-0.00956	-0.00019	0.003	0.13844	4.0945	0.25
64	7	6.215	1.0032	184740	0.48878	0.04317	0.00017	-0.00147	-0.00044	0.00552	0.34172	7.9155	0.25
64	8	9.373	1.0154	185871	0.67683	0.06034	-0.00213	0.00603	-0.00033	0.00467	0.55682	9.22816	0.25
64	9	12.358	1.0122	185581	0.7937	0.09285	-0.00244	0.00796	-0.00071	0.00668	0.70711	7.6154	0.25
64	10	15.372	1.0099	185366	0.83927	0.15198	-0.00577	-0.01489	-0.00195	0.0091	0.76887	5.0591	0.25

RUN	TP	ALPHAC	QC	RE	CLSA	CDSA	CYSA	CMSA25	CNSA25	CRSA25	CLSA32	CL32CD	VRATIO
65	2	-9.24	1.022	186450	-0.53097	0.07514	0.00347	-0.02241	-0.00025	0.00191	0.38691	5.149	0.25
65	3	-6.21	1.0177	186064	-0.36708	0.05416	0.00291	-0.01533	-0.00019	0.00072	0.22241	4.1062	0.25
65	4	-3.039	1.0152	185836	-0.16407	0.03948	0.00168	-0.0178	-0.0002	0.00076	0.06646	1.6831	0.25
65	5	-0.066	1.0133	185666	0.04013	0.03247	0.00021	-0.01625	-0.00018	0.00066	0.00804	0.24764	0.25
65	6	3.195	1.0049	184897	0.27422	0.03345	-0.00056	-0.01145	-0.0002	0.00113	0.1436	4.2929	0.25
65	7	6.178	1.0042	184837	0.47412	0.04211	-0.00071	-0.00327	-0.00054	0.00327	0.32646	7.7523	0.25
65	8	9.212	1.0043	184843	0.6587	0.05854	-0.00053	0.00459	-0.00067	0.00329	0.5346	9.13239	0.25
65	9	12.413	1.0037	184795	0.78471	0.09562	-0.00257	-0.00194	-0.00038	0.00496	0.69513	7.2697	0.25
65	10	15.385	1.0153	185873	0.82858	0.15332	-0.00308	-0.0202	-0.00144	0.0078	0.75423	4.9194	0.25
65	11	18.331	1.0238	186651	0.81542	0.22392	-0.00399	-0.04644	0.00051	0.00853	0.73632	3.2883	0.25
65	12	21.292	1.0311	187317	0.77867	0.28418	-0.00692	-0.0606	0.0016	0.01331	0.68712	2.4179	0.25
65	13	24.332	1.0538	189379	0.73427	0.34699	-0.01021	-0.07834	-0.0012	0.01747	0.6292	1.8133	0.25
65	14	27.245	1.0665	190518	0.67365	0.39096	-0.01522	-0.08428	-0.00782	0.03512	0.55291	1.4142	0.25

RUN	TP	ALPHAC	QC	RE	CLSA	CDSA	CYSA	CMSA25	CNSA25	CRSA25	CLSA32	CL32CD	VRATIO
66	2	-9.27	1.0099	185314	-0.46429	0.07869	0.00402	-0.02608	-0.0009	0.00597	0.31636	4.0205	0.5
66	3	-6.226	1.0144	185736	-0.31333	0.05686	0.00317	-0.02429	-0.00067	0.00555	0.17539	3.0844	0.5
66	4	-3.062	1.0046	184839	-0.11816	0.04184	0.00195	-0.02504	-0.00068	0.00632	0.04062	0.97062	0.5
66	5	0.142	1.0006	184479	0.10099	0.03551	-0.00046	-0.02016	-0.00077	0.0056	0.03209	0.9038	0.5
66	6	3.122	1.0002	184447	0.31386	0.03674	-0.00075	-0.01826	-0.00083	0.00481	0.17584	4.7854	0.5
66	7	6.2	0.99744	184196	0.53599	0.04694	-0.00029	-0.01397	-0.00097	0.00375	0.39241	8.3601	0.5
66	8	9.292	1.0005	184487	0.72698	0.06464	-0.00353	-0.00889	-0.00068	0.00224	0.61985	9.58885	0.5
66	9	12.408	1.0041	184821	0.85018	0.09642	-0.00193	-0.00558	-0.00052	0.0026	0.78392	8.1304	0.5
66	10	15.424	1.004	184821	0.91538	0.15342	-0.00296	-0.0257	-0.00062	0.00494	0.87579	5.7086	0.5
66	11	18.374	1.0208	186366	0.88238	0.2236	-0.00465	-0.05125	0.00069	0.01259	0.82886	3.7068	0.5
66	12	21.336	1.0475	188792	0.85287	0.27599	-0.00799	-0.06413	-0.00085	0.00947	0.78763	2.8539	0.5
66	13	24.353	1.0515	189160	0.84132	0.33553	-0.00765	-0.07729	-0.002	0.01249	0.77169	2.2999	0.5
66	14	27.362	1.0456	188630	0.81807	0.39705	-0.00521	-0.08991	0.00068	0.00999	0.73992	1.8635	0.5
66	15	30.392	1.0611	190024	0.82696	0.46699	-0.00506	-0.10568	-0.0009	0.01474	0.75201	1.6103	0.5
66	16	33.337	1.0757	191333	0.80523	0.52775	-0.00462	-0.12116	-0.00254	0.0126	0.72258	1.3692	0.5

A.10 AR-5, Alternate Trailing Edge

RUN	TP	ALPHAC	QC	RE	CLSA	CDSA	CYSA	CMSA25	CNSA25	CRSA25	CLSA32	CL32CD	VRATIO
94	2	-9.299	0.99607	181708	-0.54597	0.08178	0.00196	-0.02571	-0.00001	0.00175	0.40342	4.9328	0.25
94	3	-6.073	1.0024	182296	-0.38431	0.05652	0.00141	-0.02552	-0.00004	0.00046	0.23824	4.2153	0.25
94	4	-3.124	1.0076	182778	-0.21085	0.04212	0.00108	-0.01919	-0.00001	0.00082	0.09682	2.2985	0.25
94	5	-0.021	1.0069	182729	-0.022	0.03315	-0.0006	-0.00985	0.00001	-0.0004	0.00326	0.09845	0.25
94	6	3.05	0.99964	182073	0.20268	0.03363	-0.0031	-0.01412	-0.00001	0.00051	0.09125	2.7133	0.25
94	7	6.202	0.99687	181833	0.40143	0.04346	-0.00383	-0.00868	-0.00009	0.00257	0.25434	5.852	0.25
94	8	9.139	0.99434	181613	0.57114	0.05836	-0.00087	0.00069	-0.00005	0.0028	0.43163	7.3961	0.25
94	9	12.259	0.9935	181545	0.72755	0.09127	-0.00012	-0.0005	0.00014	0.00481	0.62058	6.7994	0.25
94	10	15.214	1.0055	182651	0.79816	0.14287	-0.00116	-0.01305	0.00045	0.00686	0.71307	4.9911	0.25
94	11	18.267	1.0169	183690	0.81784	0.20081	-0.00191	-0.03151	0.00164	0.00599	0.7396	3.6831	0.25
94	12	21.226	1.0253	184462	0.76975	0.27847	-0.0019	-0.05768	0.00062	0.00706	0.67535	2.4252	0.25
94	13	24.158	1.0263	184554	0.6364	0.32711	-0.00361	-0.05838	0.0013	0.00807	0.50768	1.552	0.25
94	14	27.198	1.031	184988	0.60846	0.36493	-0.00919	-0.05882	-0.00017	0.00421	0.47462	1.3006	0.25
94	15	30.227	1.0446	186214	0.56624	0.3969	-0.01012	-0.06415	-0.00315	0.01382	0.42609	1.0735	0.25
94	16	33.121	1.0548	187129	0.56584	0.43738	-0.00265	-0.0726	-0.00141	0.01047	0.42564	0.97317	0.25

RUN	TP	ALPHAC	QC	RE	CLSA	CDSA	CYSA	CMSA25	CNSA25	CRSA25	CLSA32	CL32CD	VRATIO
95	2	-9.16	0.99661	181877	-0.51587	0.0755	0.00269	-0.02147	-0.00018	-0.00042	0.37052	4.9073	0.5
95	3	-6.179	1.0044	182595	-0.364	0.05526	0.00256	-0.01793	-0.00003	0.00032	0.21961	3.9737	0.5
95	4	-3.052	1.0093	183050	-0.18425	0.03913	0.00102	-0.01146	-0.00003	-0.0008	0.07909	2.0209	0.5
95	5	-0.008	1.0127	183370	0.0006	0.03113	-0.00099	-0.01169	-0.00016	-0.00016	0.00001	0.00048	0.5
95	6	3.066	1.0083	182975	0.21371	0.03067	-0.00067	-0.00716	-0.00018	-0.00022	0.09879	3.2206	0.5
95	7	6.053	1.0025	182455	0.41537	0.04088	-0.00329	-0.00092	-0.00015	-0.00053	0.2677	6.5486	0.5
95	8	9.273	1.0011	182327	0.59831	0.05743	-0.00471	0.00768	-0.00021	0.00097	0.4628	8.0579	0.5
95	9	12.2	1.0026	182475	0.74877	0.08434	-0.00566	0.0113	-0.00006	0.00222	0.64793	7.6822	0.5
95	10	15.289	1.0088	183044	0.82943	0.13905	-0.00536	-0.00059	0.00018	0.0041	0.75539	5.4327	0.5
95	11	18.286	1.0146	183579	0.85022	0.19332	-0.00501	-0.01231	0.00113	0.00395	0.78397	4.0553	0.5
95	12	21.211	1.0204	184107	0.80487	0.27481	-0.00356	-0.04218	-0.00375	-0.00399	0.72208	2.6276	0.5
95	13	24.213	1.0217	184228	0.73869	0.33217	0.00408	-0.05474	-0.00656	-0.01698	0.63488	1.9113	0.5
95	14	27.232	1.0428	186126	0.60396	0.3669	0.00792	-0.06339	0.00235	-0.01535	0.46937	1.2793	0.5
95	15	30.168	1.0539	187124	0.61693	0.40817	0.0046	-0.06109	0.00169	-0.00976	0.48457	1.1872	0.5
95	16	33.119	1.0499	186771	0.57875	0.44058	0.00177	-0.06692	0.00281	-0.00982	0.44028	0.99933	0.5

RUN	TP	ALPHAC	QC	RE	CLSA	CDSA	CYSA	CMSA25	CNSA25	CRSA25	CLSA32	CL32CD	VRATIO
96	2	-9.174	1.0156	183714	-0.59254	0.07933	0.00365	-0.01336	0	-0.00069	0.45612	5.7494	0
96	3	-6.166	0.99014	181408	-0.43853	0.05763	0.00287	-0.0026	0.00008	-0.00029	0.2904	5.0386	0
96	4	-3.071	1.0094	183165	-0.23184	0.04056	0.00211	-0.00693	0.00004	-0.00018	0.11163	2.7524	0
96	5	-0.068	1.0196	184094	-0.02427	0.02947	0.00135	-0.00254	0.00007	-0.00073	0.00378	0.12835	0
96	6	3.077	1.0113	183353	0.17213	0.02955	0.0009	0.008	0.00012	-0.00163	0.07141	2.4164	0
96	7	6.038	1.0056	182836	0.3886	0.03973	-0.00116	0.01183	0.00003	-0.00158	0.24225	6.0975	0
96	8	9.265	1.0053	182811	0.56277	0.05641	-0.00308	0.01477	0.00009	-0.00059	0.42217	7.4837	0
96	9	12.178	1.0066	182939	0.67904	0.08686	-0.00334	0.01539	0.00019	0.00003	0.55956	6.4422	0
96	10	15.222	1.0087	183136	0.64662	0.15757	-0.00231	-0.0154	-0.00461	-0.0195	0.51996	3.2998	0
96	11	18.181	1.0137	183595	0.55029	0.21232	-0.00361	-0.03448	-0.00038	0.00205	0.40821	1.9226	0
96	12	21.113	1.0367	185663	0.54936	0.27709	-0.00383	-0.0478	-0.0007	0.00032	0.40718	1.4695	0
96	13	24.185	1.0354	185552	0.55424	0.31879	-0.00349	-0.04473	-0.00052	0.00248	0.41261	1.2943	0
96	14	27.148	1.0312	185178	0.52223	0.35098	-0.0067	-0.04576	-0.00214	0.00896	0.37739	1.0752	0
96	15	30.193	1.0372	185722	0.51825	0.3836	-0.00705	-0.05249	-0.00338	0.01172	0.37308	0.97259	0
96	16	33.095	1.0433	186268	0.52318	0.42543	-0.00264	-0.05755	-0.00206	0.00658	0.37843	0.88952	0

A.11 Center Body

RUN	TP	ALPHAC	QC	RE	CLSA	CDSA	CYSA	CMSA25	CNSA25	CRSA25	CLSA32	CL32CD	VRATIO
100	2	-9.062	1.0157	183309	-0.28083	0.13693	0.00991	-0.05001	-0.00024	0.00083	0.14882	1.0869	0
100	3	-6.033	1.0084	182663	-0.19373	0.11046	0.01504	-0.05201	-0.00068	-0.00304	0.08527	0.77195	0
100	4	-2.987	1.0042	182291	-0.1081	0.09079	0.00673	-0.05401	-0.00024	0.00237	0.03554	0.39149	0
100	5	-0.085	1.0019	182105	-0.03986	0.0778	0.00954	-0.05562	-0.00063	0.00358	0.00796	0.10228	0
100	6	3.061	1.0049	182382	0.03222	0.07313	0.00912	-0.01979	-0.00173	0.00424	0.00578	0.0791	0
100	7	5.964	1.0038	182295	0.10323	0.07175	0.00326	0.00615	-0.00019	0.00185	0.03317	0.46223	0
100	8	9.028	1.0008	182038	0.18885	0.08065	-0.00121	0.02483	0.0012	0.00227	0.08207	1.0175	0
100	9	12.001	1.0007	182042	0.29572	0.09472	-0.01107	0.02411	0.00003	0.00234	0.16081	1.6977	0
100	10	14.993	1.0057	182506	0.39975	0.11602	-0.0081	0.02008	0.00051	0.00288	0.25275	2.1784	0
100	11	18.059	1.0096	182874	0.52813	0.15041	-0.00872	0.02542	0.00054	-0.00277	0.3838	2.5517	0
100	12	20.977	1.0076	182699	0.65486	0.19595	0.02099	0.02353	-0.00152	-0.00669	0.52993	2.7044	0
100	13	24.016	1.0027	182273	0.77155	0.25751	0.01467	-0.00029	-0.00066	0.00524	0.67772	2.6318	0
100	14	27.062	0.99644	181709	0.81665	0.49791	0.00609	-0.17255	-0.00007	0.01194	0.73799	1.4822	0
100	15	30.084	1.0074	182732	0.93702	0.60436	-0.00281	-0.19133	0.00292	0.00513	0.90704	1.5008	0
100	16	33.003	1.0062	182651	1.0857	0.74066	-0.01592	-0.22738	0.003	0.01132	1.1313	1.5274	0

RUN	TP	ALPHAC	QC	RE	CLSA	CDSA	CYSA	CMSA25	CNSA25	CRSA25	CLSA32	CL32CD	VRATIO
101	1	-9.012	4.9764	406517	-0.25484	0.11489	-0.0644	-0.05056	0.00099	0.06854	0.12865	1.1197	0
101	2	-6.028	5.0961	411402	-0.16841	0.08798	-0.05566	-0.04947	0.00047	0.06486	0.06911	0.78551	0
101	3	-3.001	5.0034	407668	-0.08384	0.06772	-0.05707	-0.04141	0.00025	0.06661	0.02428	0.3585	0
101	4	-0.011	4.9902	407149	-0.01101	0.05441	-0.06339	-0.03058	-0.00008	0.06738	0.00115	0.02122	0
101	5	2.986	5.0169	408263	0.05526	0.05218	-0.05914	-0.00923	-0.00155	0.06974	0.01299	0.24891	0
101	6	5.996	4.9672	406260	0.13226	0.05175	-0.06875	0.01473	-0.00098	0.06635	0.0481	0.92955	0
101	7	9.005	4.9699	406389	0.21641	0.0581	-0.07975	0.02945	-0.0009	0.06709	0.10068	1.7328	0
101	8	11.94	4.9856	407050	0.31123	0.0712	-0.07943	0.03351	-0.00132	0.06665	0.17363	2.4388	0
101	9	15.067	5.0266	408737	0.42442	0.09693	-0.07952	0.03475	-0.00181	0.06602	0.2765	2.8527	0
101	10	18.036	5.0483	409636	0.54124	0.12994	-0.07741	0.02782	-0.00219	0.06486	0.39819	3.0644	0
101	11	21.002	4.9701	406466	0.66337	0.17595	-0.07683	0.01975	-0.00237	0.06437	0.54029	3.0707	0
101	12	24.027	4.9883	407226	0.79278	0.23792	-0.06945	-0.00074	-0.00244	0.0629	0.70588	2.9669	0
101	13	27.06	4.9676	406391	0.93173	0.31763	-0.07365	-0.03859	-0.00188	0.06561	0.89937	2.8315	0
101	14	30.032	5.0277	408858	1.0789	0.4301	-0.07424	-0.09417	-0.0003	0.06441	1.1207	2.6056	0
101	15	33.056	5.0094	408125	1.1207	0.64092	-0.11055	-0.18452	0.01093	0.07466	1.1864	1.8511	0

RUN	TP	ALPHAC	QC	RE	CLSA	CDSA	CYSA	CMSA25	CNSA25	CRSA25	CLSA32	CL32CD	VRATIO
102	1	-9.013	9.86903	572933	-0.24875	0.08806	0.02758	-0.02657	0.00094	-0.02205	0.12406	1.4089	0
102	2	-6.023	9.99005	576448	-0.15774	0.06105	0.03657	-0.02766	0.00055	-0.02306	0.06265	1.0261	0
102	3	-3.09	10.057	578393	-0.07731	0.04132	0.03552	-0.0203	0.00082	-0.02383	0.0215	0.52028	0
102	4	0.068	10.072	578836	-0.00207	0.0301	0.01539	-0.0033	0.00097	-0.01964	0.00009	0.00313	0
102	5	2.912	10.018	577293	0.06383	0.02267	0.0252	0.01303	0.00075	-0.02093	0.01613	0.71144	0
102	6	6.063	10.026	577515	0.13877	0.02527	0.01222	0.03595	0.00078	-0.018	0.0517	2.0459	0
102	7	9.001	10.042	578001	0.22123	0.03236	0.0045	0.04968	0.00096	-0.01627	0.10406	3.2156	0
102	8	11.938	10.022	577419	0.31785	0.04755	0.00361	0.05572	0.00073	-0.01606	0.1792	3.7687	0
102	9	15.027	10.016	577269	0.43417	0.07315	0.00834	0.05328	0.00032	-0.01829	0.28608	3.9109	0
102	10	18.081	10.042	578017	0.5526	0.1093	0.04389	0.04539	0.00022	-0.02374	0.41078	3.7585	0
102	11	20.97	10.015	577240	0.67253	0.15559	0.0396	0.03424	0.00054	-0.02401	0.55152	3.5447	0
102	12	24.049	10.002	576852	0.80525	0.21858	0.0351	0.01173	0.00006	-0.02081	0.7226	3.3058	0
102	13	27.045	9.97251	576002	0.93886	0.29488	0.01447	-0.02116	0.00008	-0.0186	0.9097	3.085	0
102	14	30.104	9.92124	574519	1.0921	0.40245	0.01494	-0.06703	0.00232	-0.01931	1.1412	2.8357	0
102	15	33.026	9.97863	576183	1.1105	0.61079	-0.01973	-0.17023	0.01139	-0.00346	1.1702	1.9158	0

RUN	TP	ALPHAC	QC	RE	CLSA	CDSA	CYSA	CMSA25	CNSA25	CRSA25	CLSA32	CL32CD	VRATIO
103	1	-9.077	19.809	811597	-0.24805	0.08357	0.00797	-0.02496	0.00143	-0.01189	0.12354	1.4783	0
103	2	-5.959	19.809	811567	-0.15181	0.05739	0.01471	-0.02345	0.0009	-0.01419	0.05915	1.0306	0
103	3	-3.013	19.784	811031	-0.07305	0.04036	0.02515	-0.01399	0.0006	-0.01902	0.01974	0.4891	0
103	4	-0.012	19.822	811783	-0.0015	0.03053	0.00835	0.00092	0.00076	-0.01665	0.00006	0.0019	0
103	5	2.927	19.801	811324	0.06439	0.02673	0.00266	0.02106	0.00068	-0.01425	0.01634	0.61133	0
103	6	6.043	19.813	811554	0.14002	0.02415	0.04594	0.03927	0.00046	-0.02467	0.05239	2.1693	0
103	7	9.025	19.786	810942	0.22619	0.03126	0.03944	0.05254	0.00057	-0.02345	0.10757	3.4411	0
103	8	12.027	19.897	813208	0.32227	0.04635	0.04458	0.05879	0.00072	-0.02477	0.18295	3.947	0
103	9	14.985	19.88	812816	0.43361	0.07137	0.04351	0.05604	0.00087	-0.02373	0.28553	4.0008	0
103	10	17.975	19.967	814575	0.54928	0.1055	0.03867	0.04851	0.00086	-0.02238	0.40709	3.8587	0
103	11	21.098	20.038	815984	0.67334	0.15269	0.0309	0.03583	0.00113	-0.02052	0.55252	3.6185	0
103	12	24.009	19.982	814825	0.7963	0.21064	0.02932	0.01626	0.00227	-0.02126	0.71058	3.3735	0
103	13	27.079	20.035	815887	0.93446	0.29153	0.02306	-0.0172	0.00398	-0.02157	0.90332	3.0985	0
103	14	30.006	19.754	810130	1.0824	0.3954	0.01943	-0.06064	0.00316	-0.02028	1.1261	2.8481	0
103	15	33.073	19.816	811367	1.0999	0.61074	-0.01537	-0.17393	0.00806	0.00039	1.1535	1.8887	0

RUN	TP	ALPHAC	QC	RE	CLSA	CDSA	CYSA	CMSA25	CNSA25	CRSA25	CLSA32	CL32CD	VRATIO
104	1	-9.094	40.722	1161985	-0.24956	0.09144	0.0116	-0.02182	0.00072	-0.01135	0.12467	1.3633	0
104	2	-5.953	40.703	1161577	-0.15163	0.06552	0.02032	-0.01973	0.00048	-0.01475	0.05905	0.90123	0
104	3	-2.993	40.557	1159291	-0.07141	0.04771	0.01522	-0.01127	0.00056	-0.01778	0.01908	0.39993	0
104	4	-0.049	40.702	1161204	0.00075	0.03845	0.01363	0.00467	0.00094	-0.01868	0.00002	0.00053	0
104	5	3.003	40.536	1158685	0.0658	0.02981	0.0447	0.02287	0.00056	-0.02171	0.01688	0.56627	0
104	6	5.928	40.28	1154896	0.13466	0.02974	0.03825	0.04084	0.00032	-0.01883	0.04941	1.6616	0
104	7	9.072	40.211	1153764	0.22849	0.03774	0.02524	0.05437	0.00001	-0.01533	0.10922	2.8938	0
104	8	11.988	40.278	1154583	0.32371	0.05319	0.02768	0.06017	-0.00011	-0.01557	0.18418	3.4626	0
104	9	15.065	40.311	1154902	0.43586	0.0785	0.02829	0.05759	-0.00021	-0.01589	0.28775	3.6658	0
104	10	18.03	40.035	1150797	0.55887	0.11172	0.00309	0.04583	-0.00122	-0.00934	0.4178	3.7398	0
104	11	20.98	40.136	1152115	0.67817	0.15654	0.00764	0.03464	-0.00074	-0.01095	0.55847	3.5676	0
104	12	24.065	40.069	1151037	0.80554	0.21983	0.0214	0.01486	0.00051	-0.01661	0.72299	3.2888	0
104	13	27.028	40.002	1149964	0.93904	0.29896	0.02253	-0.01606	0.00179	-0.01899	0.90997	3.0438	0
104	14	30.035	39.898	1148355	1.0885	0.40651	0.0165	-0.05574	0.00226	-0.01716	1.1356	2.7934	0
104	15	33.077	39.582	1143671	1.1156	0.64393	-0.03939	-0.18563	0.00347	0.00732	1.1783	1.8298	0

VITA

Robert Vets received a Bachelor of Science and Master of Science degrees in Mechanical Engineering and Mechanics from Drexel University in Philadelphia. He has worked for Viking Yachts, General Motors, STI Optronics, and the Boeing Company. For fifteen years he was a senior engineer/scientist, systems engineer, and engineering manager on the Airborne Laser program.